AD-A041 107 LOCKHEED-GEORGIA CO MARIETTA ENGINEERING STRUCTURAL --ETC F/G 11/6
ACOUSTIC EMISSION MONITORING OF CRACK PROPAGATION ON THE EXPEDI--ETC(U)
DEC 76 W M PLESS, C D BAILEY, J M HAMILTON F33615-75-C-5249
UNCLASSIFIED LG77ER-0042 AFML-TR-76-214 NL

1 OF 2
AD
A041107

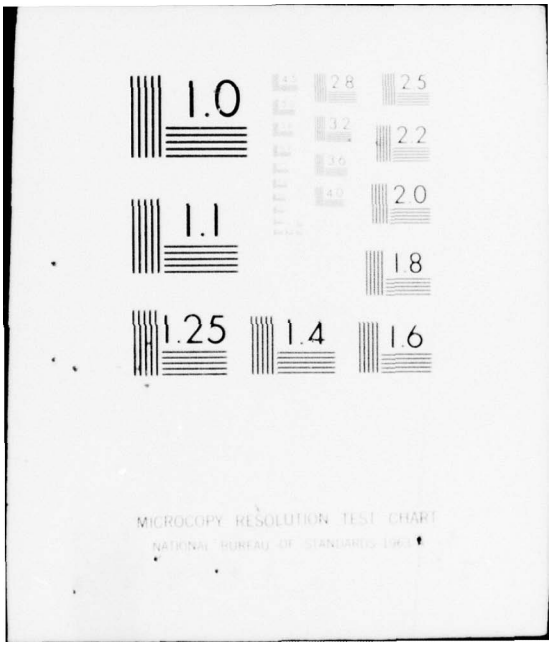
1.0
1.1
1.25
1.4
1.6
2.8
2.5
3.2
2.2
3.6
2.0
4.0
1.8
MICROCOPY RESOLUTION TEST CHART
NATIONAL BUREAU OF STANDARDS 1963

AD A041107

AFML-TR-76-214

ACOUSTIC EMISSION MONITORING OF CRACK PROPAGATION ON THE EXPEDITED WING FATIGUE TEST ARTICLE (X993)

LOCKHEED-GEORGIA COMPANY
DIVISION OF LOCKHEED AIRCRAFT CORPORATION
MARIETTA, GEORGIA 30063

D D C
RECEIVED
JUN 28 1977
C

DECEMBER 1976

FINAL REPORT JUNE 1975 - OCTOBER 1976

Approved for public release; distribution unlimited

AD No. _____
DDC FILE COPY

AIR FORCE MATERIALS LABORATORY/LLP
NONDESTRUCTIVE EVALUATION BRANCH
METALS AND CERAMICS DIVISION
WRIGHT-PATTERSON AIR FORCE BASE, OHIO 45433

NOTICE

When Government drawings, specifications, or other data are used for any purpose other than in connection with a definitely related Government procurement operation, the United States Government thereby incurs no responsibility nor any obligation whatsoever; and the fact that the Government may have formulated, furnished, or in any way supplied the said drawings, specifications, or other data, is not to be regarded by implication or otherwise as in any manner licensing the holder or any other person or corporation, or conveying any rights or permission to manufacture, use, or sell any patented invention that may in any way be related therein.

This report has been reviewed and cleared for open publication and/or public release by the appropriate Office of Information (OI) in accordance with AFR 190-17 and DODD 5230.9. There is no objection to unlimited distribution of this report to the public at large, or by DDC to the National Technical Information Service (NTIS).

This technical report has been reviewed and is approved for publication.

RICHARD R. ROWAND
Technical Manager for NDE
Nondestructive Evaluation Branch
Metals and Ceramics Division

D. M. FORNEY, JR., Chief
Nondestructive Evaluation Branch
Metals and Ceramics Division

Copies of this report should not be returned unless return is required by security considerations, contractual obligations, or notice on a specific document.

AIR FORCE - 31 MAY 77 - 425

SECURITY CLASSIFICATION OF THIS PAGE (When Data Entered)

REPORT DOCUMENTATION PAGE

READ INSTRUCTIONS BEFORE COMPLETING FORM

1. REPORT NUMBER: AFML-TR-76-214	2. GOVT ACCESSION NO.
3. RECIPIENT'S CATALOG NUMBER	
4. TITLE (and Subtitle): ACOUSTIC EMISSION MONITORING OF CRACK PROPAGATION ON THE EXPEDITED WING FATIGUE TEST ARTICLE (X993).	5. TYPE OF REPORT & PERIOD COVERED: Final Technical Report. June 1975 to October 1976.
6. PERFORMING ORG. REPORT NUMBER: LG77ER-0042	
7. AUTHOR(s): William M. Pless, Cliff D. Bailey, James M. Hamilton	8. CONTRACT OR GRANT NUMBER(s): F33615-75-C-5249
9. PERFORMING ORGANIZATION NAME AND ADDRESS: Engineering Structural and Materials Laboratory Dept. Lockheed-Georgia Company, 86 S. Cobb Drive Marietta, Georgia 30063	10. PROGRAM ELEMENT, PROJECT, TASK AREA & WORK UNIT NUMBERS: Project 7531
11. CONTROLLING OFFICE NAME AND ADDRESS: Nondestructive Evaluation Branch, Metals & Ceramics Branch, Air Force Materials Laboratory (LLP) Wright-Patterson Air Force Base, Ohio 45433	12. REPORT DATE: December 1976 13. NUMBER OF PAGES: 128p.
14. MONITORING AGENCY NAME & ADDRESS (if different from Controlling Office)	15. SECURITY CLASS. (of this report): Unclassified 15a. DECLASSIFICATION DOWNGRADING SCHEDULE

16. DISTRIBUTION STATEMENT (of this Report)

Approved for Public Release; Distribution Unlimited

17. DISTRIBUTION STATEMENT (of the abstract entered in Block 20, if different from Report)

18. SUPPLEMENTARY NOTES

19. KEY WORDS (Continue on reverse side if necessary and identify by block number)

Acoustic Emission, Nondestructive Testing, Aircraft Structure, Fatigue Crack Detection, Structural Monitoring System, Fractographic Analysis

20. ABSTRACT (Continue on reverse side if necessary and identify by block number)

This final report describes work accomplished, under USAF contract, whose objective was to evaluate the ability of acoustic emission techniques to detect crack growth in a large full-production aircraft wing fatigue test article subjected to simulated flight spectra. Fatigue cracks were propagated at seventeen selected pre-damaged fastener holes in eight test areas on the test article. The flight load spectra consisted of fifty variable tension-tension gust cycles followed by 1/2 of a compressive ground cycle. Sixteen of the fastener holes were monitored with a 32-channel acoustic emission flaw locator system containing a

DD FORM 1 JAN 73 1473 EDITION OF 1 NOV 65 IS OBSOLETE

UNCLASSIFIED

SECURITY CLASSIFICATION OF THIS PAGE (When Data Entered)

DDC REPRODUCED JUN 28 1977 DISSEMINATION C

410 259

20. Abstract (continued)

computer, CRT monitor, input/output teleprinter console and tape recorder. Linear and triangular sensor arrays were used to detect and locate cracks. Twelve fatigue cracks were detected at fifteen fastener holes monitored where crack growth occurred. Acoustic emission data were correlated to crack growth data, determined through fractographic analysis, for several of the test cracks. Complex structural features which were accommodated successfully for detection of AE across joints are described.

SUMMARY

This program was conducted to evaluate the ability of Acoustic Emission (AE) techniques to detect crack growth in the structure of a full-size aircraft wing fatigue test article during simulated flight loading spectra. Some technique variations were developed to accommodate features which are characteristic of aircraft wing structure. The events leading up to the program provide some insight into the significance of the effort. In 1973, crack growth was monitored in relatively simple structural specimens without the necessity of acoustically isolating the specimen from either the loading machine or the shop environment (Ref. 1). At that time, very little was known about the background noise level in aircraft structure in the signal-level range and frequency range in which subcritical crack growth is detectable. In 1974, the structure-borne background noise was measured (Ref. 2) during flight on a C-5 cargo airplane. The results showed that the constant level of noise in the frequency range above 500 KHz was low enough in flight to permit detection of crack growth. The next step was to demonstrate that crack growth can be monitored in production-size aircraft structure. About this time the Air Force C-5 System Project Office (SPO) began negotiations to initiate the program: "Crack Propagation Testing on the Expedited Wing Fatigue Test Article (X993)". This provided a unique opportunity for monitoring crack growth in several locations on a full-size aircraft wing test article. (Usually, if a crack is located, the damage is repaired prior to additional testing.) This program provided the test article, fatigue cycling conditions, and visual crack monitoring necessary for developing correlations with AE data. After very detail planning, the AE program was conducted in "piggyback" fashion on the C-5 SPO Crack Propagation Program.

Work on the AE Monitoring program was commenced in late May 1975. The program schedule was planned to coincide with the C-5 SPO funded program conducted to study crack propagation under simulated flight-by-flight load spectra. Under the latter program, 2000 simulated flights plus 100 identical "precrack" flights were applied to the C-5A Expedited Wing Fatigue Test Article (X993) and crack growth in eight test areas on the specimen right wing were visually monitored. Each test area contained at least one test hole which had either a sharp-notched sawcut or a fatigue crack as an initial condition. There were a total of 17 test holes, five having initial fatigue cracks. The 100 "precrack" flights were begun on 18 June 1975. The first test flight was applied on 25 June 1975 and the 2000th test flight was completed on 8 January 1976.

The acoustic emission system used in this program was a commercial 32-channel AE flaw locator system which uses triangulation techniques to detect and locate AE sources. Linear and triangular arrays are simultaneously usable with the system. The system computes source coordinates, threshold crossing counts, time of arrival differentials; displays and prints out AE event data in real time; records AE threshold, and the sensor array size and location are variable. Two calibration techniques were used to set up and functionally check the system and to determine source locations in the structure.

The AE flaw locator system was installed to monitor eight areas on the test article. Seven of the test areas were instrumented. The eighth area, not containing test holes or known cracks, was located on the outer wing to serve as an AE noise baseline test area. Calibrations were performed in each monitored test area to determine accuracy of source location and to establish operating gains for the AE system. Array sizes ranged from 8 inches between transducers to as large as 48 inches. These dimensions approached the smallest and largest arrays useable on the C-5A wing. Arrays were successfully used across wing panel and web-to-cap joints assembled with fasteners and fay-surface sealant. Acoustic emission detection capabilities proved good in a wide variety of structural applications.

Acoustic emission from crack growth was detected at 12 of the 15 test holes which were monitored and where crack growth actually occurred. Material containing one crack was removed after flight 1200 and a fractographic analysis was made on the crack surfaces. A very good correlation was made between the acoustic emission and fractographic data, showing a linear relationship between AE rate and crack growth rates. Material containing the test holes from the other test areas was removed following all load tests and fractographic analyses were conducted. Additional correlations between AE and crack growth were made on three test holes.

The program "AE Monitoring of Crack Propagation on the Expedited Wing Fatigue Test Article" was successful. Crack propagation was monitored in many different locations and operational parameters for various structural configurations were developed. Cracks in obscure locations such as under large splice plates, at bolt holes in the faying surfaces of joints and under fastener heads were located and the crack growth monitored. We at Lockheed consider these developments sufficient evidence to demonstrate that the second major milestone in the effort to adapt AE to service aircraft has been achieved. This is not intended to imply that all problems have been solved, but we believe that a firm technology base now exists to warrant initiating a program effort to demonstrate that AE techniques can be used to detect and monitor crack growth on an aircraft in flight.

FOREWORD

This is the final report on the "Acoustic Emission Monitoring of Crack Propagation on the Expedited Wing Fatigue Test Article (X993)" Program. The work was funded by the Air Force Materials Laboratory, Air Force Wright Aeronautical Laboratories (AFSC), and was monitored by the Air Force Materials Laboratory under Contract No. F33615-75-C-5249 (Project No. 7351). Captain William J. Jacques (AFML/LLP) was the Program Monitor. The program was performed from 15 May 1975 through 29 October 1976. Major efforts of the program included installation of the acoustic emission system for monitoring the X993 Wing Fatigue Test Article, monitoring the test article through 2100 test flights, and analyzing and correlating the data.

This program was conducted concurrently with a separate program under Contract AF33(657)-15053, Change Order P00972 (dated 6 January 1975) titled "Crack Propagation Testing on the Expedited Wing Fatigue Test Article (X993)", which was funded by the C-5A SPO and which provided the test article and flight-by-flight loads. Exchange of test data between the two programs was accomplished through a cooperative arrangement. Fractographic analyses were made of cracks in test areas on the C-5A SPO Program and the results were available to the ASD/AFML program.

Both programs were conducted at the Lockheed-Georgia Company, Air Force Plant 6, Marietta, Georgia. Mr. C. D. Bailey was the Program Manager for the Acoustic Emission program. Messrs. W. M. Pless and J. M. Hamilton conducted a major part of the acoustic emission test work, and Mr. Hamilton had the additional responsibility of performing the analysis of the AE test data. Messrs. Bailey and Pless assisted in the correlation of AE data with crack growth data. Mr. D. M. Anderson of the Metallurgical Group performed the fractographic analyses of the fatigue crack surfaces from the test article.

This final report is issued under the Lockheed internal No. LG77ER-0042.

TABLE OF CONTENTS

SECTION		PAGE
I	Background	1
II	Program Objectives and Approach	2
III	Discussion	3
	3.1 Experimental Approach	3
	3.1.1 Test Article Description and Test Areas	3
	3.1.2 Test Loads	3
	3.1.3 Acoustic Emission Equipment	7
	3.1.4 AE Sensor Arrays	7
	A. Configurations and Installation	7
	B. Triangular Array Characteristics	12
	C. Program Array Configuration & Modification	14
	3.1.5 Transducer Calibration	14
	3.1.6 AE System Calibration	14
	3.1.7 Admiralty Materials Laboratory AE System	16
	3.1.8 Special Tests	16
	A. AE Sensitivity Tests	16
	B. Acoustic Attenuation in Structure	18
	C. Time Delay Across a Joint	20
	D. Transducer Resonances	20
	3.2 Experimental Results	23
	3.2.1 Summary of Program Data and Data Analysis Procedures	23
	A. Program Data	23
	B. Analysis Procedure	23
	3.2.2 System Operating Parameters	24
	3.2.3 Discussion of Crack Propagation Results	27
	A. Crack Propagation Summary and Analysis Method	27
	B. Fractographic Analysis of Test Crack Surfaces	27
	C. Examination of Non-Test Areas	29

SECTION		PAGE
	3.2.4 Discussion of Acoustic Emission Results	30
	3.2.5 Correlations of AE with Crack Growth	34
	A. General	34
	B. Detection	34
	C. Correlation to Crack Growth Data	36
	3.2.6 Source Detectability	45
IV	Conclusions	46
V	Recommendations	48
	APPENDIX A	51
	APPENDIX B	53
	APPENDIX C	56
	APPENDIX D	60
	APPENDIX E	84
	APPENDIX F	86
	APPENDIX G	102
	APPENDIX H	105
	APPENDIX I	110
	References	115

LIST OF ILLUSTRATIONS

FIGURE		PAGE
1	C-5A X993 Expedited Wing Fatigue Test Article	4
2	View of X993 Right Wing Inner Wing Box, Rear Beam	5
3	Test Areas and Array Locations on the X993 Wing Fatigue Test Article	6
4	X993 Unit Flight Load Spectrum	8
5	Block Diagram of AE Source Location System	9
6	Console and Data Terminal for the 32-Channel AE Source Location System	10
7	Time Relationships for the Linear and Triangular Arrays	11
8	Error Relationships for the Triangular Array	13
9	AML Transducer Installations	17
10	Ringdown Counts Exceeding Threshold Versus System Gain	19
11	Oscilloscope Traces of Transducer Outputs from which Resonant Frequencies were Computed	21
12	Section of Center Wing Removed to Investigate Presence of Suspected Crack	31
13	Section of Outer Wing Removed to Investigate Presence of Suspected Crack	31
14	Portion of Structure from Test Area 4 Containing Crack Suspect Areas 4A and 4B	32
15	Portion of Structure from AE Test Area 9 Containing Crack Suspect Area 9A	33
16	Crack Growth History of Crack 'N'	38
17	Correlation of AE with SEM View of Crack 'N' Surface	39
18	AE Versus Time for Crack N at Flights 791-800	41
19	Amplitude of AE Signals During Flights 791 and 792	43
20	Comparison of Crack Length and AE Versus Test Flights for Test Crack 4H	44
21	Comparison of Crack Length and AE Versus Test Flights for Test Crack 5J	44

LIST OF ILLUSTRATIONS (Continued)

FIGURE		PAGE
	APPENDIX C	
C1	Acoustic Emission Array Data as Programmed into the System	57
C2	Acoustic Emission Array Data Format	58
C3	Examples of the Post Test Analysis Program Input Data Formats	59
	APPENDIX D	
D1	Test Area 1, Array 0/1, Test Holes A, B and C	63
D2	Test Area 2, Array 1/2, Test Holes D, E, O, P, & Q	64
D3	Test Area 2, Array 7/2, Test Holes D and E	65
D4	Test Area 3, Array 2/3, Test Holes F and G	66
D5	Test Area 4, Array 4/4, Test Hole H	67
D6	Test Area 5, Array 3/5, Test Holes I, J and K	68
D7	Test Area 6, Array 5/6, Test Hole L	69
D8	Test Area 8, Array 7/8, Test Hole N	69
D9	Test Area 9, Array 6/9, No Known Cracks	70
D10	View of Triangular Array 0 in Test Area 1 (Flts 1201-1400)	71
D11	View of Triangular Array 0 in Test Area 1 (Flts 801-1200)	72
D12	View of Triangular Array 1 in Test Area 2 (Flts 401-1200)	73
D13	Split View of Triangular Array 1 in Test Area 2 (Flts 1201-2000)	74
D14	View of Triangular Array 7 in Test Area 2	75
D15	View of Triangular and Linear Array 2 in Test Area 3 (All Flts)	76
D16	View of Triangular Array 4 in Test Area 4 (Flts 141-1200)	77
D17	View of Triangular Array 4 in Test Area 4 (Flts 1201-2000)	78
D18	View of Triangular Array 3 in Test Area 5 (Flts thru 1200)	79

LIST OF ILLUSTRATIONS (Continued)

FIGURE		PAGE
D19	View of Triangular Array 3 in Test Area 5 (Flts 1201-2000)	80
D20	View of Triangular Array 5 in Test Area 6 (Flts 437-2000)	81
D21	View of Triangular Array 7 in Test Area 8 (Flts thru 1200)	82
D22	View of Triangular Array 6 in AE Baseline Area 9 (Flts 801-2000)	83
	APPENDIX F	
F1	Conditions at Test Holes A, B, and C in Test Area 1	89
F2	Conditions at Test Holes D and E and O, P, and Q in Test Area 2	90
F3	Conditions at Test Holes F and G in Test Area 3	91
F4	Conditions at Test Hole H in Test Area 4	92
F5	Conditions at Test Holes I, J and K in Test Area 5	93
F6	Conditions at Test Hole L in Test Area 6	94
F7	Conditions at Test Hole N in Test Area 8	95
F8	Crack Growth versus Cumulative Test Flights	96
F9	Photomacrographs of Test Crack Surfaces	99
	APPENDIX H	
H1	AE Representations from Test Area 1	106
H2	AE Representations from Test Area 2	106
H3	AE Representations from Test Area 2	107
H4	AE Representations from Test Area 3	107
H5	AE Representations from Test Area 5	108
H6	AE Representations from Test Area 4	108
H7	AE Representations from Test Area 6	109
H8	AE Representations from Test Area 8	109
	APPENDIX I	
	Accumulative AE Events Versus Test Flights for Four Test Cracks	114

LIST OF TABLES

TABLE		PAGE
1	Acoustic Emission Array Configurations and Modifications	15
2	Typical Acoustic Emission Transducer Operating Resonances	22
3	Summary of X993 Crack Propagation and AE Program Test Areas	28
4	Summary of Relative AE Activity	35
G1	Visual Crack Measurements	104
I1	Appendix I. Cumulative AE Events for X993 Test Cracks and AE Sources	113

SECTION I

BACKGROUND

The assurance of structural integrity is a major requirement of the service life maintenance procedures for military aircraft. This generates requirements for reliable and cost effective nondestructive test (NDT) techniques for detecting small fatigue cracks. Such cracks usually originate in obscure locations such as under fastener heads and in the faying surfaces of lap joints. Techniques currently being used, such as X-ray, eddy current, and ultrasonics are not entirely satisfactory in terms of the large number of manhours required to search for the cracks and the aircraft down-time that make these techniques very costly for large aircraft. Reliability of these techniques can be poor. Clearly, a significant advancement in NDT techniques is needed.

The Acoustic Emission (AE) technique has demonstrated potential to help fulfill this need. Acoustic emission flaw location techniques have been used to locate crack extensions and monitor crack growth in aircraft structural test specimens during flight-by-flight spectrum loading (Reference 1). This was accomplished without acoustically isolating the specimen from the loading mechanism or the noisy shop environment. Also, acoustic emission structure-borne noise measurements have been made on a C-5A aircraft during flight, (Contract No. F33(657)-74-C-0588 (Reference 2)). The results showed that above 500 KHz the structure-borne noise level is low enough for the AE signals from crack extension to be detected.

The current program was considered the next step in the long-term plan to develop an AE system for in-service aircraft applications. It was conducted to demonstrate that crack extensions can be detected in a full-size aircraft wing test specimen during cyclic loading conditions. The program is unique in that the resources necessary to conduct the program were available at a minimum cost and in the proper time frame for conducting the program. It was conducted concurrently with a C-5A Special Project Office funded program, "Crack Propagation Testing on the Expedited Wing Fatigue Test Article (X993)". On the C-5A program, the test article was flight-by-flight loaded and crack propagation in eight areas was monitored visually and with conventional NDT techniques.

Initially, a 1200-flight (approximately 5000 cyclic test hours) program was planned. However, crack growth did not proceed in the test areas as anticipated and the test program was extended in 400 flight-by-flight increments to 2000 total flights. In addition, 100 "precrack" flights were applied to initiate the tests. Following the 2000 flights, a series of loadings were applied to the test article for residual strength studies, which contributed some growth to most test cracks, but these tests were not a part of the current program. Fractographic analysis was conducted on the fracture

surfaces at the completion of all tests. The acoustic emission program used the same test article and the results of the C-5A program were available for the evaluation of relationships between AE event data, crack growth rates, fractographic data, and cyclic loading conditions. Likewise, the results of the AE program were available to the C-5A crack propagation testing program for real-time crack growth surveillance.

SECTION II

PROGRAM OBJECTIVE AND APPROACH

The objective of this program was to determine the Acoustic Emission operating parameters necessary to locate small fatigue cracks and monitor crack extensions in various structural members on a full-size C-5A aircraft wing test article. A secondary objective was to identify characteristics of an acoustic emission flaw locator system suitable for in-flight structural monitoring.

This program is an integral part of a larger effort to develop an airborne monitoring system using acoustic emission to detect cracks on aircraft. The approach was to conduct the acoustic emission program concurrently and cooperatively with a C-5A SPO funded crack propagation program using the C-5A expedited wing fatigue test article (X993). Under the C-5A SPO program, the test article was flight-by-flight loaded to produce crack propagation in eight selected test areas. The test areas were monitored visually for crack growth and inspected by NDT methods. Seven of the areas were monitored with an acoustic emission (AE) crack locator system throughout most of the applied flights and the AE data recorded on magnetic tape. Upon completion of load testing, the AE data were analyzed and correlated or compared to the crack growth data as determined by fractographic analysis.

SECTION III

TECHNICAL DISCUSSION

3.1 EXPERIMENTAL APPROACH

3.1.1 Test Article Description and Test Areas

Test Article. The acoustic emission program was conducted concurrently with and used the same test article as the C-5 SPO funded program, "Crack Propagation Testing on Expedited Wing Fatigue Test Article (X993)". The test article is a full-scale C-5A wing previously tested to 2.0 lifetimes in the C-5A Expedited Wing Fatigue Tests. The condition of the test article following the expedited fatigue tests is fully described in Reference 3, which presents the baseline configuration for the acoustic emission and crack propagation programs.

The test article is illustrated by the sketch in Figure 1, except that it does not have the leading and trailing edge structures attached as illustrated. It consists of a mid-fuselage section, left-hand inner-wing box, center wing box, right-hand wing box and right-hand outer wing box in the full production structure configuration. The test article did not contain the electrical, hydraulic and mechanical systems of a flight-configured aircraft. These systems are known to produce EMI, cavitation and mechanical noise in a flying aircraft. The wing boxes, though fay-surface sealed, did not contain fuel tank sealer and, of course, did not contain fuel - conditions which have been found to affect sound transmissibility in the structure. Only the right-hand wing was involved in the crack growth study. The right-hand inner wing is shown in Figure 2 with the rear beam exposed.

Test Areas. In the crack propagation study program, eight areas on the right inner wing were selected in which to initiate and propagate fatigue cracks. The eight areas initially contcined, in toto, five existing fatigue cracks and 12 artificial flaws (sharp-notched sawcuts). The locations of these areas on the wing are shown in Figure 3, including the seven test areas monitored in the acoustic emission program. One additional area on the outer wing lower surface containing no known flaws was selected to be monitored as a baseline area. A description of each area is presented in Appendix A.

3.1.2 Test Loads

The test article was flight-by-flight loaded to 2000 identical test flights to propagate fatigue cracks in the eight test areas. Prior to beginning the test unit flights, 100 pre-crack unit flights (identical to the test flights) were applied to initiate crack growth in the test holes having sawcut flaws. Loads were applied to the wing by means of hydraulic jacks and whipple-tree/pad arrangements applied to upper and lower surfaces along the entire span of the wing. These can be seen to some extent in Figure 2.

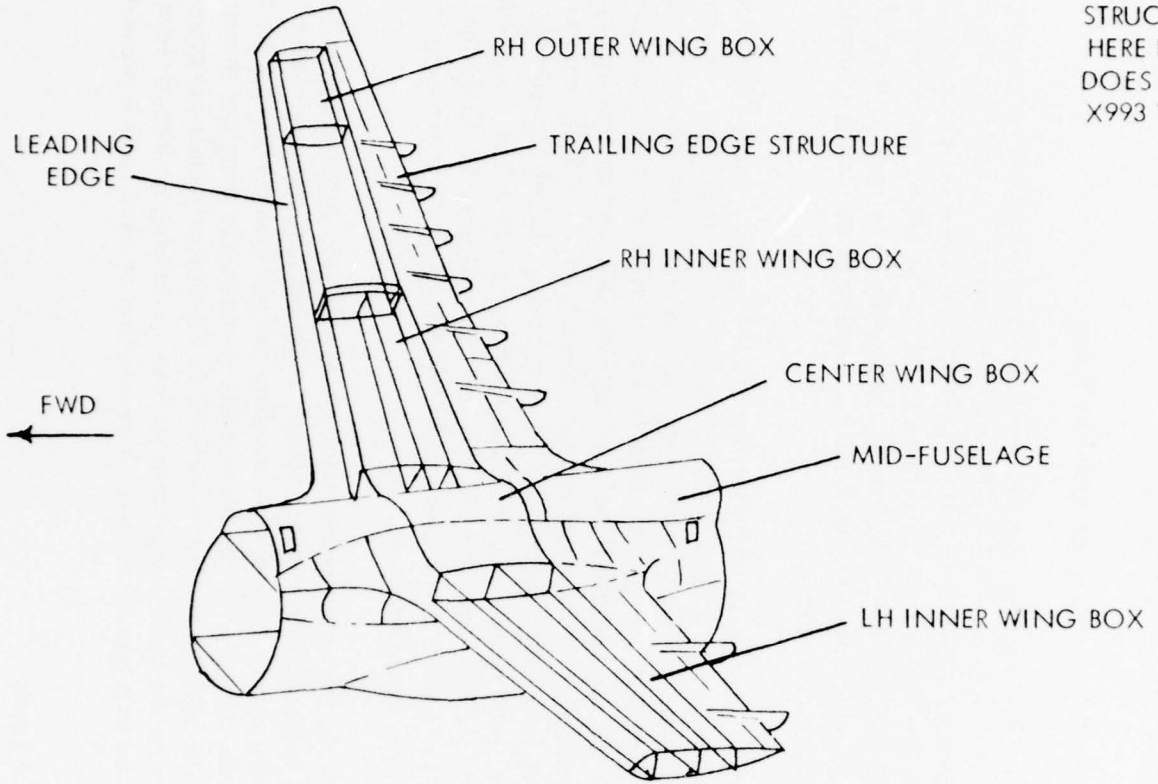

FIGURE 1. C-5A X993 EXPEDITED WING FATIGUE TEST ARTICLE

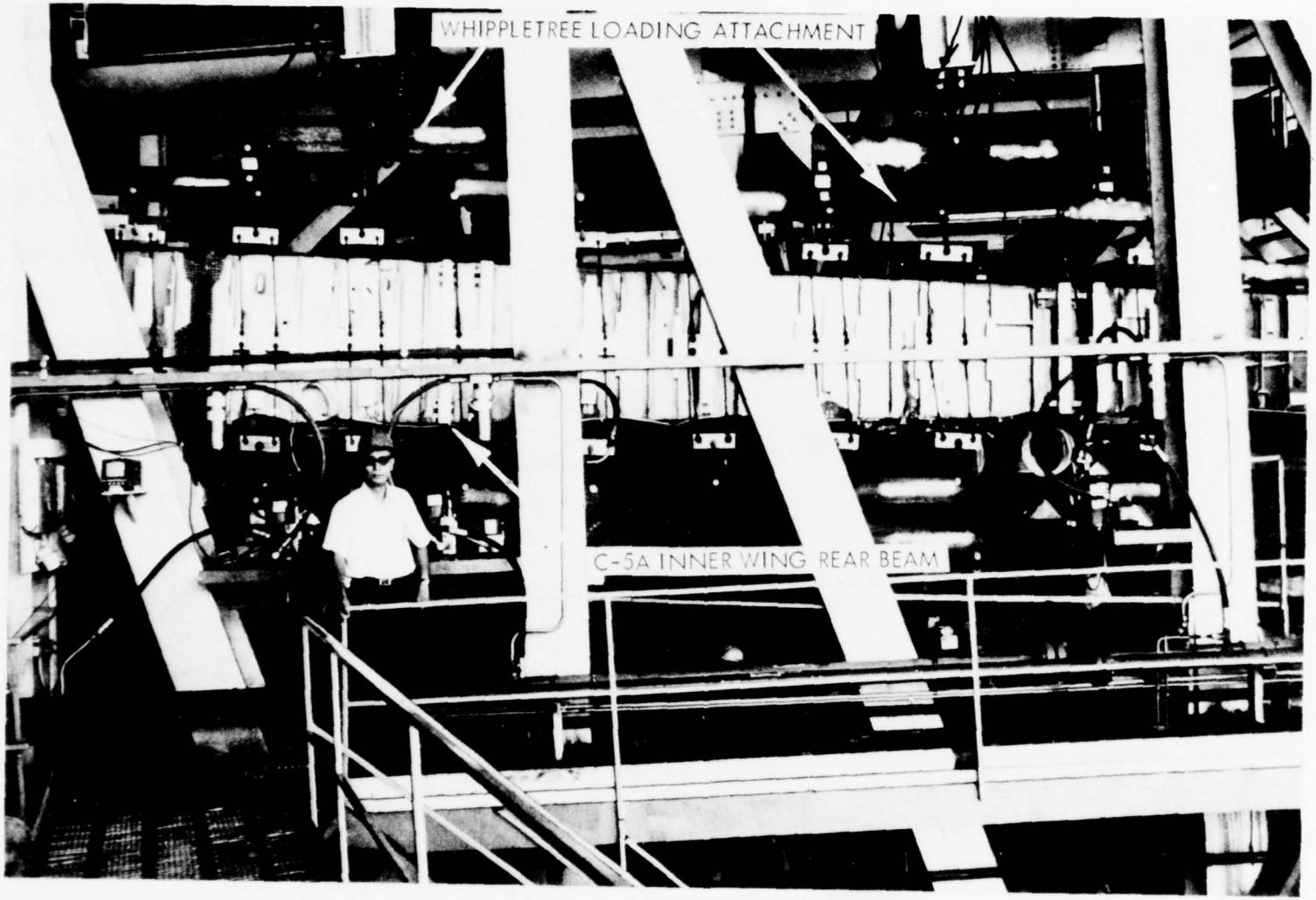

FIGURE 2. VIEW OF X993 RIGHT WING INNER WING BOX, REAR BEAM

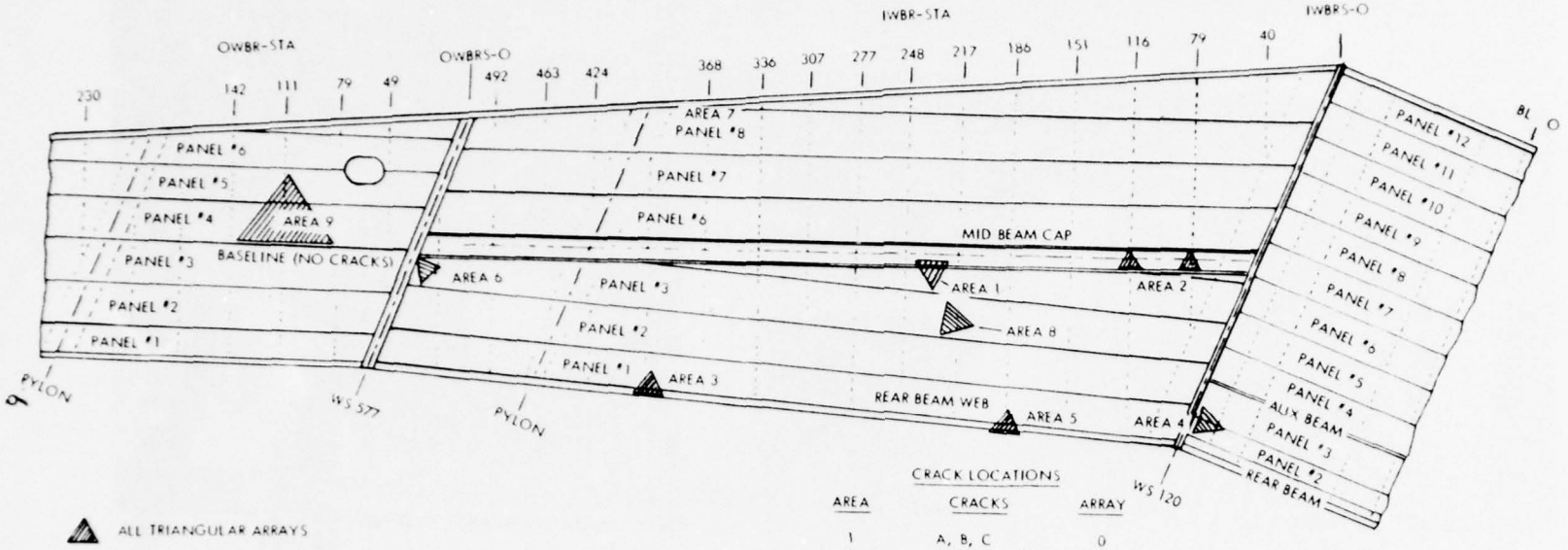

ALL TRIANGULAR ARRAYS

X993 WING LOWER SURFACE
RIGHT SIDE VIEW LOOKING UP

CRACK LOCATIONS

AREA	CRACKS	ARRAY
1	A, B, C	0
2	D, E; O, P, Q	1, 7
3	F, G	2
4	H	4
5	I, J, K	3
6	L	5
7	M	--
8	N (REMOVED)	--
9	NONE	6

REVISED 2 OCTOBER 1975

FIGURE 3. TEST AREAS AND ARRAY LOCATIONS ON X993 (CONFIGURATION FOR TEST FLIGHTS 801 THROUGH 1600)

The simulated flight spectrum is described by the diagram in Figure 4. The unit flight spectrum contains a total of 50 flight cycles and 0.5 ground (down bending) cycles. The flight cycles are divided into five groups of increasingly greater tension-tension loads varying about a constant mean load. Variable sets of marker loads (Reference 5) were applied at time zero and after every 100 unit test flights. The marker loads were of constant maximum amplitude varying between the upper and lower limits of the simulated flight spectrum envelope. The purpose of the marker loads were to produce "landmark" striations among fatigue crack growth striations for distinguishing the crack growth increments occurring between each block of 100 flights. It should be noted that the 225 total marker loads contributed to crack growth although these contributions were not defined in the fractographic analyses. During the later discussions of crack growth, the contributions from the markers will, therefore, not be mentioned.

3.1.3 Acoustic Emission Equipment

A commercially-available 32-Channel Acoustic Emission Source Location System* was used in the detection, processing, recording and analysis of acoustic emission events. This system is capable of simultaneously monitoring a maximum of eight arrays, with two or four transducers in each array; accepting input data at a rate of more than 3000 events per second; and processing data sets at a rate of approximately 100 points per second. A block diagram is shown in Figure 5 and a photograph of the console is shown in Figure 6. The transducers and basic components of the system are described in Appendix B.

Dunegan/Endevco S750 and D9202 transducers were used as sensors. Their outputs were fed into 40-db gain preamplifiers which were connected to the AE console through 100-ft. signal cables. Additional gain variable from 0 to 60 decibels was available in the console. The system computer determined time of arrival differentials between array transducers and provided AE event data to a CRT monitor, to the teleprinter and to the magnetic tape recorder - all components of the AE system.

3.1.4 AE Sensor Arrays

A. Configurations and Installation. Two array configurations are possible with the system used with the supplied software program. One is a 2-transducer linear configuration and the second is a 3-transducer equilateral triangle configuration with a 4th transducer located in the center of the triangle. These are illustrated in Figure 7. The linear array is useful where all potential flaw sites lie along a straight-line path. The system displays all signals as though the sources lay on that line. The linear array displays the source according to the time difference in arrival of the signal at the two transducers.

*Model 1032, Dunegan/Endevco, San Juan Capistrano, Calif.

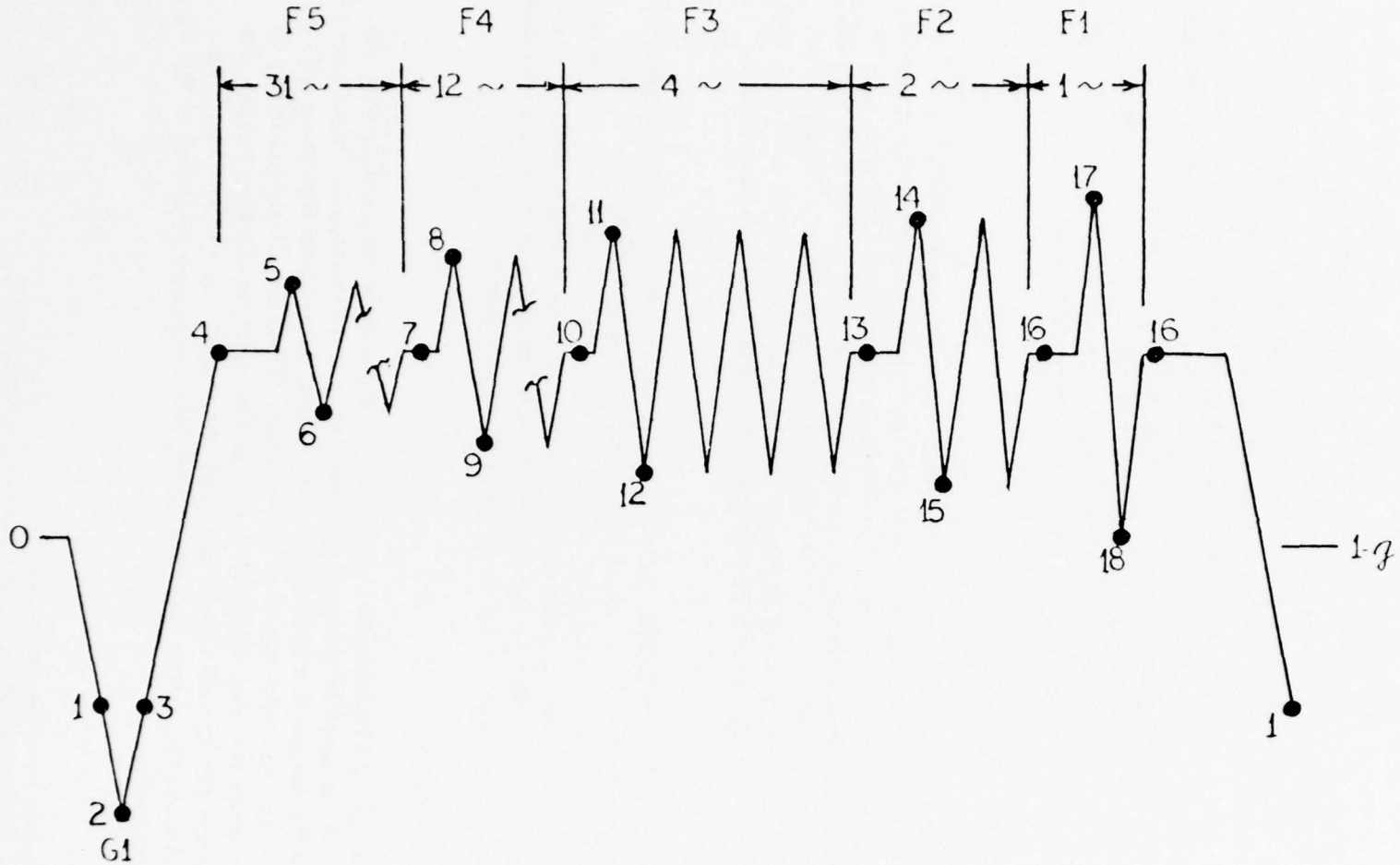

FIGURE 4. X993 UNIT FLIGHT LOAD SPECTRUM

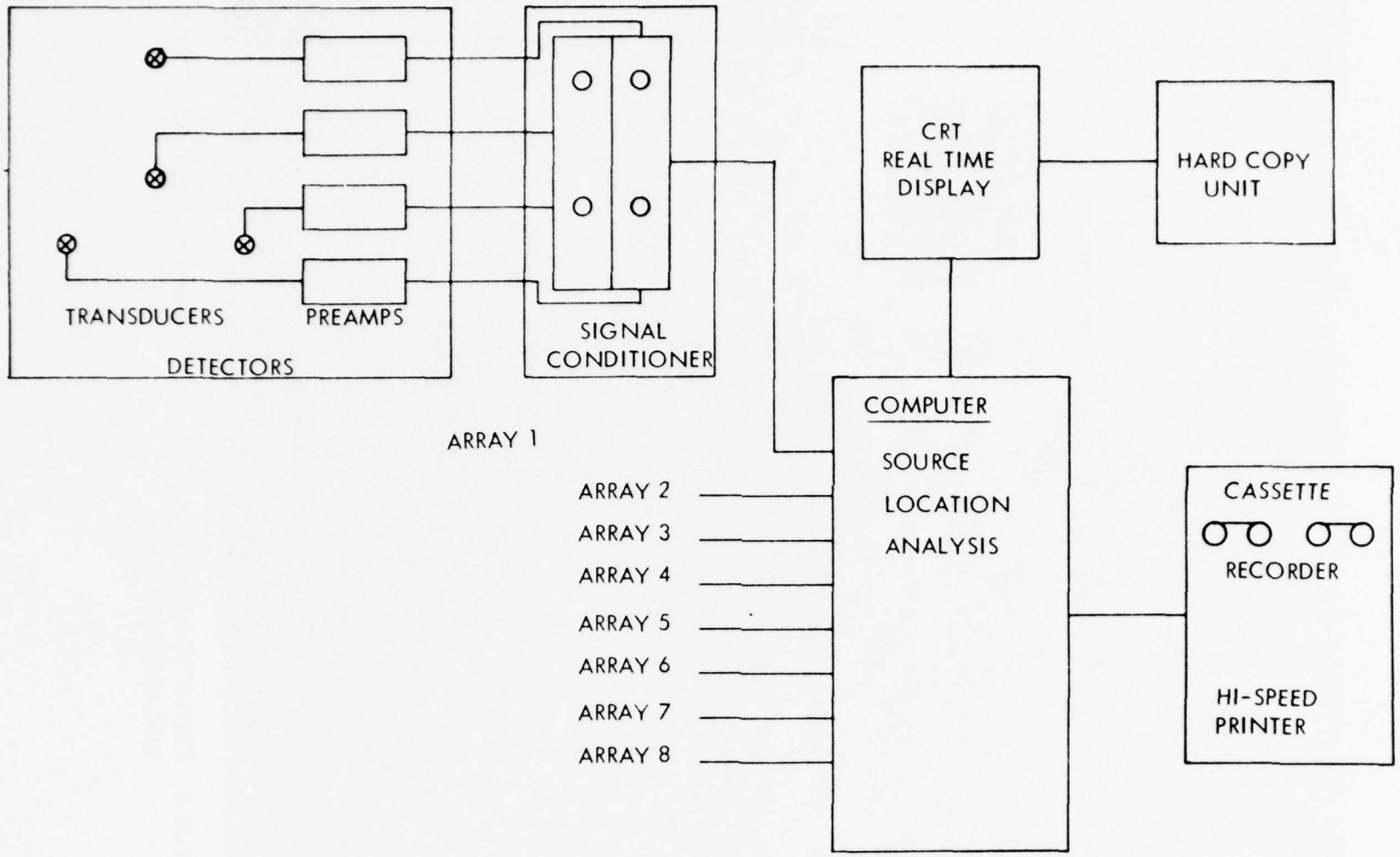

FIGURE 5. BLOCK DIAGRAM OF AE SOURCE LOCATION SYSTEM

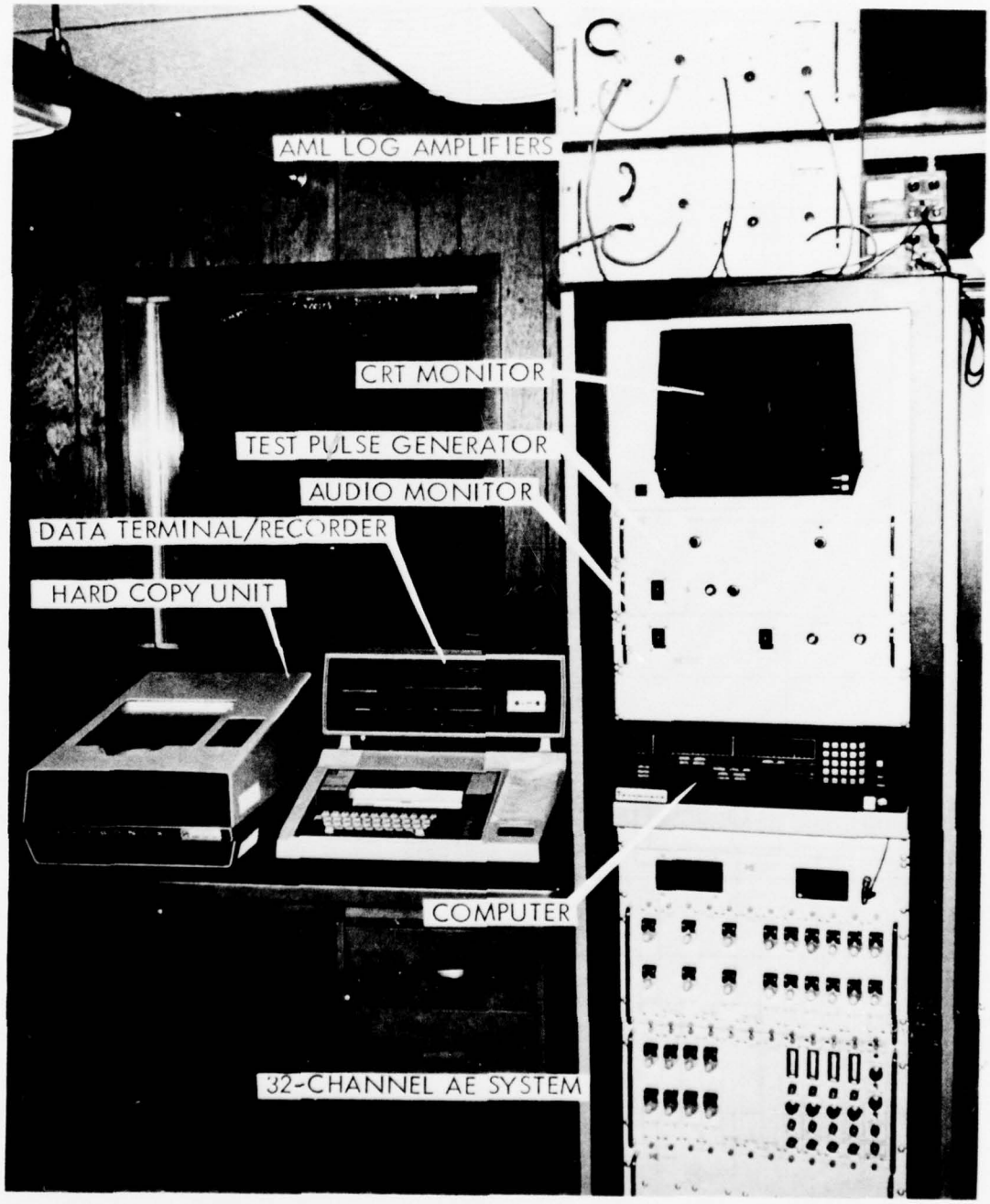

FIGURE 6. CONSOLE AND DATA TERMINAL FOR 32-CHANNEL AE SOURCE LOCATION SYSTEM

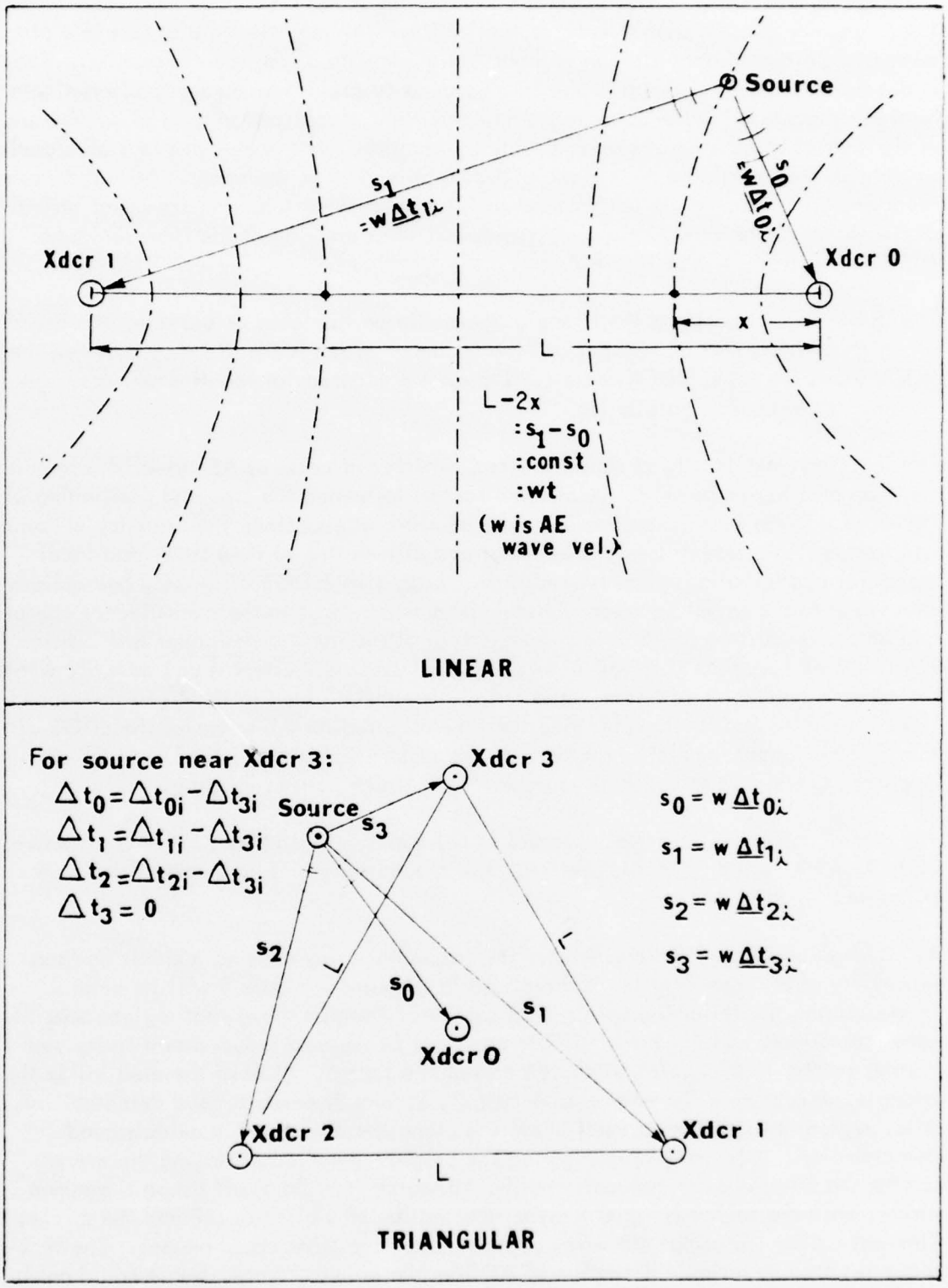

FIGURE 7. TIME RELATIONSHIPS FOR THE LINEAR AND TRIANGULAR ARRAYS

The triangular array is useful where potential flaw sites may lie more or less in a plane or can be projected onto a plane without losing identity of the source location. The 2-dimensional characteristics of the triangular array provides a means to discriminate between random structure-borne noise and persistent, localized sources of AE because of the spatial allocation of signal display information. The system displays all signals as through they originate on a plane, i.e., a plan view of the array. All valid source locations are displayed in accordance with the respective time differences of arrival of the signal of the three remaining transducers after arriving at the first transducer (XDCR), as illustrated in Figure 7.

The three XDCR's defining the triangle apexes lie on the locus of a circle, the center of which is the center of XDCR 0 and the radius of which is the distance between the XDCR 0 and the other XDCR centers. The system accuracy at locating sources is greater within the circle than outside it.

The locations and density of signal sources, whether of noise or AE, usually determines the type of array to be used. Additional factors influence the size and positioning of the array. These factors include structure acoustic attenuation, the presence of joints and fastener attachment areas, the number and distribution of flaw sites, and local structural configuration. The type of array, array size (EDGE distance), and calibration value (wave travel between transducers) must be input to the computer for operation and proper processing of AE data. An example of the input data format is shown in Figure C1 of Appendix C for all arrays. In the first line, letters A or L identify whether the array is triangular or linear. The EDGE distance is given in inches in the second line. The third and fourth lines give the time required for AE to travel the EDGE distance. The format for typing the data on the system teleprinter is in Figure C2 of Appendix C which also contains explanations for each column heading.

The transducers were adhesively bonded to the structure with Hysol EA 9421 adhesive, Parts A and B, which is a quick setting, low shear strength, room temperature cure adhesive.

B. Triangular Array Characteristics. The triangular array does not exhibit uniform sensitivity or detectability in all directions in its plane. Figure 8 will be helpful in visualizing the following points of discussion. Analysis shows that regions near the apex transducers will not have reliable coverage because of reduced sensitivity and greater scatter in triangulation coordinates of the source. Most of the area inside the triangle, except near the apex transducers (1, 2, and 3) exhibits good detectability. Also, regions outside the triangle bordering along the bisectors $\overline{OP}$ exhibit good detectability. A technique used during the program involved arranging the array so that the three apex transducers and the AE source (test hole) all lie on a common circle, with the source lying at P - the intersection of a bisector $\overline{OP}$ and the circle. This was called "rotating" the array so that these conditions could be met. The technique resulted in reliable detection of AE from the growing crack, but it could not be applied in every test area because of structural limitations or the presence of multiple test holes in the test area.

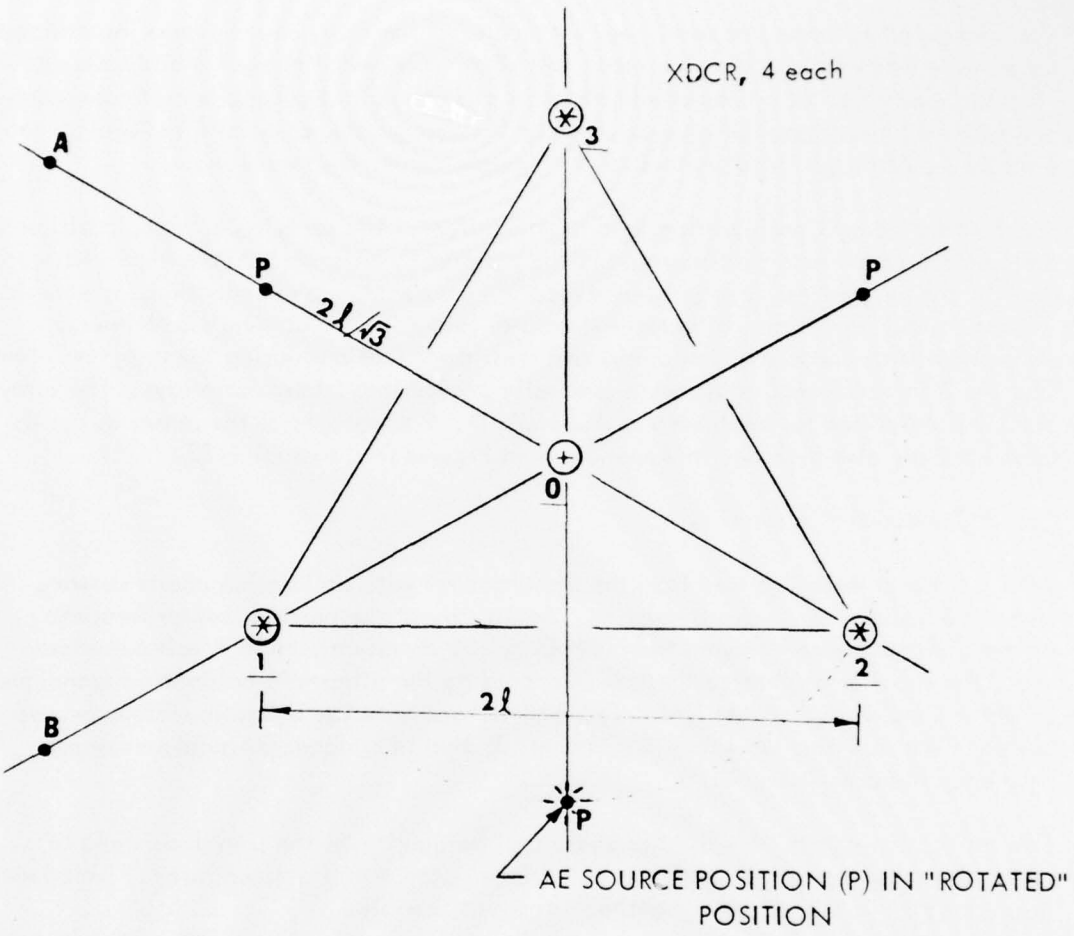

DIMENSIONAL RELATIONSHIP:

$\underline{(1,2)} = \underline{(1,3)} = \underline{(2,3)} = 2\ell$

LOCATIONAL ERROR RELATIONSHIPS:

- ERROR IS MINIMUM NEAR XDCR 0.
- WHEN $\overline{OA} = \overline{OB} = 2\ell$, ERROR $\delta t_B = 1.67 \cdot \delta t_A$
- ALSO, ERROR $\delta t_p < \delta t_A < \delta t_B$

FIGURE 8. ERROR RELATIONSHIPS FOR THE TRIANGULAR ARRAY

The triangulation errors are small near the center of the array, but become increasingly large away from the center. The errors are also larger near the apex transducers and "behind" them than at a comparable distance at some point between apex transducers. For example, the triangulation error is sixty percent greater at point B in Figure 8 than at point A, although the distances to the triangle center are the same.

C. Program Array Configurations and Modifications. The array type, size, positioning and configuration were modified during the program in order to achieve improved source display characteristics, greater source location assurance, noise reduction, or experimentation with the effects of various structural features such as wing panel joints. Table I gives the history of the arrays and their modifications during the program. Note that the 5 initial linear arrays were gradually phased into triangular arrays. The array history is described for each area in Appendix D. Photographs of the sensor arrays in each area are also included in Appendix D in Figures D10 through D22.

3.1.5 Transducer Calibration

All transducers were supplied from the manufacturer with calibration charts showing transducer sensitivity versus frequency. Sensitivity at the nominal center frequency of the S750 transducers ranged from -76 db to -80 db referenced to 1 volt per microbar. The supplier calibrated the transducers using the ultrasonic calibration technique in which a pulser transducer is coupled face to face with the unknown transducer and pulsed. The resulting waveform is compared to that of a standard transducer whose frequency response is known.

The calibration charts were used to evalutate the quality of the transducers and to select those having similar responses to be incorporated into a given array. Transducers in an array were, therefore, "matched" as far as possible.

A technique having some similarities was used during the program to test the response of a transducer any time it was in question. The output of the transducer was viewed on a CRT to determine the relative sensitivity of the transducer. The D9202 transducers were calibrated by the supplier using the spark bar method of calibration. The sensitivity ranges of these transducers were the same as the S750 units.

3.1.6 AE System Calibration

In-Situ Calibration and Functional Checks - Two methods were used during the program to provide calibration and functional checks on the system. One method used an S750 transducer bonded on the structure within or near each array to transmit single or multiple acoustic pulses into the structure. When working properly, each transducer of the array senses the test pulses and the system computes the source location coordinates, counts the ringdown pulses, and stores the relevant data in the minicomputer. The CRT monitor displays the array and pulser transducer relative locations and the printer types the arrival time differentials for each transducer, the source coordinates, ringdown counts, and computer time for functional verification. On the basis of these data, the system gain controls and software calibration values can be adjusted as necessary

TABLE I. ACOUSTIC EMISSION ARRAYS AND MODIFICATIONS

Area	Test Holes	Array No.	Type XDCR	(Size - Inches) Type of Array	Flights	Remarks
1	A, B, C	0	S750	(20) Linear	Precrack 1 - T-Flt 800	Installed Inside Wing Box
			S750	(15) Triangular	T-Flt 801 - 1200	Installed Outside Wing Box
			S750	(18.5) Triangular	T-Flt 1201 - 1400	Wing Panel Splice Included, Outside
2	D, E, O, P, Q	1	S750	(39) Linear	Precrack 1 - 100	Installed on Cap, Inside Wing Box
	D, E, O, P, Q		S750	(15) Triangular	T-Flt 1 - 400	Installed on Web, Inside
	O, P, Q		D9202	(17) Triangular	T-Flt 401 - 1200	Installed on Web, Inside
	D, E		D9202	(15) Linear	T-Flt 550 - 1200	Installed on Cap, Inside
	O, P, Q		D9202	(10) Triangular	T-Flt 1201 - 2000	Installed on Cap, Inside
	D, E	7	D9202	(12) Triangular	T-Flt 1201 - 2000	Installed on Cap, Outside
3	F, G	2	S750	(20) Linear	Precrack 1 - T-Flt 800	Installed on Cap
			S750	(24) Triangular	T-Flt 801 - 2000	Cap - Panel Joint Included
			AML	(20) Linear	T-Flt 401 - 1600	AML System, Installed on Cap
4	H	4	S750	(9) Linear	Precrack 1 - T-Flt 140	
			S750	(8) Triangular	T-Flt 141 - 1200	
			S750	(15) Triangular	T-Flt 1201 - 2000	Wing Panel Splice Included
5	I, J, K	3	S750	(12.5) Triangular	Precrack 1 - T-Flt 400	
			D9202	(12) Triangular	T-Flt 401 - 1200	
			D9202	(12) Triangular	T-Flt 1201 - 2000	Beam Web-Cap Joint Included
6	L	5	S750	(15) Linear	Precrack 1 - T-Flt 100	
			S750	(14.5) Triangular	T-Flt 101 - 435	
			S750	(14.3) Triangular	T-Flt 437 - 2000	"Rotated" About Test Hole L
8	N	7	S750	(20) Triangular	Precrack 1 - T-Flt 437	
			S750	(13.5) Triangular	T-Flt 438 - 1200	"Rotated" About Test Hole N
9	None	6	S750	(20) Triangular	Precrack 1 - T-Flt 800	
				(48) Triangular	T-Flt 801 - 2000	Wing Panel Joint Included

to achieve desired operation. This method of calibration produces repetitive constant-amplitude pulses and tends to cause the S750 receiver transducers to resonant between 640 and 760 KHz (see Section 3.1.8(D)).

A second method of calibration involves a proprietary technique developed separately from this program. It provides a sharp rise-time acoustic pulse which is input at a very small point and closely simulates crack growth AE. The completely self-contained handheld unit provides only nonrepetitive single pulses whose amplitudes, like AE, are distributed statistically about a mean amplitude. This method tends to cause the S750 transducer to resonate at frequencies between 440 and 580 KHz (see Section 3.1.8(D)). The system adjustment routines are essentially the same as described for the previous method. These two methods have been used throughout most of the program to provide a reliable check on the calibration and functioning of the system, and to derive acoustic propagation data.

A third method was attempted but abandoned after a short trial period. It involved bonding a 1" x 1" x 4" cantilever-beam stress corrosion specimen to the structure and activating it with a salt-water solution. The chief advantage was that it produced real crack growth AE, but had the disadvantages that: it required bonding to the structure, its large contact area (1 sq. in.) prohibited high source location resolution, and the signals were random in time and amplitude and could not be caused to appear at the moment desired.

3.1.7 Admiralty Materials Laboratory AE System

The AE Instrumentation from Admiralty Materials Laboratory, England, was installed during the inspection period following the 400th unit flight and prior to start-up for flight 401. The system's logarithmic amplifiers are shown in Figure 6 atop the 1032 AE Flaw Locator cabinet. The AML transducers were installed on a 1-inch wide lip on the aft edge of the rear beam cap in Test Area 3 at inner wing box rib station 401, lower surface, as shown in Figure 9. The transducers were installed in parallel with the 2 transducers of linear array 3 of the 32-channel system. The signals from the AML transducers were input to the 32-channel system for approximately 100 unit flights out of each 400 flights to provide a basis for comparison.

The Admiralty Materials Laboratory systems consist of two 60 to 100 db variable gain logarithmic amplifiers, two 100-ft lengths of supershielded transmission cables, and two specially designed high-Q transducers. The signals from the AML amplifiers are routed into the primary 32-channel AE system and from there on the operation is identical to that described in Section 3.1.3. Since each AML amplifier can process only one transducer input, the system was operated as a linear array.

3.1.8 Special Tests

A. AE Sensitivity Tests. To determine the amplification needed to detect crack growth acoustic emission (AE) in 7075-T6511 aluminum alloy, a preflawed coupon

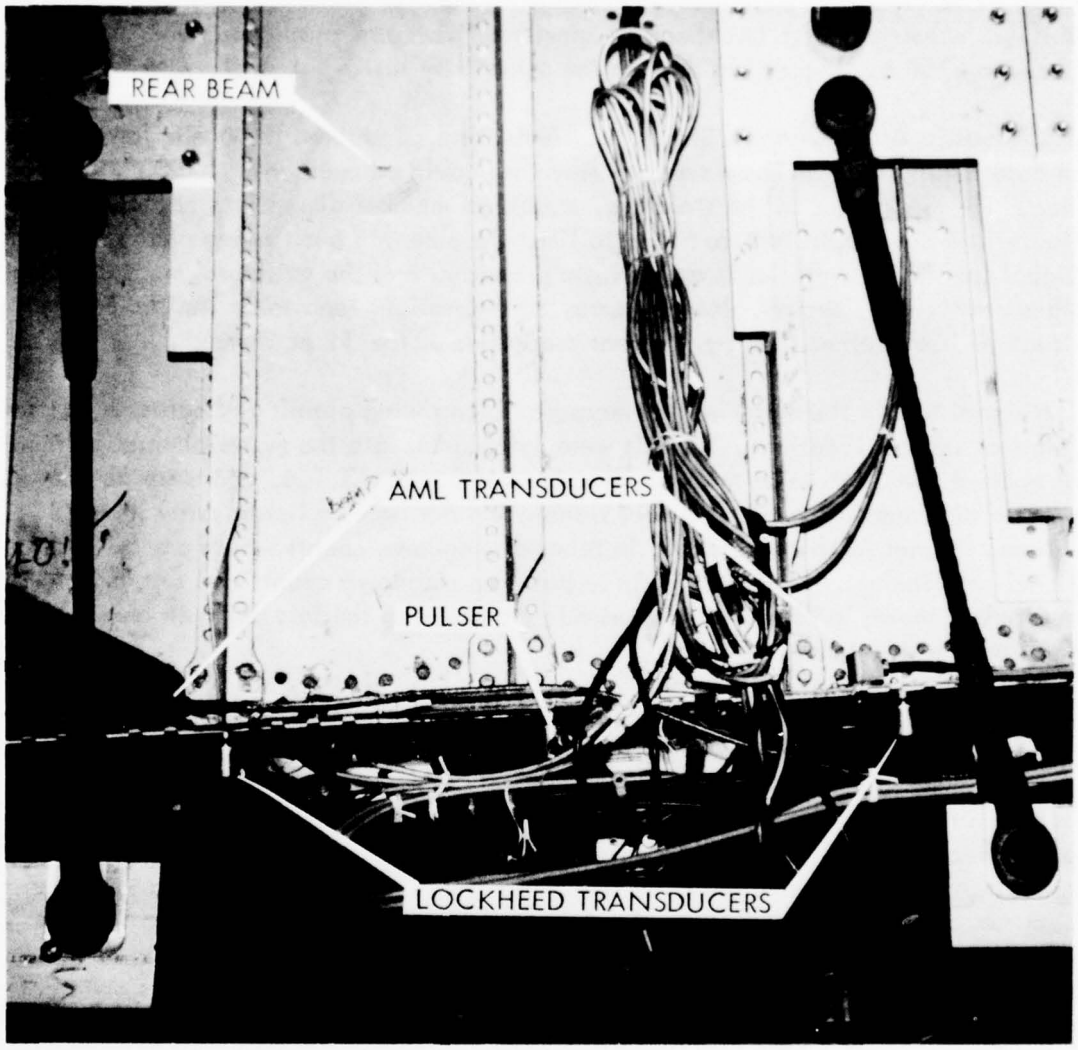

FIGURE 9. AML TRANSDUCER INSTALLATIONS

specimen of this material was fatigue cycled to failure and the AE monitored in the frequency range of 500 KHz to 1000 KHz. Total voltage gains of 65 to 80 db were found to be sufficient for reliable detection without overamplifying background noise. This was consistent with Lockheed's experience from past programs. The Dunegan/ Endevco S750 transducer was used in the sensitivity test.

B. Acoustic Attenuation in Structure. Tests were conducted to obtain data for use in determining the maximum size of array that could be used on the X993 wing specimen. The signal loss in the structure, structural member dimensions and array configurations are constraints that tend to limit the size and positioning of the arrays. Signal loss in the material is an intrinsic property, and the structural member dimensions are fixed by design. Hence, array configurations tend to be limited by the structure itself rather than by inherent properties of the AE equipment.

The signal loss in the material was measured along wing planks and across wing plank joints at several locations. Signals were introduced into the material through the use of each of the calibration methods described in Section 3.1.6, and were detected at precise distances using two receiver transducers acting as a linear array in the 1032 system. Signal levels were noted in terms of ringdown counts which are related to signal amplitude. A correlation curve between ringdown counts and system gain (in decibels), shown in Figure 10, was used in determining the loss between any two locations on the structure.

Attenuation is not a smooth function of distance in the structure, but is affected strongly by reflections from edges, fastener holes, risers, and other features. Attenuation across joints is also affected by fasteners, lap area, variations in sealant adhesion and thickness, and possibly other factors. Because of phase interference and reflections, signal levels can increase or decrease greatly over a very short distance. A single attenuation value taken at a given distance or across a joint then becomes almost ambiguous, for a second measurement very near the same location may yield a considerably different value. It is often sufficient under these conditions only to determine that the signal can be reliably detected between two points or to determine the average attenuation between the two points as an aid to adjusting the gain.

The signal level over a 2-foot distance along a panel does not drop appreciably. The greatest attenuation measured at a 4-foot distance in area 9 was less than 9 decibels. Attenuation across joints was measured at 11 to 16 decibels between outer wing box panels 3 and 4 in test area 9, 3 to 4 decibels between rear beam cap and inner wing box panel 1 in test area 3, about 21 decibels between inner wing box panels 4 and 5 in test area 1, and 9 decibels between center wing box panels 1 and 2 in test area 4. The wide variations in attenuation are due to many factors related to the joints. The low attenuation value obtained in test area 3 is probably related to the wide lap joint containing two rows of fasteners as opposed to the narrow, one-fastener-row joints in the other areas.

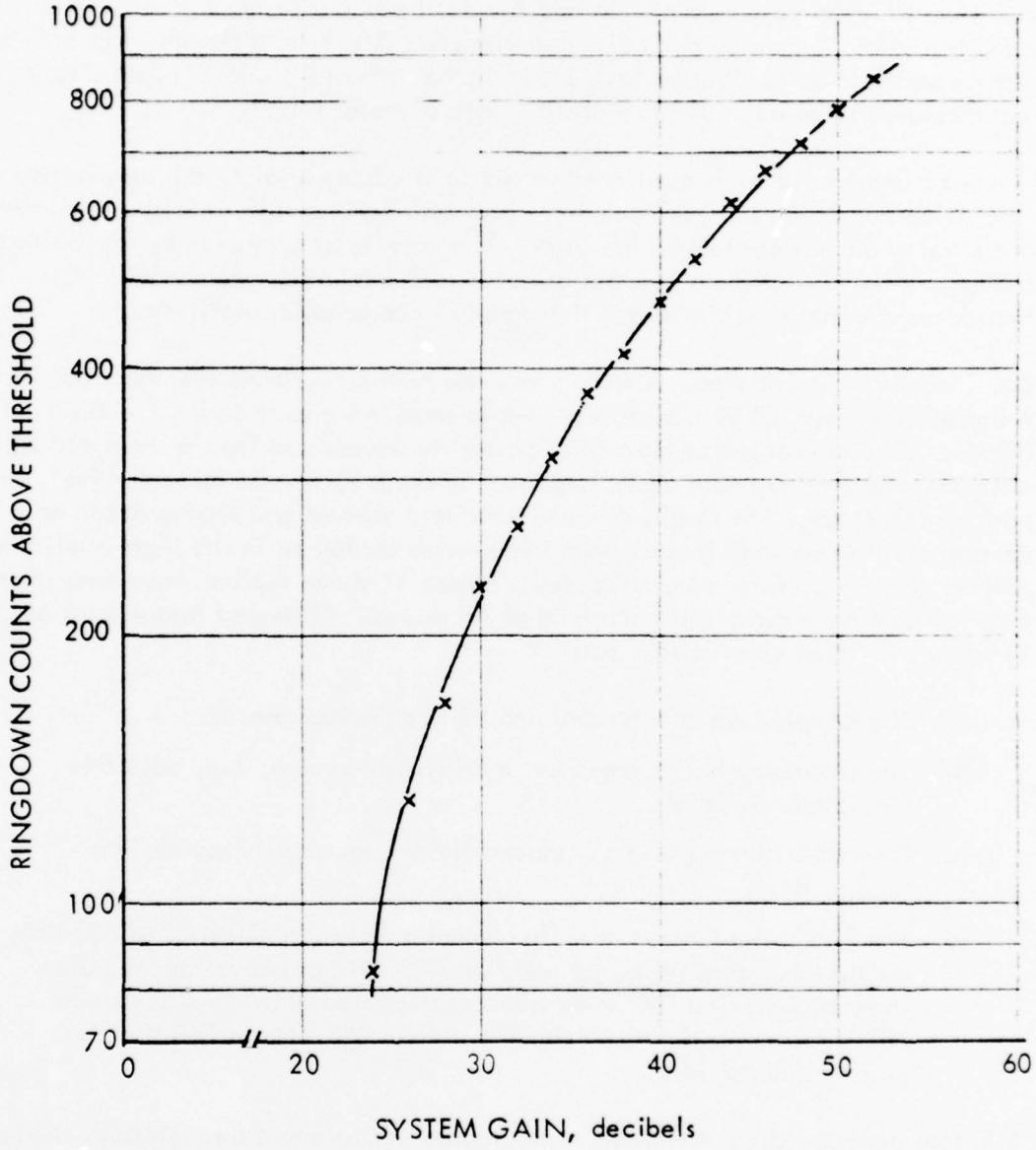

FIGURE 10. RINGDOWN COUNTS EXCEEDING THE THRESHOLD VERSUS SYSTEM GAIN FROM WHICH SIGNAL AMPLITUDE DIFFERENCES CAN BE DETERMINED (IN DECIBELS)

C. Time Delay Across a Joint. In addition to the signal losing intensity when it transits a joint, a time delay is also experienced. The time differential in area 9 was measured to be equivalent to 1-11/16 inches of metal travel. In area 1, it was measured to be equivalent to about 1 inch of metal travel.

When a triangular array is positioned so that it straddles a joint, the attenuation and time delay caused by the joint requires compensation in system gain and a compression of the array dimensions toward the joint. The array must appear to be an equilateral triangle in the time domain whether or not it really is in the geometric domain. Each transducer channel should also see the signal at comparable amplitudes.

D. Transducer Resonances. A study was made of the operating resonances of the installed S750 and D9202 transducers used to sense AE events during the 2000 unit flights. Simulated signals from a S750 pulser transducer and from a simulated AE source were input alternately near each transducer in areas 2, 5, and 6, respectively, to perform this study. The resulting waveforms were viewed and photographed on a storage oscilloscope and the resonant frequencies contained in the high-amplitude portion of the waveform were computed. Figure 11 shows typical waveforms photographed from each array and each type of AE source. Observed frequencies are listed in Table 2. Other observations are:

(a) The complex waveforms contained 2 or more resonances.

(b) The resonance had a dependence on type of source, i.e, pulser vs simulated AE signal.

(c) Resonances for a given transducer did not necessarily repeat from time to time.

(d) The S750 transducers typically resonated between 420 KHz to 560 KHz for the simulated AE signal and from 700 KHz or above for the pulser induced AE. The D9202 transducers resonated between 420 KHz to 580 KHz for simulated AE signal and from 580 KHz to 760 KHz for pulser-induced AE.

A further understanding of transducer resonance was attained through study of the transducer response curves. The 6 db points on the transducer response curves for the S750 transducers are generally at 550 and 950 KHz and for the D9202 at 380 to 650 KHz. Between these frequencies there may be one or more peaks at which the transducer will oscillate, depending to some extent on characteristics of the source AE. Filtering of low frequencies is achieved both by the transducer and the preamplifier. The transducer is essentially a bandpass filter having a sensitivity roll-off of 12-16 db octave on either side of the peak so that at 300 KHz the sensitivity is reduced by at least 8 db. The preamplifier has a high-pass filter which attenuates signals 48 db per octave below 350 KHz. The result of the transducer and preamplifier frequency response and filtering is that signals below 300 KHz have little likelihood of being processed by the system.

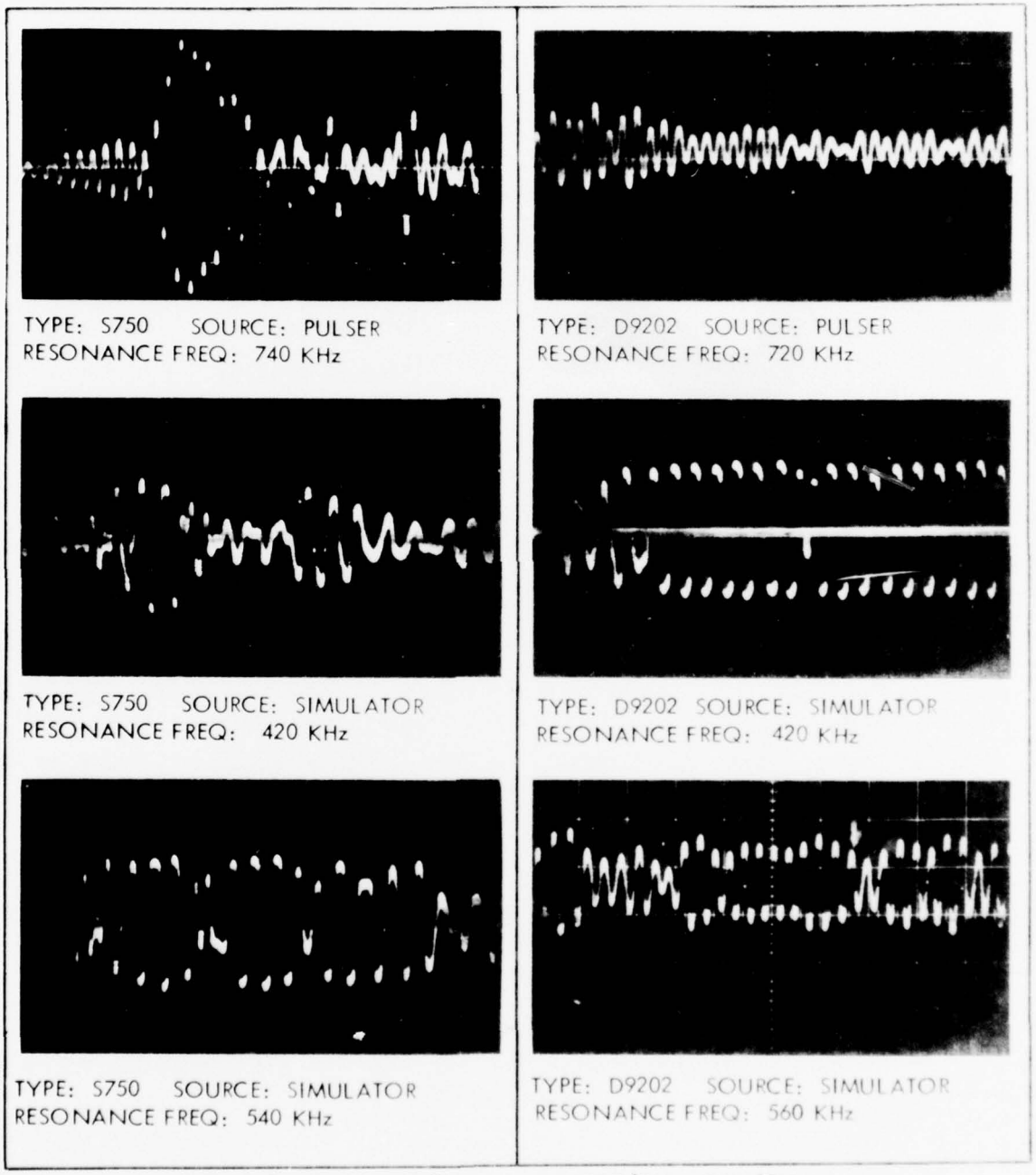

FIGURE 11. OSCILLOSCOPE TRACES OF TRANSDUCER OUTPUTS FROM WHICH RESONANT FREQUENCIES WERE COMPUTED FOR TWO TYPES OF TRANSDUCERS AND SOURCES

TABLE 2

TYPICAL ACOUSTIC EMISSION TRANSDUCER OPERATING RESONANCES
C-5A X993 TEST ARTICLE

Transducer S/N	Transducer Type *	Resonant Frequency KHz	AE Source	Location
AC08	D9202	580	** S750 Transducer	Area 2
AC08	D9202	480	AE Simulator	Area 2
AC05	D9202	500	AE Simulator	Area 2
AC06	D9202	580	AE Simulator	Area 2
AC15	D9202	560	AE Simulator	Area 2
AC04	D9202	480	AE Simulator	Area 5
AB29	D9202	720	**S750 Transducer	Area 5
AB29	D9202	400	AE Simulator	Area 5
AC10	D9202	420	AE Simulator	Area 5
AB83	D9202	500	AE Simulator	Area 5
AB83	D9202	520	AE Simulator	Area 5
944	S750	700	AE Simulator	Area 6
444	S750	740	**S750 Transducer	Area 6
444	S750	560	AE Simulator	Area 6
263	S750	460	AE Simulator	Area 6
947	S750	540	AE Simulator	Area 6
947	S750	420	AE Simulator	Area 6

* Dunegan/Endevco Models

** Transducer was driven at a pulse repetition rate of 1000 pulses per second

3.2 EXPERIMENTAL RESULTS

3.2.1 Summary of Program Data and Data Analysis Procedures

A. Program Data. Acoustic emission data processed from the 32-channel system during the flight-by-flight load cycles were recorded on magnetic tape cassettes for future reference and analysis. The data were also displayed in real time on the CRT monitor in the form of event histograms, ringdown count histograms, and array data point displays. Paper hard copies were made, on command, of any desired CRT display. Numerical data could also be typed out on the system teleprinter in the format and content shown in Figure C2 of Appendix C.

During 2100 unit flights, acoustic emission signals were observed and recorded from 12 of the 16 test holes monitored. Three nontest locations, in addition to the test holes, emitted repetitive and persistent acoustic emission to the extent that crack growth was suspected. The AE test data collected during the tests include:

a. 60 cassette tapes containing complete information on the AE events.

b. 1700 hard-copy paper printouts of the AE event data as displayed on the CRT in real time.

c. A daily laboratory log to facilitate correlation between the fatigue testing and the AE data and other information.

In addition to these data, test article load and visual crack growth information was readily available at any time. Fractographic crack growth data were available upon completion of each fractographic evaluation.

About 85 percent of all flights were monitored during the program; therefore, AE data are not available for all flights. Personnel were not available to man the AE system on a 3-shift per day basis. The missed flights probably do not significantly affect the information concerning acoustic emission sources, since the percentage of flights which were monitored is sufficiently high to reveal practically all the active sources and information about their relative activity.

B. Analysis Procedure. The AE data were analyzed by using the Post-Test Analysis Program (PTAP)-VTS-C2 and the system computer to extract prescribed data from the data tapes. The PTAP is stored in the computer, then additional information, machine time period of interest (flight number) and desired y-variable (counts or events) are input according to one of the formats shown in Figure C3 of Appendix C. The stored program processes the information from a particular data tape which is played back to the computer. The result is an x-y bargraph displayed on the CRT monitor showing the total counts or events (y-axis) versus machine time (x-axis) while the data were taped. When complete, the bargraph can be recorded on the paper hard-copy machine which facilitates correlation to the flight load chart referred to previously as Figure 4.

Such information can be extracted for any array if the AE source coordinates are known. The coordinates for the test holes and other locations of interest were determined during the previous calibration activities and recorded for use during the analysis. Each test hole where AE activity was seen during the flights was interrogated through the PTAP. Acoustic emission data correlation is made to the flight spectra and the flight spectra is correlated to fatigue crack growth through fractographic examination.

Data extraction from the tapes is accomplished entirely with the AE source location instrumentation using its computer, software, keyboard, and cassette recorder, real-time CRT display unit, and hard copy unit. Before analysis could be accomplished in an efficient, meaningful manner, however, it was necessary to set up a systematic procedure for properly interrogating the tapes for extraction of categorized data. Since a tape may contain an uncertain number of flights, instrumentation stops and start-ups, interrupted machine clock times, and other variables, the analyst must determine the general contents of the tape and the ranges of the analytical variables. This is done by referring to the daily data log made during the fatigue tests and by playing the tapes back to note where the "landmarks" occur.

The procedure set up for characterizing the contents of the tapes is an important step in the total data analysis routine and is given in Appendix E for reference.

After all tapes have been characterized using this procedure, the analyst has a complete compilation of information about the contents of individual data tapes. He is therefore able to select any tape containing a flight or flights desired to be analyzed. The AE data within those flights can then be efficiently extracted and plotted in terms of AE "counts" or "events" for any transducer array or test area.

3.2.2 System Operating Parameters

One purpose of this program was to determine the operating parameters suitable for an airborne acoustic emission flaw detector, pursuant to development of such a system as an ultimate goal. Among these parameters are, chiefly:

(1) transducer type and frequency
(2) detection threshold
(3) system gain per channel
(4) transducer array configurations
(5) structural limitations
(6) system characteristics - electronic processing, noise suppression and data handling

The first five items were evaluated during the program. Only generalizations about desirable system characteristics can be made presently relative to Item 6. Specific characteristics of an airborne AE flaw detector system are yet to be formulated because the demand for such a system has not been realized to the extent that definite design goals exist.

Transducers. The two types of transducers used during the program (S750 and D9202) which are described in Sections 3.1.3 and 3.1.8D, were off-the-shelf commercial units for general purpose laboratory or non-severe environment applications. Their operating frequencies are roughly the same and seem to respond from 480 to 580 KHz. Areas having relatively high structure-borne noise levels such as the mid-beam area may require operation in the vicinity of 750 KHz. The sensitivities (about 80 db/microbar) of these transducers are adequate for aircraft use and the D9202 models exhibited a 10 to 16 decibel greater sensitivity to signals and noise in the areas where both types had been installed. The differential models also suppress EMI transients.

Neither of the transducers should be used, as is, on flying aircraft because they are not "flight hardened". Experience from related programs at Lockheed shows that air-borne transducers must be hermetially sealed and "hard wired" to eliminate the external connector. These are minimum requirements for airborne transducers.

System Gain. It is desirable that the gain of each channel be independently adjustable to compensate for sensitivity differences among transducers, suppress noise and compensate for signal losses across joints. For a detection threshold of 0.1 volt in the signal processing section, a total voltage gain of at least 70.5 decibels is required for detection of a 30 microvolt signal appearing at the transducer output. Since electronic noise generated in the preamplifiers is usually about 6 microvolts, total gains above 85 db greatly decrease the signal/noise ratio at the 0.1 volt detection threshold. With that gain, the detection threshold must be increased to improve the signal/noise ratio. Such high gains are practical only when the structure-borne noise levels are very low.

A channel fixed gain of 40 db was provided by each preamplifier. Additional gain adjustable from 0 to 60 db was available for each channel in the signal conditioning section. Typically, these were set for 26 db to 40 db of additional gain. The low gains were generally selected for high noise areas to reduce the noise background and amplify the highest AE signals. The more sensitive transducers were operated at lower total gains. To reduce noise effects, gains for arrays in the high noise areas were set relatively low (68 to 72 db, typical). In moderate and low noise areas, gains were at higher settings (74 to 80 db, typical).

The four transducer channels in the triangular array were often operated at different gains varying from 2 to 6 db to compensate for differences in channel sensitivity (due to transducers and coupling). Equalization in output was accomplished by adjusting the gains to get the same audio output from each channel using the AE system's audio monitor described in Appendix B.

Detection Threshold. The purpose of the detection threshold setting is to block noise and superfluous low-level acoustic emission. Even without structure-borne noise produced by test or flight loading, the preamplifier itself produces an rms noise of about 6 microvolts. For reliable AE detection, the threshold is set to a value which will block most of the noise while passing sufficient AE signals to provide information about

the source. For a given threshold setting, there is a unique gain for which signals of some specified minimum amplitude can be detected. The threshold was adjustable in our AE system by means of a 3-turn limited 10-turn potentiometer which provided selection of threshold settings from zero to 3 volts. For most of the testing, this was set between 0.2V to 1.0V. Since a single detection threshold adjustment in the AE system controls the detectable signal level for all 32 channels, the threshold is not independently adjustable for each channel. Therefore, it was not possible to optimize the gain and threshold to achieve the best signal-to-noise ratio independently for each array. Instead, the threshold was normally adjusted in an empirical fashion to achieve acceptable results for the array in the noisest area. The channel gain controls were also adjusted independently to achieve good AE detection. Since noise is not constant over an aircraft structure, it is desirable to incorporate separate threshold adjustments for each array.

Array Size and Configuration. Experience was gained during the program with a variety of array sizes and configurations which were described and illustrated in Section 3.1.4. Summarized, these include:

1. Linear arrays from 9 to 39 inches long.
2. Triangular arrays for 8- to 48-inch EDGE distance.
3. Triangular arrays straddling a single joint, with one or two transducers opposite the flawed member.
4. Triangular arrays with one and two double-row of fasteners intervening.
5. Triangular arrays positioned so that the test hole is at a precise location with respect to the other transducers (e.g., array is "rotated" about test hole as described in Section 3.1.4B).
6. Triangular arrays divided by integral risers with the defect in the riser.

The small arrays tend to exhibit considerable scatter in their source location displays. The larger arrays tend to reduce scatter, but reduce spatial resolution also. The triangular arrays proved to be the only practical configuration for use on the test article since it can provide two-dimensional information about source location. Even along purely linear structural features such as a joint or a row of fasteners, the one-dimensional linear array was not adequate for reliable detection and location of crack growth. The reason for this was that structural noise coming from near by regions of the structure often made differentiation between noise and AE very unreliable.

Structural Factors. Structural characteristics are the greatest limiting factors for AE transducer array size and type. Structural members such as wing panels and webs are long in one direction, but relatively narrow in width (about 20 inches for wing panels). Even in the long direction, they are divided periodically by rows of fasteners. Our experience has shown that panel joints and rows of fasteners scatter and attenuate AE signals and probably produce wave mode conversions. The size of the array, therefore, becomes restricted.

The 48-inch triangular array approaches the largest triangular array size that can be accommodated on the wing skin structure without straddling more than one plank joint. Two joints would require a gain compensation (increase) of 22 to 32 decibels, which would prohibitively amplify structural noise while losing signal amplitude through scatter at the joints and fasteners. Having a joint within an array may actually be beneficial due to its ability to block low level noise from some sources, providing the amplification can be kept to a minimum.

The placing of arrays to accommodate structural features while maintaining the array physical requirements is illustrated by array modifications made to monitor the final 800 unit flights (1201-2000) as described in Section 3.1.4C. The array configurations and their positioning were made simple as possible at the start of the program to test the feasibility of the monitoring system. As the program progressed, the arrays were modified to test more complex situations and to evolve more practical arrays to accommodate structural features. From these experiences, it appears that sufficient versatility exists in a system of this type to permit monitoring of a great variety of complex structure within the airplane.

3.2.3 Discussion of Crack Propagation Results

A. Crack Propagation Summary and Analysis Method. Test holes initially contained existing fatigue cracks or 0.05 or 0.1-inch sawcut crack starters made either at the corner of the hole or through the entire hole wall. Crack propagation during the test program was measured from the bounds of the initial predamage conditions at the hole and is given in Table 3 in dimensions along the surface (S) or along the 45 degree line (45°) extending from a hole corner. Table 3 summarizes the initial conditions at the test holes and the final crack growth dimension contributed by test loads applied during the program. The crack lengths for all test cracks except 8N, 1A, and 1B include also growth increments induced by additional loads applied following the 2000 test flights. The length given for test cracks resulting from initial fatigue cracks is the total crack length since the increments added during the flight tests were not determined in all cases.

Crack dimensions were determined by cutting and breaking the test pieces open along the crack plane direction and photographing the fatigue crack surfaces along with a 0.01-inch division scale. A direct comparison of the photographed crack surfaces with the scale provides a reasonably accurate measurement of total crack size. Where fatigue cracks existed prior to start of the tests, an electron microscope was used to determine the position of striations produced by the first marker loads applied at the beginning of the tests. Crack extensions which occurred during the program are thus determined.

B. Fractographic Analysis of Test Crack Surfaces. A total of 18 fastener test holes were selected in nine test areas on the X993 right wing to study fatigue crack propagation in the crack propagation program.

TABLE 3
SUMMARY OF X993 CRACK PROPAGATION AND AE PROGRAM TEST AREAS

X993 TEST AREA	TEST HOLE	TYPE OF PREDAMAGE+	PROGRAM CRACK GROWTH+, IN.	AE CATEGORY
1	A B C	Thru Cut .05, F Thru Cut .10, F & A Thru Cut to F Edge	0.365(S) F 0.362(S) F ---	Array O
2	D E O P Q	Thru Cut .05 U Existing Crack, U Existing Crack, U Existing Crack, U Existing Crack, U	0.087(S) U 0.228 (45°) 0.303 (45°) 0.125 (45°) 0.133 (45°)	Array 1* Array 7** Array 1
3	F G	Corner Cut .05, A Corner Cut .05, F & A	0.035 (45°) A 0.055 (45°) F 0.035 (45°) A	Array 2
4	H	Corner Cut .10, A	0.175 In (45°)	Array 4
5	I J K	Thru Cut .05, U Thru Cut .05, L Thru Cut .05, U & L	0.050 (S) U 0.247 (S) L 0.033 (S) U 0.050 (S) L	Array 3
6	L	Corner Cut .10, A	0.020 (45°)	Array 5
7	M	Thru Cut .05, F		Not Monitored
8	N	Existing Crack, F & A	0.32 (S) F 0.30 (S) A	Array 7*
9 (AE)	None	None		Array 6 AE Baseline

*Precrack Flts 1-100 and Test Flights 1-1200

**Test Flts 1201-2000

+A = AFT (Side of Hole), F = Forward, U = Upper, L = Lower
(S) = Crack Growth Measured Along Surface (45°) = Crack Growth Measured Along 45° Line WRT Surface and Hole Wall

One of these, 9R, was added during the test program and was not monitored for AE Another test hole region, 8N, was removed from the test structure for analysis at the end of test flight 1200, and the fractographic/AE history for this one was first reported in the Second Quarterly Progress Report.

Fractographic examinations were made on the crack surfaces to analyze crack growth. Generally, 10X to 300X binocular microscopes, scanning electron microscopes (SEM), and transmission electron microscopes (TEM) were used to determine crack growth history and to make crack growth measurements. An x-y micrometer stage was used to obtain macromeasurements with the binocular microscopes. Micromeasurements pertaining to specific propagation events were obtained with the SEM and TEM. The TEM was used to record the fine spacings between marker loads. The SEM was used to locate the transition between major types of loading.

Corner cracks were measured along three directions: a 45° line starting at the hole-to-surface corner and bisecting the hole and surface apex, along the surface axis and along the hole axis. Throughcracks were measured along one or more lines running parallel to the surface axis. Summaries of crack growth at each test area are given in Appendix F.

In-test crack length measurements were made of each test crack aperiodically, after every 25 to 75 unit test flights. Where possible, these measurements were made using an accurate triangular technique. The technique description and the final results of the measurements are given in Appendix G.

C. Examination of Non-Test Areas. Two (2) non-test crack suspect areas existed in test area 4 and one (1) non-test crack suspect area existed in AE test area 9. These suspect areas were called 4A, 4B, and 6A in previous reports (6A will subsequently be called 9A). In each case, portions of the structure anticipated to contain the suspect area were cut from the X993 wing test article following completion of all fatigue and residual strength testing programs. The probable source locations were determined by applying simulated AE signals at various points on the structure until the simulated coordinates coincided with the coordinates actually received. Thorough visual and NDT inspections were performed in the areas prior to removal.

Suspect Areas 4A and 4B - These areas were assumed to be in the center wing panel No. 3 in a region adjacent to the W.S. 120 joint and the panel No. 3/panel No. 2 splice. This assumption was based on the signal coordinates provided by the AE instrumentation, the relatively high AE activity and the AE amplitudes experienced during the test flights. This indicated that the suspect flaws were in the same piece of structure upon which the array transducers were bonded, as opposed to being in an adjacent faying member.

Since this region was buried between inner and outer splice straps, NDE was not accomplished until the splice straps were removed. An automatic eddy current bolt-hole scanner was used to inspect holes along the W.S. 120 and Panel 3/2 splice. No

cracks were found. A 5" x 6" section of panel 3 containing the suspect holes was removed for inspection in the laboratory. The diagram in Figure 12 shows where the material was removed from panel 3. After a thorough cleaning, the section was observed under a 30X binocular microscope, particularly along the corner edges of the bolt holes. No fatigue damage was visible at the hole edges. The section was then cut into five pieces through the bolt holes to provide access for more sensitive NDI. A careful fluorescent penetrant inspection using Magnaflux ZL-22 penetrants was performed on the inside hole surfaces with magnified (20x) viewing to search for very small hole surface cracks. Figure 14 is a photograph of the section of panel 3 showing where the cuts were made through the holes to provide inspection access. No crack-like indications were seen on any of the hole surfaces. Of the several components in the W.S. 120 wing joint build-up, only the panel was given a detailed inspection for cracks.

Suspect Area 9A - Persistent localized emissions in AE reference area 9 led to anticipation of a suspect crack in outer wing panel No. 4/panel No. 5 splice near OWBR Station 116. Visual and eddy current NDI were performed in the area as well as at other potential locations of this source several times during the final 800 test flights. The AE simulator was used in an attempt to define the coordinates. A definite source for the emissions could not be identified by these means. Following completion of the structural tests, a portion of the wing planks containing the panel 4/panel 5 splice joint was sawed out for more intensive inspection. Figure 13 is a diagram of the outer wing area showing where the section was removed. Figure 15 contains photographs of this section. Careful visual, eddy current and fluorescent penetrant NDI were performed on this section in the laboratory without finding crack indications in the immediate suspect area. Finding tiny cracks was the object of this investigation. Respective of the limitations of the NDI methods used in this case and the case preceding, no cracks were detected. An old, stop-drilled crack (initiated during the previous 2-lifetime testing of X993) was discovered at point U in Figure 15. No additional growth could be detected at this crack, but the possibility exists that the fretting of the old crack surface produced the steady emission identified as suspect 9A.

3.2.4 Discussion of Acoustic Emission Results

Acoustic emission (AE) data were extracted from the data tapes using the data reduction procedure given in Section 3.2.1B. The AE sources were identified in real time during the course of the program.

A source is defined as a small confined region denoted by definite geometric (one or two dimensions) coordinates in which there is a persistent emitter of AE signals. The emissions need not be constant, but persistent over a period of several flights. For sources relatively low in activity which provide only one or a few emissions (events) per flight, many flights may be needed to prove persistency. AE signals which arrive randomly with respect to space are not regarded as a source as defined above. Coordinates denoting a source are usually broad enough to encompass the spatial scatter that characterize emissions from the source.

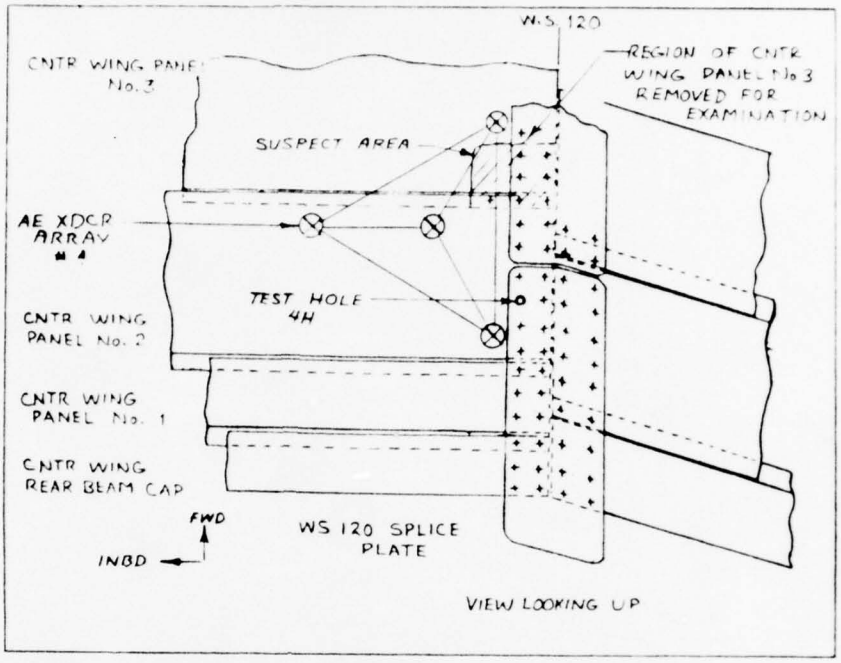

FIGURE 12. SECTION OF A CENTER WING (TEST AREA 4) REMOVED TO INVESTIGATE PRESENCE OF SUSPECTED CRACKS

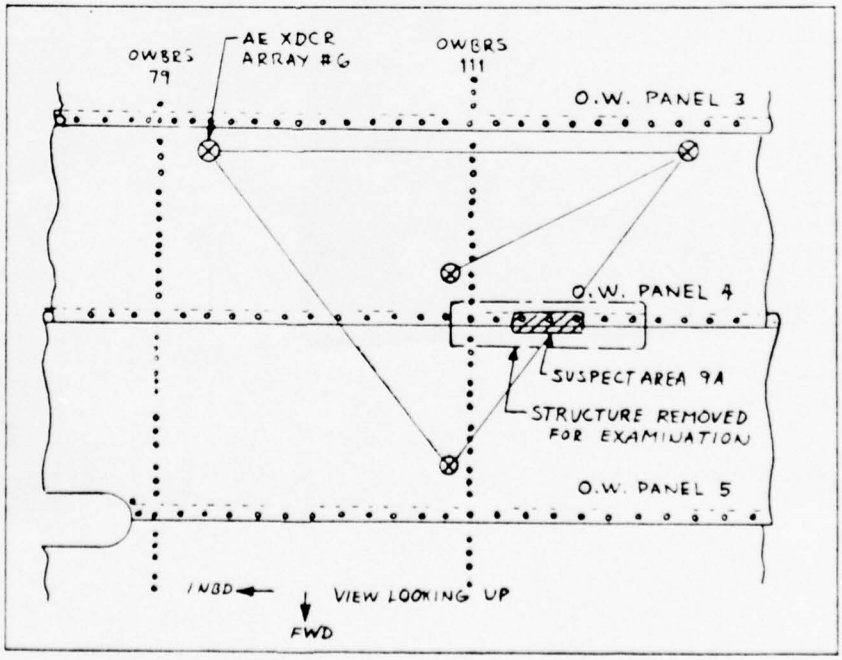

FIGURE 13. SECTION OF OUTER WING (AE TEST AREA 9) REMOVED TO INVESTIGATE PRESENCE OF SUSPECTED CRACK

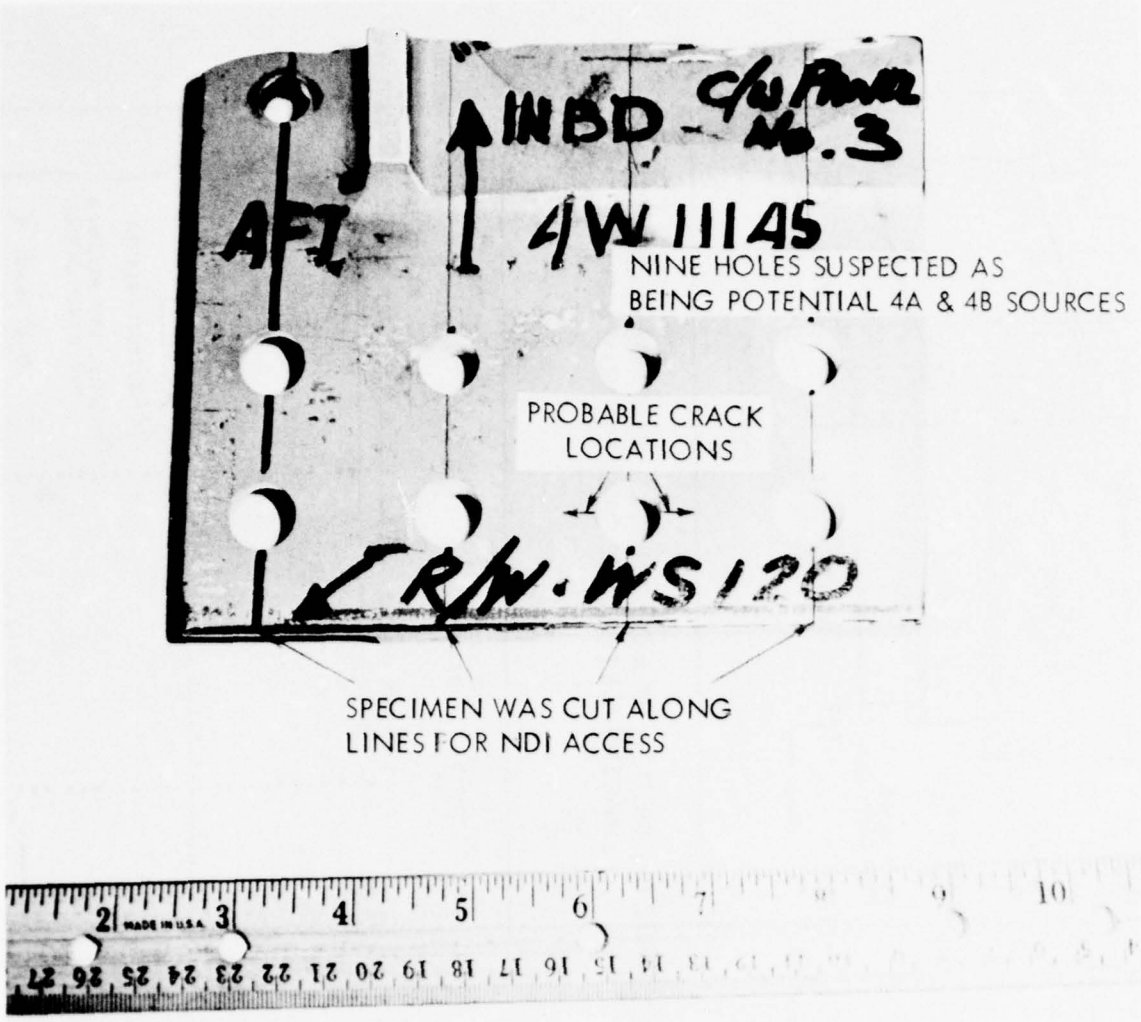

FIGURE 14. PORTION OF STRUCTURE FROM TEST AREA 4 CONTAINING CRACK SUSPECT AREAS 4A AND 4B

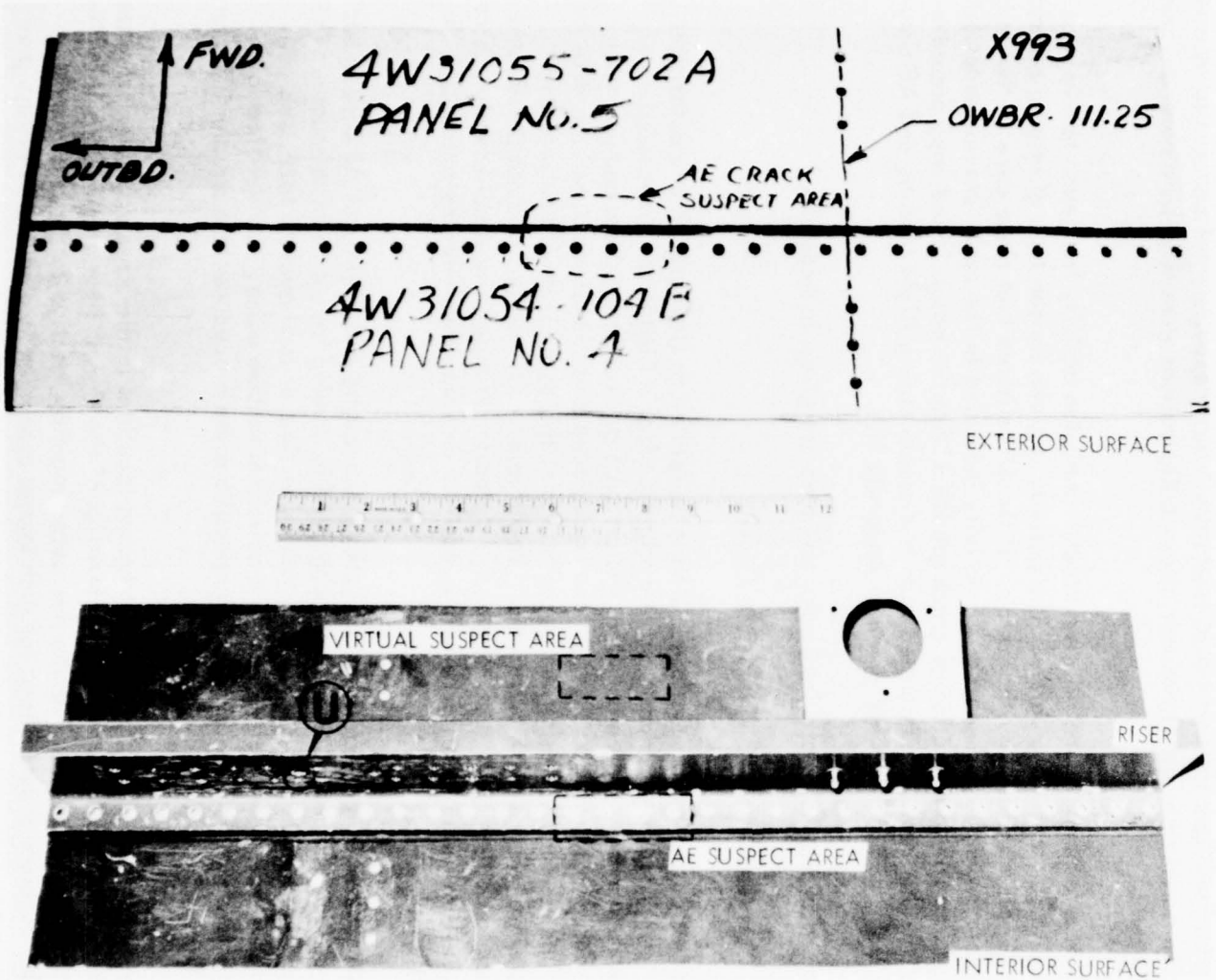

FIGURE 15. PORTION OF STRUCTURE FROM AE TEST AREA 9 CONTAINING CRACK SUSPECT AREA 9A .

The seven test areas monitored on the X993 right wing during these tests contained a combined total of 16 test holes. Fractographic analysis has shown that crack growth occurred in all but one of these holes during the 2100 simulated flights.

Since the holes were analyzed after additional load tests had been made on the test article following the 2100 simulated flights, the cracks contain growth contributed by these subsequent loads. This report, however, does not present acoustic emission results obtained from the additional load tests. Many experimental changes to instrumentation parameters and transducer array configurations were made and observed prior to flight 801.

Table 4 is a summary of the relative acoustic emission activity from each test hole as received throughout the program. The activity is given for the type of array used and for the flights monitored by that array. It should be noted that since some of the early arrays were highly experimental, AE activity indicated in the table was not necessarily regarded as positive detection of crack growth within the array. Hard copy presentations of acoustic emission detected from test cracks during flight loading and AE simulations made of test holes are given in Appendix H.

Discussions of the AE results from each test area are given in Appendix I.

3.2.5 Correlations of AE with Crack Growth

A. General. Acoustic emission data must be related to flaw growth characteristics if it is to be used as a nondestructive evaluation tool. First, the flaw-produced AE must be detectable. This means that factors such as structural access and geometry, system capabilities and sensitivity, and background noise levels must be favorable for detection. Secondly, for maximum usefulness of the data, it should be relatable to the amount of flaw growth and to flaw growth rates. Of course, it is not possible in all cases to achieve both; but, obviously, detection is a definite requirement. Correlation to flaw characteristics is then a goal that may be achievable by optimizing the test conditions.

B. Detection. Detection is the collection, processing and display of AE data in such a manner that the emissions can be recognized as coming from a definite source. The emissions must be persistent over some period of time or load cycles, localized with respect to space or geometry, and separable from random noise. For verification, the emissions should be traceable through calibration procedures to a structural feature where flaw growth is likely to occur.

The presence of cracks and sawcuts at known locations in the large, complex structure provided a test bed to observe characteristics of the signals from growing cracks. The range of coordinates which define the source location relative to the array position could be accurately determined for such known cracks. Since scatter is always present, a range of coordinates within which the source will be detected had to be determined.

TABLE 4. SUMMARY OF RELATIVE AE ACTIVITY

CRACK	ARRAY TYPE	PRE TEST FLTS 0-100	TEST FLIGHTS 0-400	401-800	801-1200	1201-1600	1601-2000	NOTES
1A	L	0	P	P				(1) Crack removed at end of 1400 flts
	A				0	0(1)	(2)	
1B	L	0	0	0				(2) Not monitored during flight span
	A				N	N(1)	(2)	
1C	L	P	P	P				(3) Region of crack growth not identified
	A				N	N(1)	(2)	
2D	L	(3)	(3)	(3)	(3)			(4) Ocassional periods of very high AE activity
	A					0	0	
2E	L	(3)	(3)	(3)	(3)			(5) Crack removed at end of 1650 flts
	A					C	C	
3F	L	N	P	P				(6) Crack removed at end of 1200 flts
	A				P_R	P_R	P_R	
3G	L	P	C	P				
	A				$P_{(4)}$	$P_{(4)}$	$P_{(4)}$	
4H	L	(3)	0-140 (3)					SYMBOLS:
	A		141-400 P_R	P	P_R	P	P	L = Linear Array A = Triangular Array N = No AE Activity O = Occasional AE Activity P_R = Periodic AE Activity P = Persistent AE Activity C = Continuous AE Activity
5I	A	N	N	N	N	N	N	
5J	A	0	0	0	0	0	(5)	
5K	A	N	N	N	N	N	N	
6L	L	(3)	0-100 (3)					
	A		101-400 0	P	P	$P_{(4)}$	$P_{(4)}$	
8N	A	C	C	C	$C_{(6)}$	(2)	(2)	
2 O, P, Q	A	(2)	(2)	C	$P_{(4)}$	C	C	

Calibration procedures in which simulated AE signals injected into the structure at the test holes were used to obtain the source coordinates as the equipment recognizes them. Repeated emission buildup at these coordinates during the applied test flights then heralds crack growth which is periodically verified by visual or NDI tracking of the crack on an accessible surface. In this manner, repeated emissions were recognized at twelve of the 15 monitored test holes where crack growth actually occurred.

At the three holes where crack growth was not detected, it appeared that emission build-ups from the growing cracks were taking place, but the high local noise incidence prohibited positive detection. These three cracks, at test holes O, P, and Q were grouped together at the attachment of a vertical stiffener to the mid-beam web and lower cap juncture. Fastener-attached vertical stiffeners were also within and adjacent to this area. This proved to be the noisiest area among those monitored.

Emission buildups were not restricted to the known cracks. On numerous occasions, persistent buildups having definite coordinates occurred within most arrays. These unknown sources were designated crack suspect areas and their locations within the structure were determined. Many of the suspect areas were investigated during the program using visual and NDT inspection methods. While no cracks normally detectable by these methods were found at any of the suspect locations, several of the emission sources were traced to loose fasteners. A loose fastener is in itself a defect condition and the fact that the instrument detected these points to a potential added dimension of the AE system. Three of the detected suspect areas were selected for post-test fractographic examination. These were suspect locations 4A, 4B, and 9A, described previously.

Detection of crack growth at the known test holes was very good. Some problems which may affect positive detection were also recognized, such as high scatter at some locations, displacement of the displayed source coordinates from the true coordinates, and interference from random noise.

C. Correlation of AE with Crack Growth Data. Detection of crack growth AE does not assure that the AE data can be correlated directly with the amount of crack growth or the crack growth rate. Detection is critical for the system in its role as a structural monitoring tool. Correlation, however, extends the usefulness of the system and enables inspection and maintenance decisions to be based potentially on the AE data alone.

Correlatable AE data are chiefly dependent upon wise design and installation of the array, optimization of system gain and detection threshold, and the amount of random structural noise which can interfere with and mask real AE data. Assuming that the array and system operating parameters are favorably selected, noise is the greatest detractor to correlatable data. It is not possible to separate noise events from AE events within the coordinates defined for the source, so noise causes fluctuations in the accumulated events. Also, since the equipment imposes a brief "dead time"

following reception of a "valid" event, the reception of a noise signal can thus cause a subsequent AE event to be missed. Therefore, it follows that close correlations of AE to crack growth data will not always be possible for complex structure.

Correlations were attempted for the following test cracks: 8N, 4H and 5J. In the case of 8N, a very detailed fractographic analysis of the fatigue crack surface was accomplished using the scanning electron microscope (SEM) to locate crack growth striations. A detailed correlation of the AE data was therefore possible for this crack. For 4H and 5J, only a relatively macroscopic analysis of growth resolved for each 100 simulated flights was accomplished. Thus, a less detailed correlation of AE resulted. However, the latter represents a more practical approach relative to field level crack growth detection.

Data for other test cracks were either insufficient or too fluctuating to attempt direct correlations. From the correlations presented and from other observations, it appears that, under controlled and optimized test conditions, direct correlations are possible for most crack growth investigations.

Correlation, Test Crack 8N. Crack N, Area 8, was a relatively large crack prior to application of the initial loads. The initial crack length at the surface, including fastener hole, was 0.94 inches. Acoustic emission signals were received from growth of this crack early and continued to be received throughout the tests. After 1200 unit flights, a small piece of material containing Crack N was cut out of the wing plank for metallographic examination. Repairs were made to the structure for further testing.

A magnified view of the crack surface is shown at the top of Figure 16. Bands of different hue on the surface indicate various regions of crack growth. The surface between C and D, which includes the fastener hole, represents the initial crack which existed prior to testing. The crack then grew slowly from D to E and simultaneously C to A during the 1200 test flights (including the 100 precrack flights and the applied marker loads). The lower part of the figure is a graph of the crack growth in the region D-E which resulted from all the applied load spectra. The growth was reasonably linear over the load spectra. The increment of growth during the 100-block of flights from flight 600 to flight 700 was approximately 0.026 inches, of which slightly more than 0.005 resulted from the marker loads. Thus, the average growth during this period was 200 microinches per flight.

The crack growth data were derived by analyzing the crack surface between D and E using the scanning electron microscope (SEM). The marker load striations were searched out on the crack surface to separate and identify the growth produced during each block of 100 unit test flights. A photograph showing a SEM view of a portion of the crack surface produced during test flights 601 through 611 is presented in Figure 17.

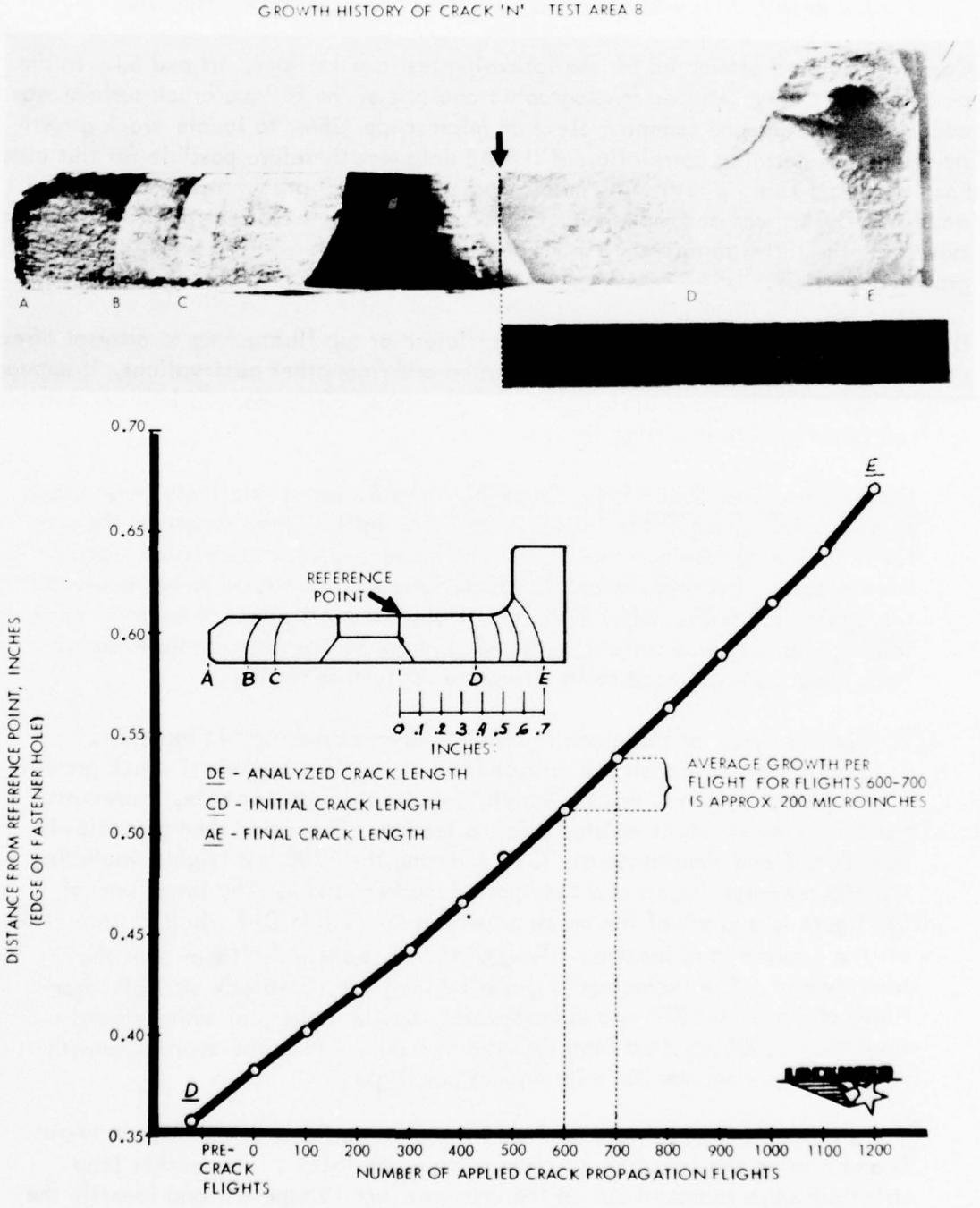

FIGURE 16. CRACK GROWTH HISTORY OF CRACK 'N'

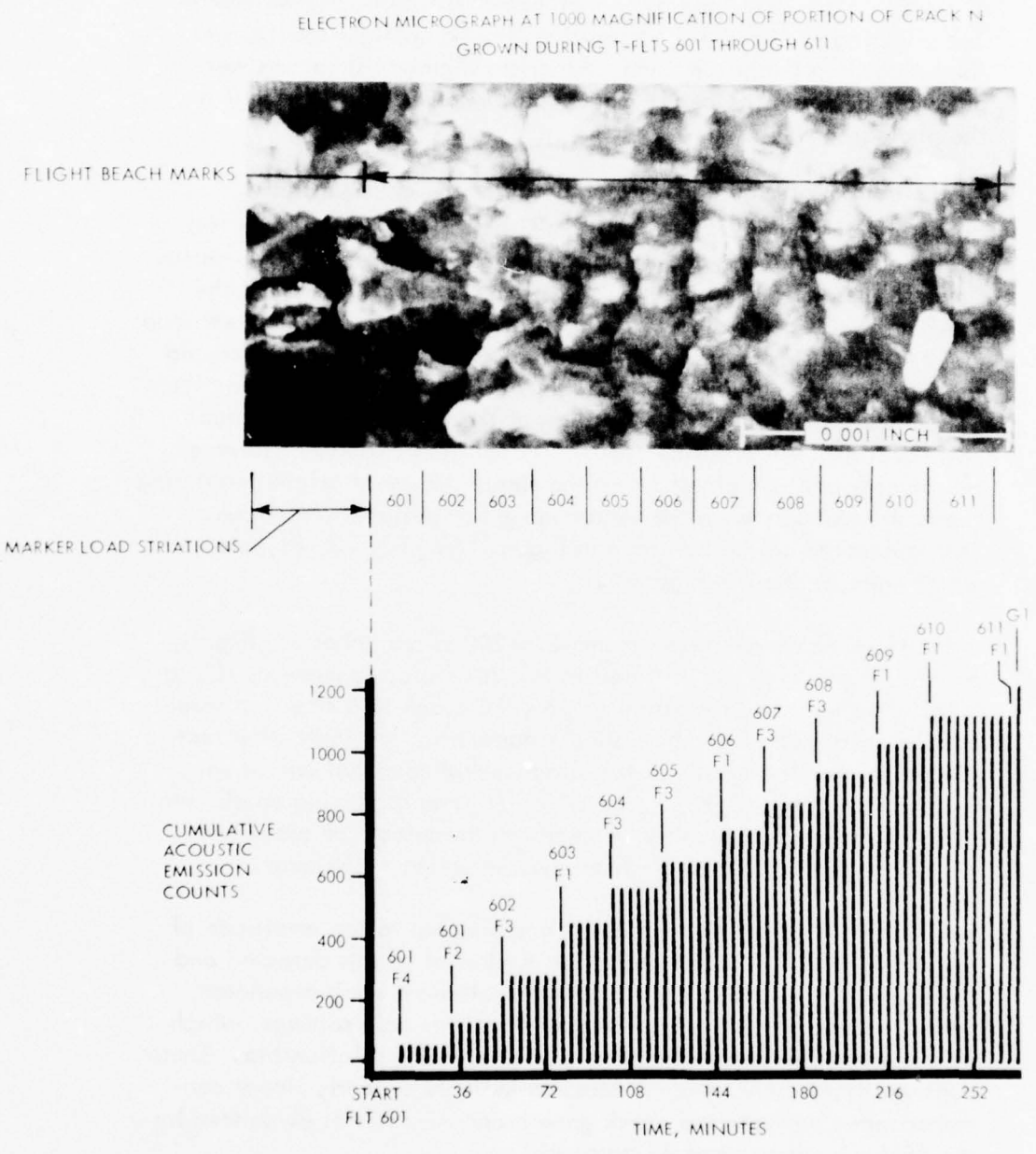

ACOUSTIC EMISSION EVENTS FROM CRACK N AT IWBRS 217, PANEL 3, AREA 8 DURING T-FLTS 601 THROUGH 611.

FIGURE 17. CORRELATION OF AE WITH SEM VIEW OF CRACK 'N' SURFACE

The marker load striations on the left of the photograph were used to identify and correlate this region of growth to the particular set of test flights. The wider set of striations to the right of this group of striations are described as "beach mark" striations and were produced during the F1-G1-F5 transitions from one flight spectrum to the succeeding flight spectrum. Finer slow-growth striations were produced between the beach marks, but are not clearly evident in the photograph.

At the bottom of Figure 17 is a bargraph of the accumulated acoustic emission (AE) received from Crack N during the same test flights depicted in the photograph. The cumulative AE counts versus time for these flights were extracted from the data tapes using the PTAP and were correlated to the recorded function generator test load curves. Each step increase at the flight condition noted was caused in most cases by detection of a single AE event occurring during the F1-G1-F5 transition. The resolution of the time bars on the graph was not sufficient to define the flight condition exactly. However, the investigations indicated that the single AE event originated during the first excursion when the load changed to a higher amplitude. This is denoted on the bargraph in Figure 17 by F2, F3, F1, etc., which were defined in Figure 4.

Since the crack growth rate is small ($\sim$200 microinches per flight), after a fatigue crack is initiated in this structure, as many as 100 to 200 flights would be necessary to grow the crack to a size that would be minimally detectable by ordinary nondestructive inspection techniques. Since the results of this program indicate that only a very few AE events per flight may be expected from a growing crack, ten to 20 flights would probably be necessary to detect the crack with AE techniques - a decided advantage over other techniques.

The height of each step increase is porportional to the amplitude of the AE signal. Of course, both the number of events detected and the number of ringdown oscillations detected are each dependent upon the detection threshold and the amplifier gain settings, which were set to achieve a reasonable signal-to-noise relationship. These considerations aside, the AE data did indicate a nearly linear correspondence between the crack growth and AE rates as evidenced by the SEM micrograph and AE bargraph.

AE data from Crack N were analyzed at other flights. Figure 18 is a bargraph showing cumulative AE versus time for test flights 791 through 800. Most of the step increases, caused by single AE events occurred at the flight transitions. At these points, the amplitudes (number of

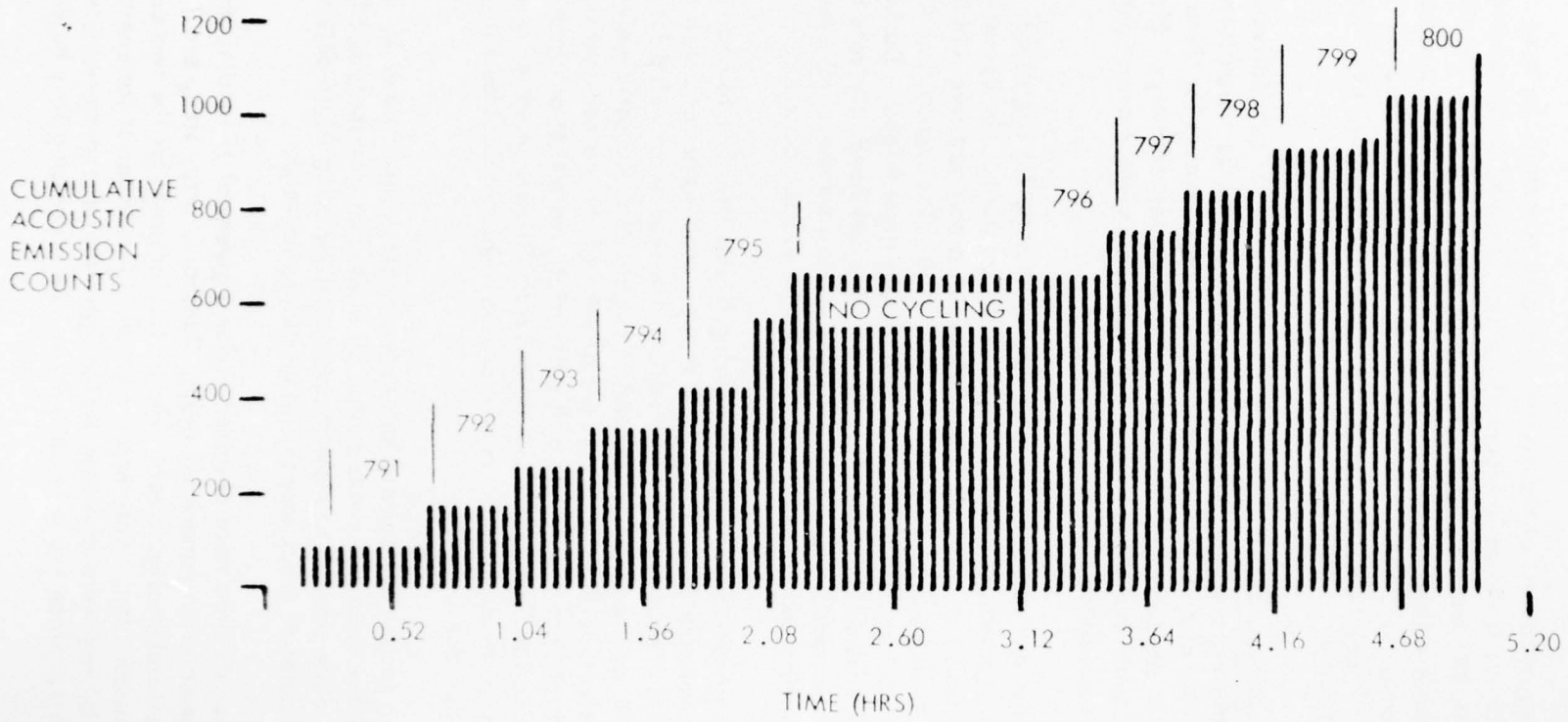

FIGURE 18. AE VERSUS TIME FOR CRACK 'N' AT FLIGHTS 791-800

ringdown counts) of the events were approximately the same. The amplitude is shown in Figure 19, which is a similar bargraph for flights 791 and 792. The flight transition at T-Flt 792 condition F1 shows a step increase of 88 counts over T-Flt 791, and the transition to T-Flt 793 showed a step increase of 82 counts. The other flight transition step increases were of similar, near constant, amplitudes.

Correlation, Test Cracks 4H and 5J. Curves for cumulative AE events and crack growth for test cracks 4H and 5J were plotted as a function of cumulative test flights. A set of curves for these test cracks are presented in Figures 20 and 21, respectively. Plots of AE counts (not shown) instead of AE events present a very similar correspondence.

For the segment of test flights shown, that is, for flights 801 through 2000, growth for crack 4H was nearly constant. The acoustic emission from the crack was accumulated at a constant rate within flights 801 through 1000 and 1201 through 1800. The cumulative AE follows the crack growth curve very well within these flights. During 200 flights from 1001 through 1200, on the other hand, the rate of AE event accumulation increased considerably for the crack growth occurring and caused a crossover in the plotted curves.

The growth for test crack 5J during flights from 801 to nearly 1600 was not constant. The growth showed small surges and slow downs before it reached the lower edge of the rear beam web prior to flight 1600, as indicated on the plot in Figure 21. Acoustic emissions received during the growth period did not show a constant accumulation rate nor did its rate coincide strictly with that of crack growth. During the flights, AE indications from 5J were observed on the AE monitor to be sporodic in arrival rate, which coincides with the plotted data.

Even though the correlations between crack growth and AE event rate for these two cases cannot be classed as extremely good, they are close enough to show the potential for using AE to determine estimates of crack length and crack growth rate.

These AE data were obtained under a given set of loading and instrumentation parameters (gain, threshold, array size, etc.) and structural configuration. The particular areas for the two cases were complex, contained a considerable number of fasteners or bolts, and were in moderate-to-high structure-borne noise environments. Since the AE system must share processing time between

Note: See Fig. 6 for description of "F" load conditions

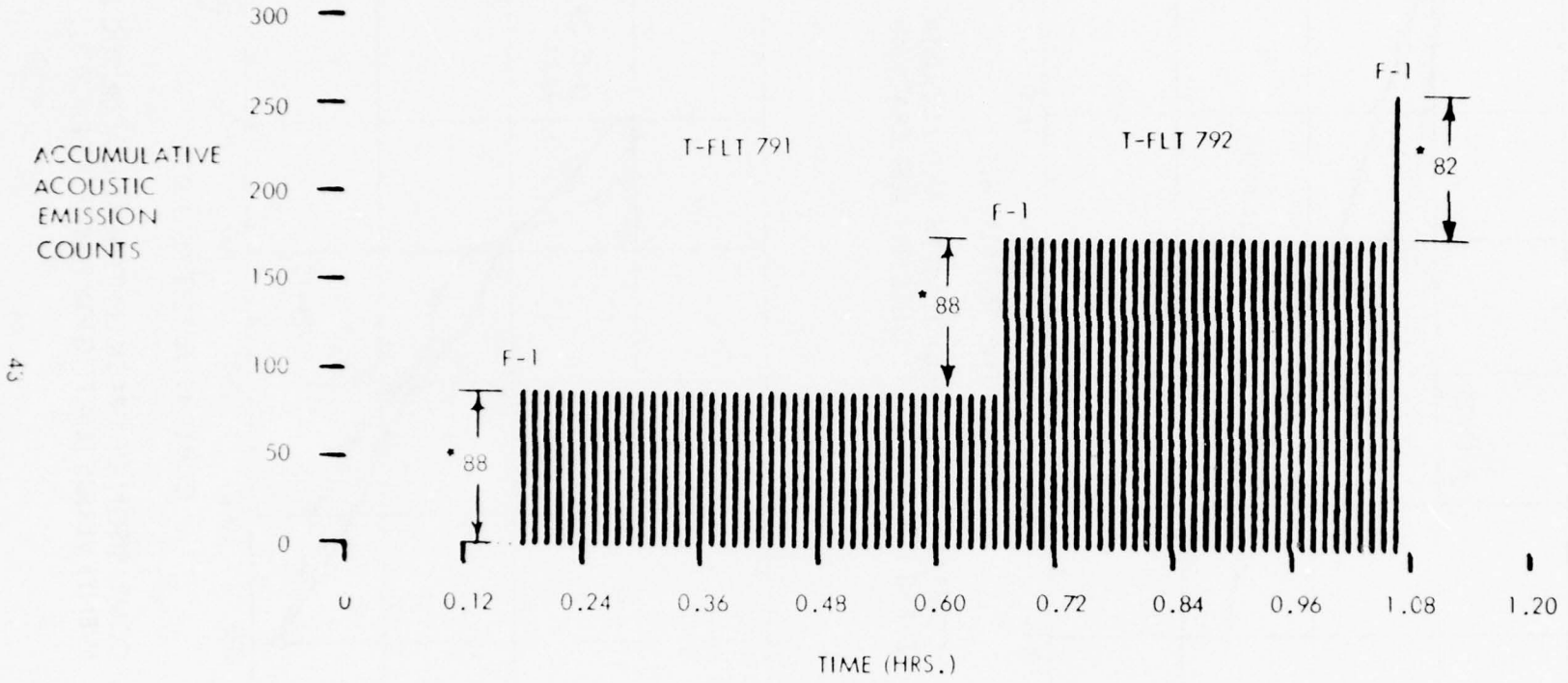

FIGURE 19. AMPLITUDE OF AE SIGNALS DURING FLIGHTS 791 AND 792

* Actual number of AE Counts in each of the 3 AE Events

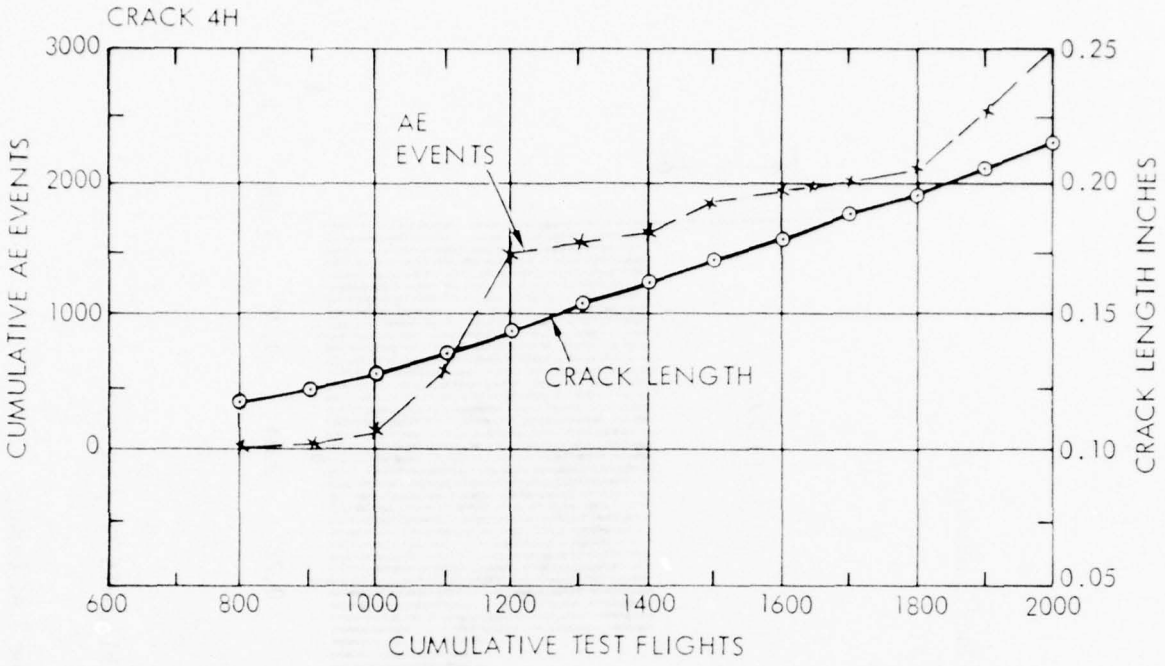

FIGURE 20. COMPARISON OF CRACK LENGTH AND ACOUSTIC EMISSION EVENTS VERSUS TEST FLIGHTS FOR TEST CRACK 4H.

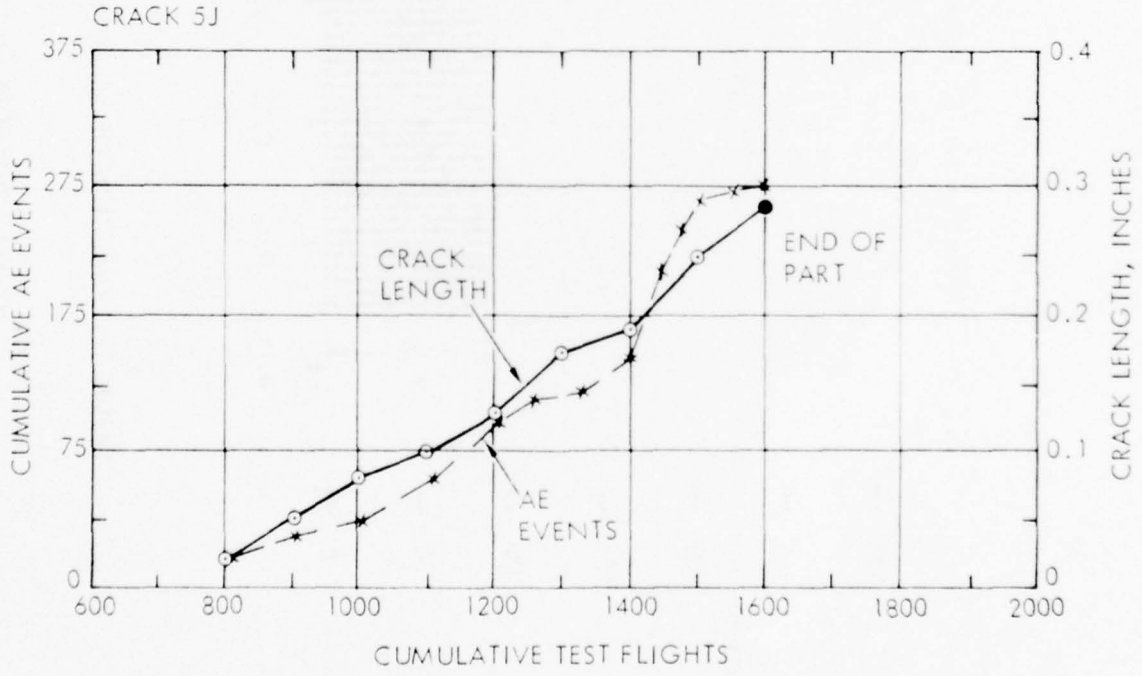

FIGURE 21. COMPARISON OF CRACK LENGTH AND ACOUSTIC EMISSION EVENTS VERSUS TEST FLIGHTS FOR TEST CRACK 5J.

noise signals and AE signals, the AE rates can be adversely affected if the structure-borne noise rate changes or if changes are made to any channel of the AE system in which sensitivity is greatly changed.

Due to such factors, apparent fluctuations in the AE rate as presented by the equipment do not necessarily mean actual fluctuations in AE from the crack source. The assumption can be made that the true AE rate caused by the growing crack very closely follows the actual rate of crack growth. But the protrayal of AE rate by the equipment depends on the selected system parameters, the system computer's time sharing responsibilities, and the structure noise environments.

3.2.6 Source Detectability

The experimental approach followed in this program was to monitor structure in test areas which contained known crack or damage at specific locations. The most probable AE source locations were, therefore, well defined and the coordinates which the equipment should compute for the known sources could be determined accurately. Thus, crack growth detection was a matter of observing whether persistent emissions were displayed within the range of defined coordinates.

Several observations of the source emissions were made which relate to the detectability. These were:

1) The locations of some known sources were accurately displayed, while
2) The locations of other known sources were displayed in a pseudo location, i.e, displaced location relatively to the true location.
3) The AE activity of some sources was relatively constant with time or flights, while
4) The AE activity of other sources was sporadic with time or flights.
5) The AE data from some sources displayed little spatial scatter, while
6) The AE data from other sources displayed considerable spatial scatter.
7) "Noise" is usually random in time and spatial origins.
8) Persistent sources with high activity other than the known, intentional sources were often present.

The odd-numbered factors above usually enhance the detection and increase the certainty that an AE source is valid. On the other hand, the even-numbered items are factors which complicate and detract from the detection process. All persistent

sources must be pinpointed within the structure and investigated. Regions containing scattered "noise" should also be investigated for possible discreet flaw sites.

Present AE equipment can provide only one detinite piece of information about a source: that an AE event has occurred. There is no means to differentiate between AE events caused by crack growth, fretting, structural slippage, expansion/contraction, microscopic metallurgical processes or other possible causes. The equipment displays the event irrespective of its cause and the investigator must resolve its meaning and determine whether it is or is not of concern to him.

Despite these potential difficulties, the fact that events are displayed on a plan view basis is a valuable tool for informing the investigator that something unusual is occurring in a narrow region of structure which he is monitoring. Much of the work involved in inspecting large areas is thus eliminated, for the inspector can limit his search to certain suspect regions and flag these regions for future periodic inspections.

SECTION IV

CONCLUSIONS

Crack growth was detected with acoustic emission techniques in complex full-scale aircraft structure loaded to simulated flight-by-flight spectra using commercially available acoustic emission equipment. Cracks were detected in structural locations where they would be very difficult or costly to detect with more commonly used NDT techniques because of accessibility problems. Such locations were under large splice plates, in inaccessible faying members and under fastener heads. Fastener removal or structural disassembly was not necessary to apply the AE techniques.

Discrimination against background noise was successful. Flaw source location techniques using a four-transducer array to provide real-time location of each AE event in a two-dimensional x-y coordinate system was used and is considered to be essential for monitoring an area of aircraft structure. Attempts to use a one-dimensional two-transducer location system were unsuccessful. Other noise discrimination techniques used included high band pass frequency filtering with cutoff of 350 KHz and signal threshold adjusted to eliminate the constant level background noise.

The time rate of AE events received from a growing crack was astonishingly small. Typically, only one or two events were detected during a unit flight. A unit flight

consisted of 51 load cycles and required from 20 to 30 minutes to complete. It was designed to induce the same fatigue as a "typical" four-hour service flight. Correlation analysis showed that an AE event was indication that a crack extension of the order of 10^{-4} inches had occurred. This indicates that from 100 to 200 flights are required to grow a crack 0.020 inches. This is the lower limit of detectability for conventional NDT techniques. This result provides insight into some major considerations necessary for an on-board AE monitoring system; namely, the detection reliability and management of the system. Note that this test was conducted on the test article of a large cargo aircraft and may not be applicable to other types of aircraft.

The correlation between AE data and crack growth were fairly good. The results of correlation studies on 3 cracks were presented. These correlations, together with the results of other AE work on the same test article (Ref. 6) show that AE has the potential for being used to determine crack size and crack growth rate. A qualitative measure of the change in crack growth rate can be accomplished with the present technology. However, a very precise system calibration together with AE tests on duplicate specimens would be required to establish a confidence level for determining crack size and crack growth rate.

System calibration with a standard AE signal source is essential for AE monitoring on aircraft structure. The standard source must be capable of producing, on command, acoustic signals which very closely simulate AE in rise-time, pulse shape, frequency content, amplitude, and must be capable of introducing the standard signal into the test piece at a point source such as a crack tip. The standard source is needed to establish and verify sensor array parameters, set gain and threshold settings, trace source origins and determine their coordinates, determine signal losses in the material and across joints, and to verify system operation. Work is being conducted at the National Bureau of Standards on a device that promises to meet these requirements. A prototype was used on this program.

The distance over which an AE event can be detected and the layout of an array of transducers used in monitoring aircraft structure is dictated by the complexity and geometry of the structure. An AE event can be reliably detected across one joint assembled with mechanical fasteners but not across two joints. Likewise, an AE signal can be detected across one row of fasteners but not reliably across two rows. Transducer array sizes used on this program ranged from 8 inches to 48 inches between transducers.

The background noise and the AE response characteristics of this test article may not be totally representative of in-service aircraft. Although the test article was a production-size wing structure, there are many differences which should be noted: 1) the test article had been subjected to two aircraft lifetimes of fatigue prior to starting the monitoring program. This probably accounts for some of the spurious flaw source signals encountered during the tests, 2) the load was applied to the structure by servo-controlled hydraulic jacks through mechanical linkages attached to the

structure. The relative magnitude of the background noise generated by the method of loading and that produced by aerodynamic lift is not known, 3) the tests were conducted at room temperature with no attempt to simulate flight environment, 4) the test article consisted of the load carrying box structure without any of the mechanical, hydraulic, or electrical flight systems installed. The electrical controls for these systems are known to generate a severe EMI environment for AE system operation, 5) the fuel tank sections of the test article were not integrally sealed and hence did not contain aircraft fuel. This test condition probably enhanced the AE signal transmission characteristics.

SECTION V

RECOMMENDATIONS

Acoustic emission technology for aircraft applications is in its infancy and only a few general solutions have been developed to solve the many problems peculiar to monitoring the many types of complex aircraft structure. Basically, the results of this AE monitoring program have demonstrated that AE techniques can be used to monitor crack growth in a limited number of locations on a production-size wing fatigue test article during simulated flight loading. The major problems associated with long-term unattended AE system operational reliability in the various aircraft mission profiles and flight environment have only been talked about. A melding of the highly sophisticated aircraft electronic technology and the existing AE technology can solve the problems necessary to produce an on-board AE system that can be successfully demonstrated. Consequently, we believe that any future work be very carefully coordinated to include the aircraft electronics, the structural design for the selected application, and the aircraft mission profile.

We recommend that future work be done to define the general requirements of a practical on-board AE system. Factors to be determined include detailed definition of the major elements of the system and its operation, including the sensors, amplification and signal processing, data storage, data analysis and interpretation, calibration and checkout procedures, system maintenance, and inspection/verification procedures. Of primary importance are considerations for the separation of on-board and ground-based functions and portions of the system; how the data should be handled and by whom; under what conditions should a source be regarded as a flaw suspect and how or when to verify.

It is further recommended that for any aircraft on which an AE system is installed, there be a full-scale specimen of the identical structure available for on-ground system development and evaluation. The value of this approach is that it permits sensor arrays to be defined, optimized and verified so that an identical proven array can be installed at the same location on the aircraft; permits prior detection and resolution of problems; noise sources can be eliminated, minimized or avoided; provides a test bed for evaluation of peculiar results that may be obtained on the aircraft; and provides a ready means to trace a source to its structural origin when verification problems are reported from the fleet.

APPENDICES

APPENDIX A

APPENDIX B

APPENDIX C

APPENDIX D

APPENDIX E

APPENDIX F

APPENDIX G

APPENDIX H

APPENDIX I

APPENDIX A

DESCRIPTION OF TEST AREAS

APPENDIX A

DESCRIPTION OF TEST AREAS

Area 1 consists of a portion of the lower surface mid-beam spanwise splice containing test holes A, B, and C at IWBRS(s) 240, 234.75, and 229.50, respectively. The test holes contained initial sawcut flaws in either one or both members of the splice on fore- or aft-sides of the hole.

Area 2 consists of a portion of the lower mid-beam cap riser-to-web splice from IWBRS 96 to 136. Test holes D and E which contain initial sawcut flaws are at IWBRS 100.25 and 96, respectively. Test holes O, P, and Q contained existing fatigue cracks and are located in the stiffener base attachment area at IWBRS 134.5.

Area 3 consists of a portion of the rear beam cap at IWBRS 396. Test holes F and G are along the aft edge of the cap/hinge-half attachment area. Both test holes contained initial sawcut flaws.

Area 4 consists of test hole H in center wing panel No. 2 at the W.S. 120 wing joint. The bolt hole contains an initial sawcut flaw and is covered by a chordwise splice plate on the exterior lower surface.

Area 5 is a portion of the rear beam lower cap-to-web splice between IWBRS 178 to 194. The area contains test holes I, J, and K, which had initial sawcut flaws in the web. The area is bracketed inboard and outboard by two external stiffeners and is divided by one internal stiffener which presents a double row of fasteners.

Area 6 is a portion of inner wing skin panel No. 4 at the W.S. 577 wing joint which is covered with a chordwise splice plate on the lower exterior surface. Test hole L in this area contained an initial sawcut flaw.

Area 7 consists of the inner wing panel No. 9 runout at IWBRS 337 at the front beam and contains test hole M. The hole contained an initial sawcut flaw. This area was not monitored for acoustic emission.

Area 8 consists of a portion of the inner wing panel No. 2 to panel 3 spanwise splice in the vicinity of IWBRS 217.25. The area contained test hole N which had an existing fatigue crack at the start of the tests.

APPENDIX B

DESCRIPTION OF ACOUSTIC EMISSION SYSTEM COMPONENTS

APPENDIX B

DESCRIPTION OF ACOUSTIC EMISSION SYSTEM COMPONENTS

1. Transducers: (a) S750 - Single-ended with a peak frequency response generally above 700 KHz. The sensitivity at the resonant frequency ranged from approximately -80 db to -76 db referenced to 1 volt per microbar. Calibration was accomplished by the supplier* using the ultrasonic technique and comparison with a standard transducer.

   (b) D9202 - This is a differential transducer for elimination of common-mode electrical noise and has a sensitivity peak between 450 to 550 KHz. The peak sensitivity ranged from -80 db to -76 db referenced to 1 volt per microbar. Calibration was performed by Dunegan/Endevco using the Spark Impact Bar Technique (Reference 4).

2. Preamplifier: 40 db fixed gain with a peak output of 5V into 50 ohms. High pass filters with cutoff at 350 KHz and a 48 db per octave roll-off. Bandwidth is from 350 KHz to 2 MHz and a noise level of 5 V (rms).

3. Signal Conditioner: Adjustable gain from zero to 60 db in 1 db steps. Also, generates digital pulses for timing the signal arrivals.

4. Analog/Audio Monitor Selector and Buffers: Allows selection of an array for off-line monitoring and processing and provides an audio indication of the acoustic activity from any of the 32 channels.

5. Test Pulse Generator: Provide pulses, with amplitude of zero to 25 volts and repetition rate of one to 100 pulses per second, to a test transducer located in an array to verify normal operation and to perform periodic array calibration checks.

6. Minicomputer: Performs AE source location calculations, formats and stores data for CRT display and cassette recording, monitors keyboard for operator commands, and issues control commands for efficient system operation.

7. CRT Device: Converts digital data to precise analog voltages for CRT beam deflection for real-time display.

8. Storage Cathode Ray Tube: Displays real-time dual histograms of events and counts, providing an indication of severity and activity within all arrays or will display simultaneously the event histogram and any one of the eight arrays. This feature allows assessment of the activity within an array while monitoring the total events occurring within individual arrays.

---

*Dunegan/Endevco, San Juan Capistrano, Calif.

9. Hard Copy Unit: Produces an 8-1/2" x 11" paper hard copy of the CRT display.

10. Printer/Cassette Recorder: Contains a teleprinter and a dual cassette recorder. The teleprinter keyboard allows the operator to enter calibration data and commands to the system, and the printer produces a printout of the test data, post-test analysis results, and computer responses to commands. The dual cassette recorder allows simultaneous recording of real-time data and playback of previously recorded data. The recorder is also used to enter programs into the computer.

APPENDIX C

1032 FLAW LOCATOR SYSTEM INPUT/OUTPUT DATA FORMATS

APPENDIX C

```
ARRAY  0

  LINE,ARR,OFF A
  EDGE=12
  CAL VALUE=1100
  MAX DT=1100

ARRAY  1

  LINE,ARR,OFF A
  EDGE=10
  CAL VALUE=910
  MAX DT=910

ARRAY  2

  LINE,ARR,OFF A
  EDGE=23.5
  CAL VALUE=2145
  MAX DT=2145

ARRAY  3

  LINE,ARR,OFF A
  EDGE=12.5
  CAL VALUE=1145
  MAX DT=1145

ARRAY  4

  LINE,ARR,OFF A
  EDGE=15
  CAL VALUE=1365
  MAX DT=1365

ARRAY  5

  LINE,ARR,OFF A
  EDGE=14.3
  CAL VALUE=1300
  MAX DT=1300

ARRAY  6

  LINE,ARR,OFF A
  EDGE=48.3
  CAL VALUE=4380
  MAX DT=4380

ARRAY  7

  LINE,ARR,OFF A
  EDGE=12
  CAL VALUE=1100
  MAX DT=1100

HARD. MAX DT= 4380
```

FIGURE C1. ACOUSTIC EMISSION ARRAY DATA AS PROGRAMMED INTO THE AE SYSTEM COMPUTER PER THE DUNEGAN/ENDEVCO VESSEL TESTING PROGRAM - VERSION 4.

APPENDIX C

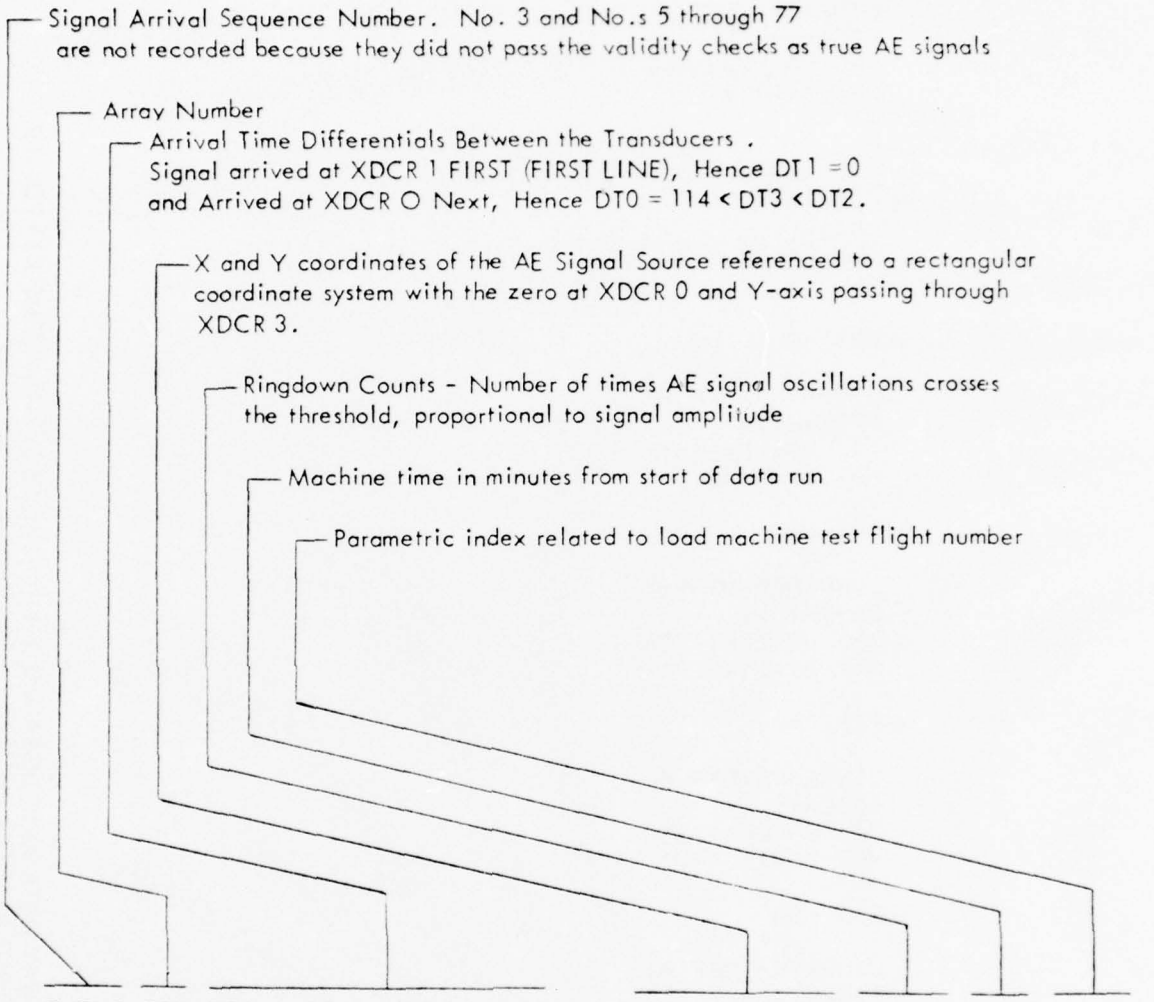

EVENT	ARY	DT0	DT1	DT2	DT3	X	Y	COUNTS	TIME	CYCLES
2	3	114	0	748	887	-3.5	-1.6	88	0	1602
4	3	161	0	845	896	-4.0	-0.9	70	0	1602
78	7	331	958	399	0	7.3	7.8	24	1	1602
102	1	37	531	78	0	4.7	3.3	299	1	1603
2111	3	84	0	746	746	-3.3	-1.8	64	187	1603

FIGURE C2. ACOUSTIC EMISSION ARRAY DATA FORMAT

APPENDIX C

Format, Counts Vs Time for Total Counts

```
D:E WTS.C.2  POST TEST ANALYSIS

MODE= T  ( TOTAL )

DATA= C  ( COUNTS )
ACTIVE ARRAYS= 7
BOUNDS:
   X: 0.0,4.5
   Y: -7.5,-3.3

VS T ( TIME )
TIME BOUNDS= 0-700

RUNS PER CASSETTE= 1
READY CASSETTE?
```

Format, Event Vs Time for Event Rate

```
D:E WTS.C.2  POST TEST ANALYSIS

MODE= R  ( RATE )

DATA= E  ( EVENTS )
ACTIVE ARRAYS= 7
BOUNDS:
   X: 0.0,4.5
   Y: -7.5,-3.3

VS T ( TIME )
TIME BOUNDS= 0-700

RUNS PER CASSETTE= 1
READY CASSETTE?
```

FIGURE C3. EXAMPLES OF THE POST-TEST ANALYSIS PROGRAM INPUT DATA FORMATS USED WITH THE 32-CHANNEL ACOUSTIC EMISSION SYSTEM

APPENDIX D

HISTORY OF ARRAYS AT EACH TEST AREA

APPENDIX D

HISTORY OF ARRAYS AT EACH TEST AREA

Area 1. Figure D1 illustrates the arrays used in Area 1. Through the 800th unit test flight, a linear array of two transducers separated by 20 inches was used to monitor Area 1 (see Figure 3). The array was installed along the splice inside the wing box to monitor crack growth at all three test holes. For flights 801 through 1200, a triangular array of four transducers was installed outside the wing box on the wing panel number 4 lower surface. From flights 1201 through 1400, the array was repositioned to include the wing plank joint. After flight 1400, cracks A, B, and C were cut out for metallographic examination.

Area 2. Figure D2 illustrates the arrays used in Area 2. Initially, a 39-inch linear array was installed spanwise along the cap to monitor all five test holes simultaneously A very high structural noise level necessitated changing to a 4-transducer triangular array which was installed on the web midway between the two sets of test holes. Acoustic emission pick-up was inhibited by multiple rows of fasteners at web stiffener attachment areas, so a new triangular array using D9202 transducers was installed on the web near the IWBRS 134.5 stiffener to monitor test holes O, P, Q and a new 15-inch linear array was installed in the vicinity of the IWBRS 97.25 stiffener to monitor test holes D and E. The last two arrays used through flight 1200 are shown in Figure D2. From flights 1201 through 2000, new triangular arrays were installed on the mid-beam cap to monitor the two sets of test holes and are shown in Figure D3.

Area 3. Arrays used in area 3 are illustrated in Figure D4. A 20-inch linear array was used through flight 800 to monitor the two test holes. In addition, the British AML transducers and cables were installed similarly in this area to provide a parallel comparison with the linear Lockheed array. A triangular array was installed to replace the linear array and was used during flights 801 through 2000.

Area 4. Arrays used in Area 4 are illustrated in Figure D5. Initially, a 9-inch linear array was installed parallel to the splice on CW Panel No. 2 to monitor the test hole, but a relatively high structural noise level necessitated changing to a triangular array following flight 140. The latter array, having an 8-inch transducer separation, was used through flight 1200 and is shown at the top of Figure D5. For flights 1201 through 2000, the array was expanded to 15 inches and included a spanwise plank joint, as shown at the bottom of the figure.

Area 5. Figure D6 illustrates the arrays used in Area 5. A 12-inch triangular array was used to monitor this area throughout the first 1200 flights, as shown in the figure. During flights 1201 through 2000, a modified 12-inch array shown at the bottom of Figure D6 folded across the web-to-cap joint was used.

Area 6. The array used in Area 6 is shown in Figure D7. Initially, a 15-inch linear array installed parallel to and near the W.S. 577 joint on inner wing panel number 4 was used to monitor crack growth in the test hole. After T-Flt 101, a triangular array was installed. After T-Flt 437, the position of this array was "rotated" about the test hole to improve the acoustic emission display characteristics and was used through flight 2000.

Area 7. This area was not monitored with the acoustic emission system.

Area 8. Figure D8 illustrates the array used in Area 8. The area was monitored with a 20-inch triangular array which was "rotated" about N after T-Flt 437 to improve the acoustic emission display characteristics.

Area 9. The arrays used in Area 9 are shown in Figure D9. A 20-inch triangular array was installed here to obtain baseline noise background data through flight 800. The size of the array was extended to 48 inches for flights 801-2000, and thus included the joint between inner wing panels 3 and 4.

APPENDIX D

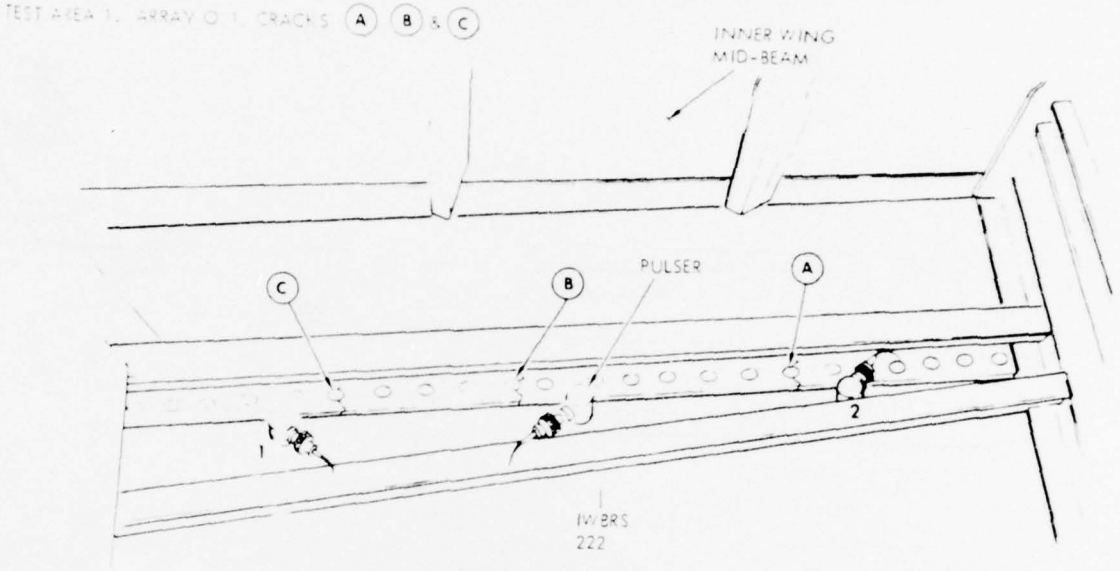

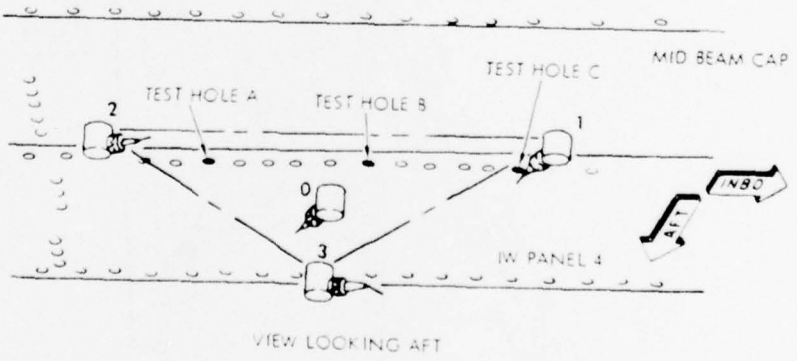

FIGURE D1. TEST AREA 1, ARRAY 0/1, TEST HOLES A, B, AND C. INITIAL LINEAR ARRAY AND FINAL TRIANGULAR ARRAY SHOWN.

APPENDIX D

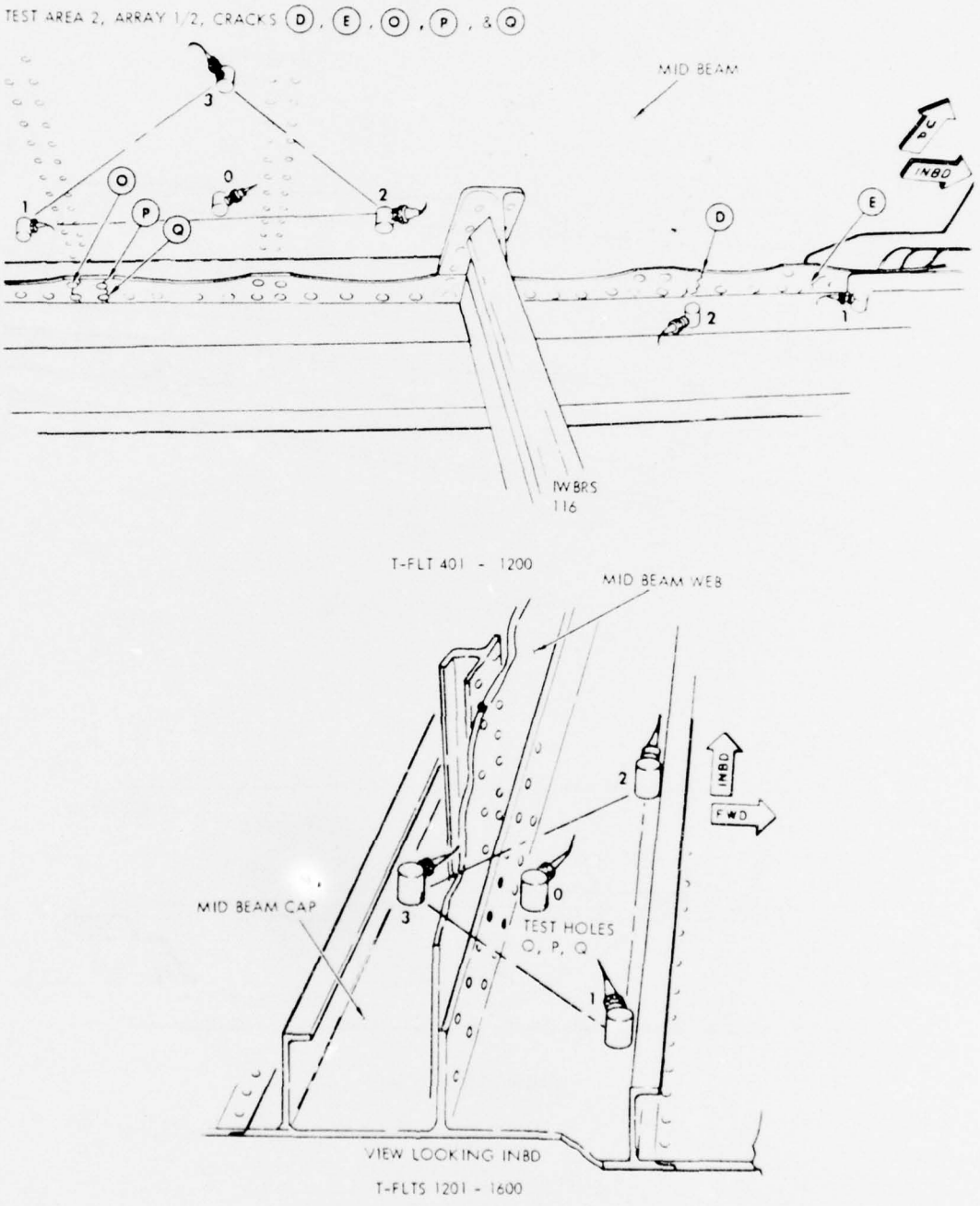

FIGURE D2. TEST AREA 2, ARRAY 1/2, TEST HOLES D, E, O, P & Q. INTERMEDIATE LINEAR ARRAY FOR HOLES D & E AND INTERMEDIATE AND FINAL TRIANGULAR ARRAYS FOR HOLES O, P AND Q SHOWN.

APPENDIX D

TEST AREA 2, ARRAY 7/2.

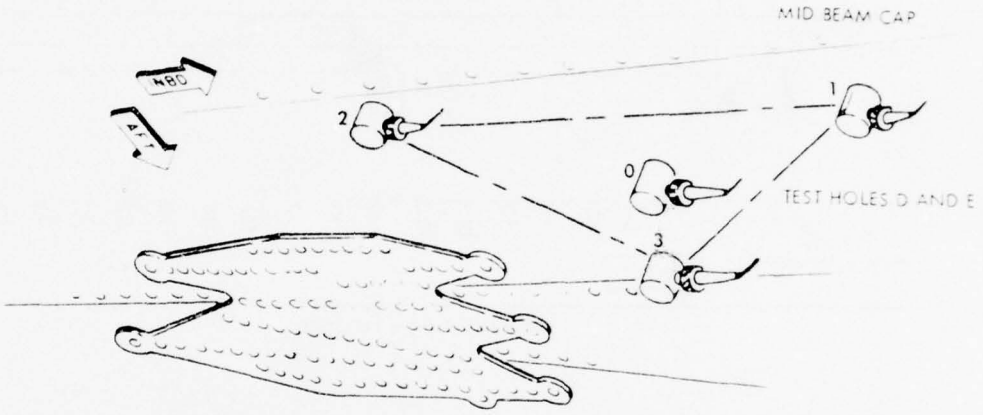

VIEW LOOKING AFT

T-FLTS 1201 - 1600

NOTE

TEST HOLES D AND E CANNOT BE SEEN FROM THE BOTTOM OF THE BEAM CAP AS SHOWN ABOVE. SEE FIGURE 11 FOR LOCATION.

FIGURE D3. TEST AREA 2, ARRAY 7/2, TEST HOLES D & E. FINAL TRIANGULAR ARRAY SHOWN INSTALLED ON LOWER SURFACE OF WING BOX.

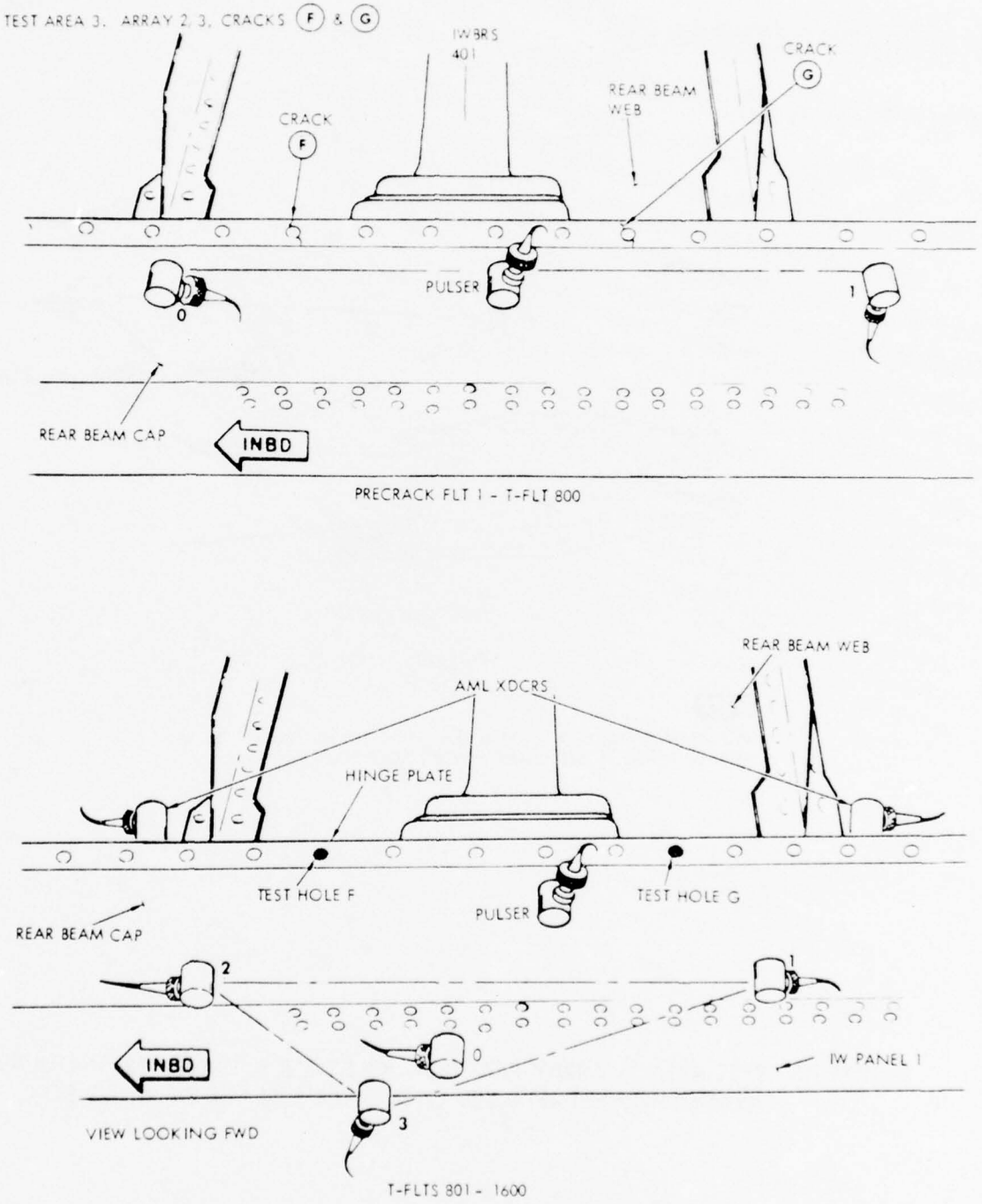

FIGURE D4. TEST AREA 3, ARRAY 2/3, TEST HOLES F AND G. INITIAL LINEAR ARRAY AND FINAL TRIANGULAR ARRAYS SHOWN.

APPENDIX D

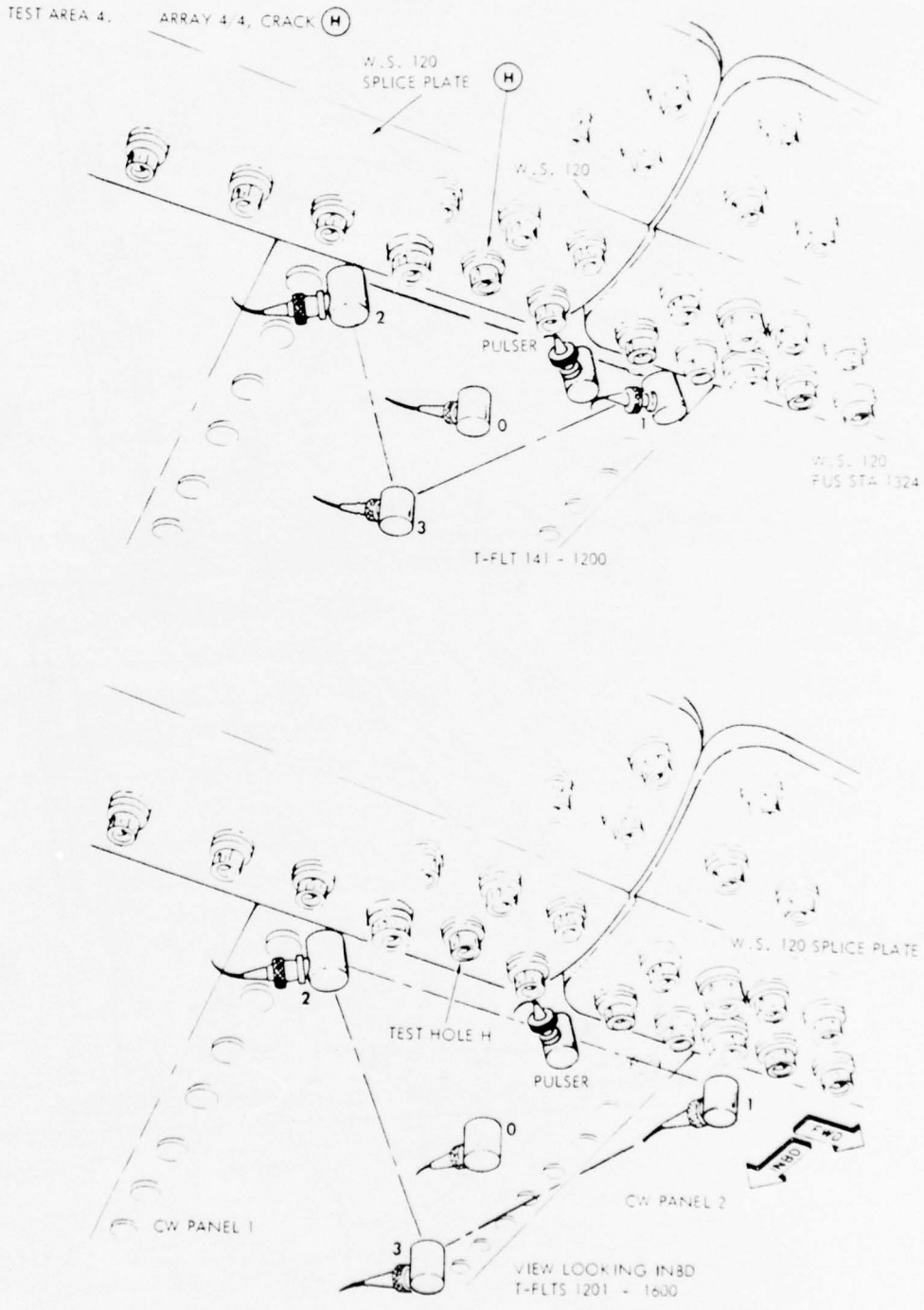

FIGURE D5. TEST AREA 4, ARRAY 4/4, TEST HOLE H. INTERMEDIATE AND FINAL TRIANGULAR ARRAYS SHOWN.

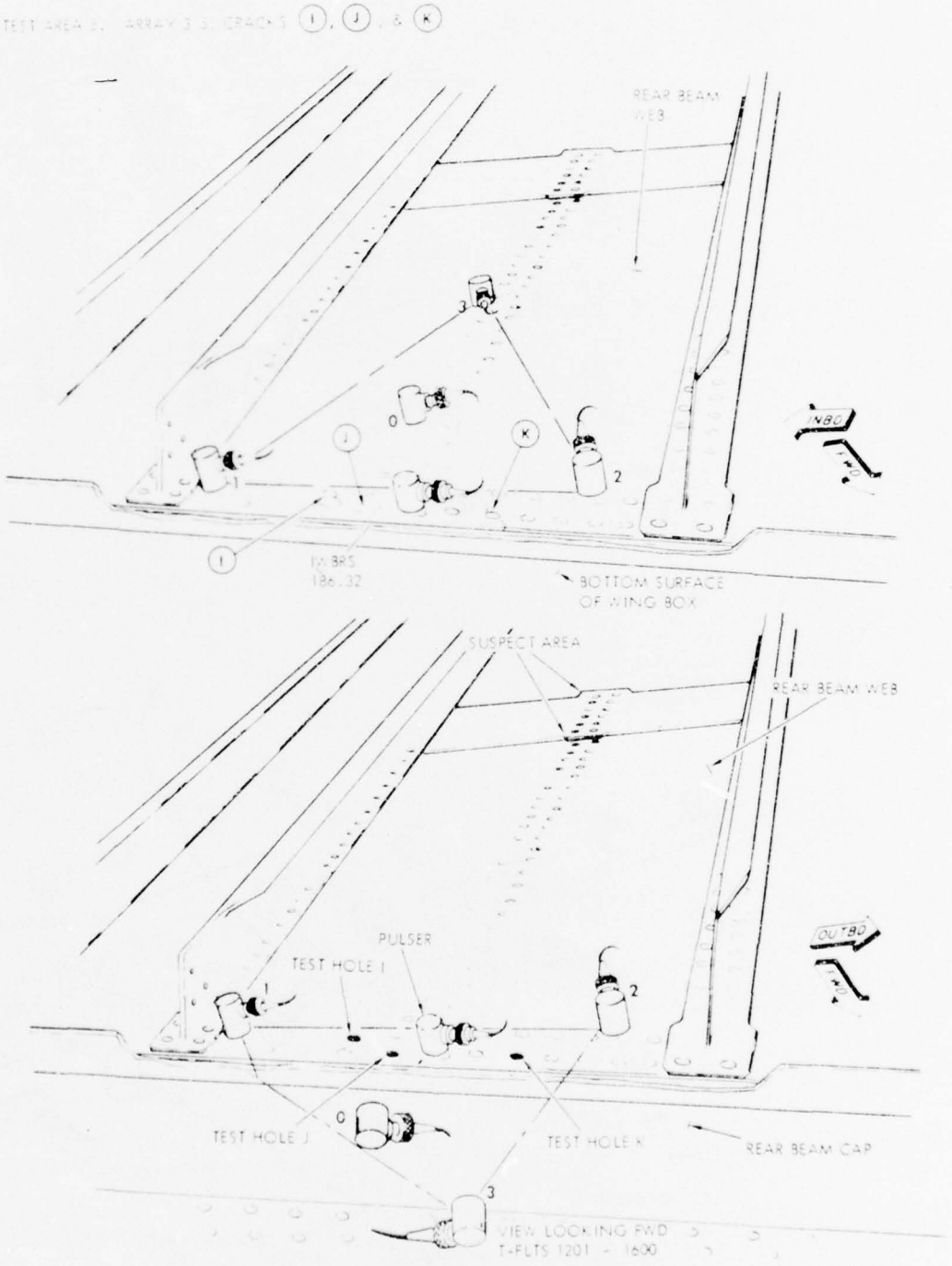

FIGURE D6. TEST AREA 5, ARRAY 3/5, TEST HOLES I, J AND K. INITIAL AND FINAL TRIANGULAR ARRAYS SHOWN.

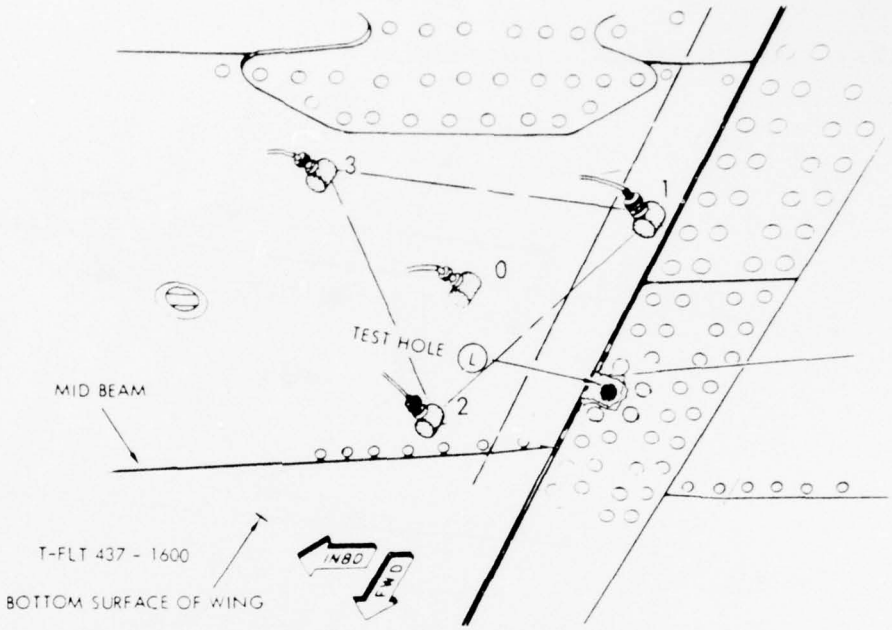

FIGURE D7. TEST AREA 6, ARRAY 5/6, TEST HOLE L. FINAL TRIANGULAR ARRAY SHOWN IN "ROTATED" POSITION.

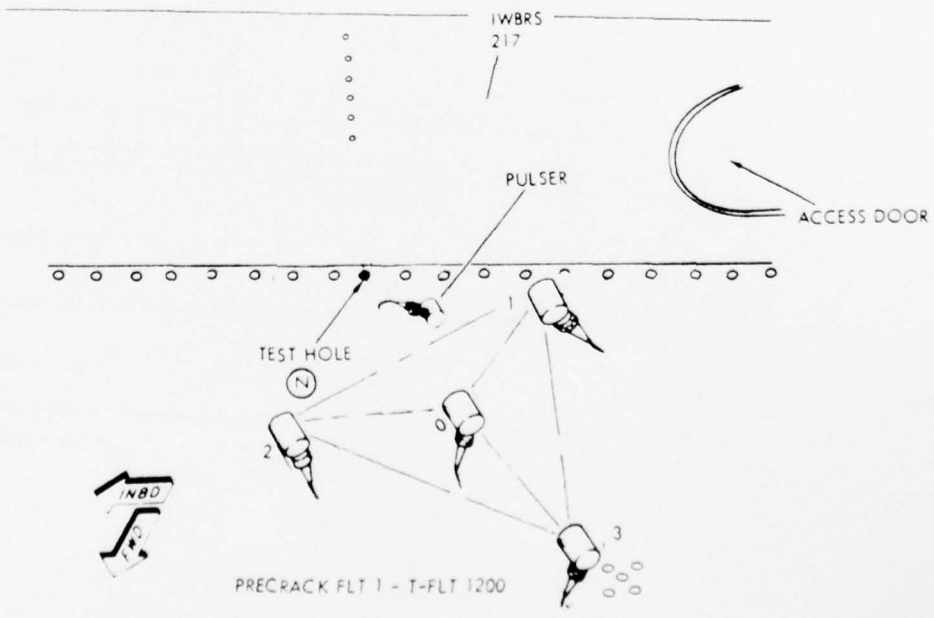

FIGURE D8. TEST AREA 8, ARRAY 7/8, TEST HOLE N, TRIANGULAR ARRAY SHOWN IN "ROTATED" POSITION.

APPENDIX D

TEST AREA 9. REFERENCE ARRAY 6/9. NO KNOWN CRACKS

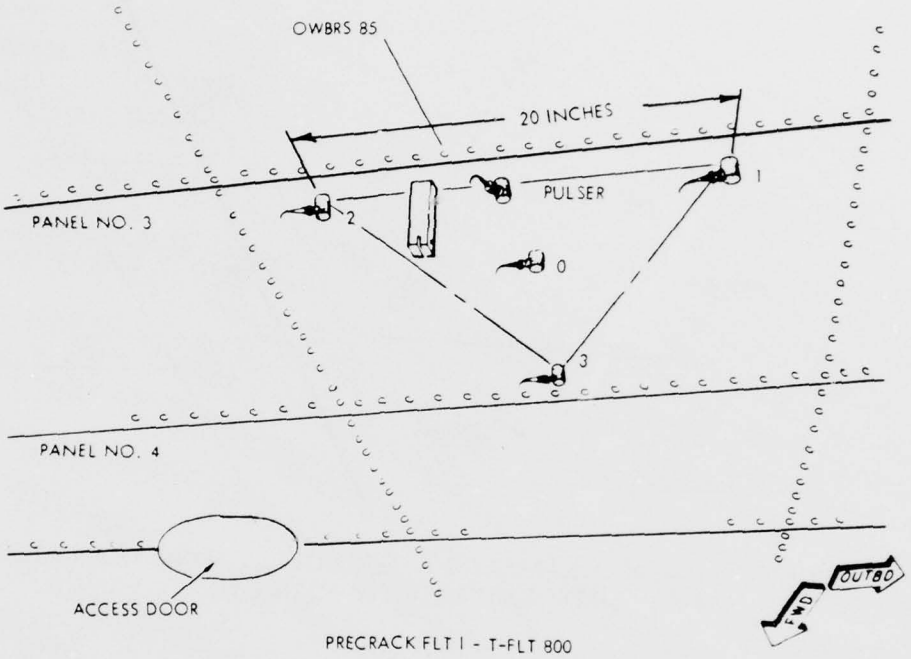

PRECRACK FLT 1 - T-FLT 800

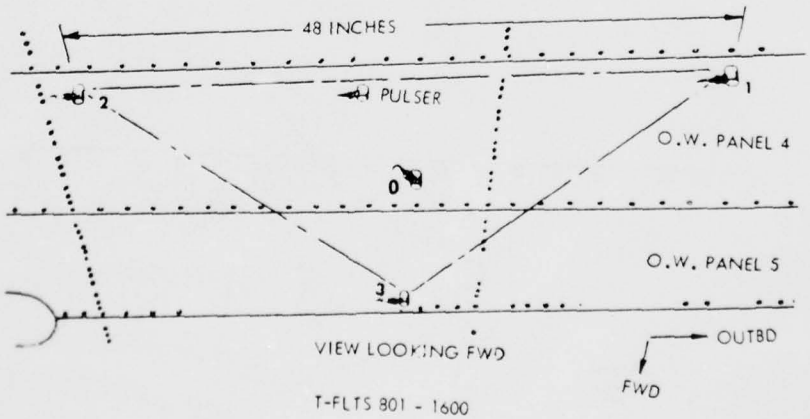

T-FLTS 801 - 1600

FIGURE D9. TEST AREA 9, ARRAY 6/9, NO KNOWN CRACKS. INITIAL AND FINAL TRIANGULAR ARRAYS SHOWN.

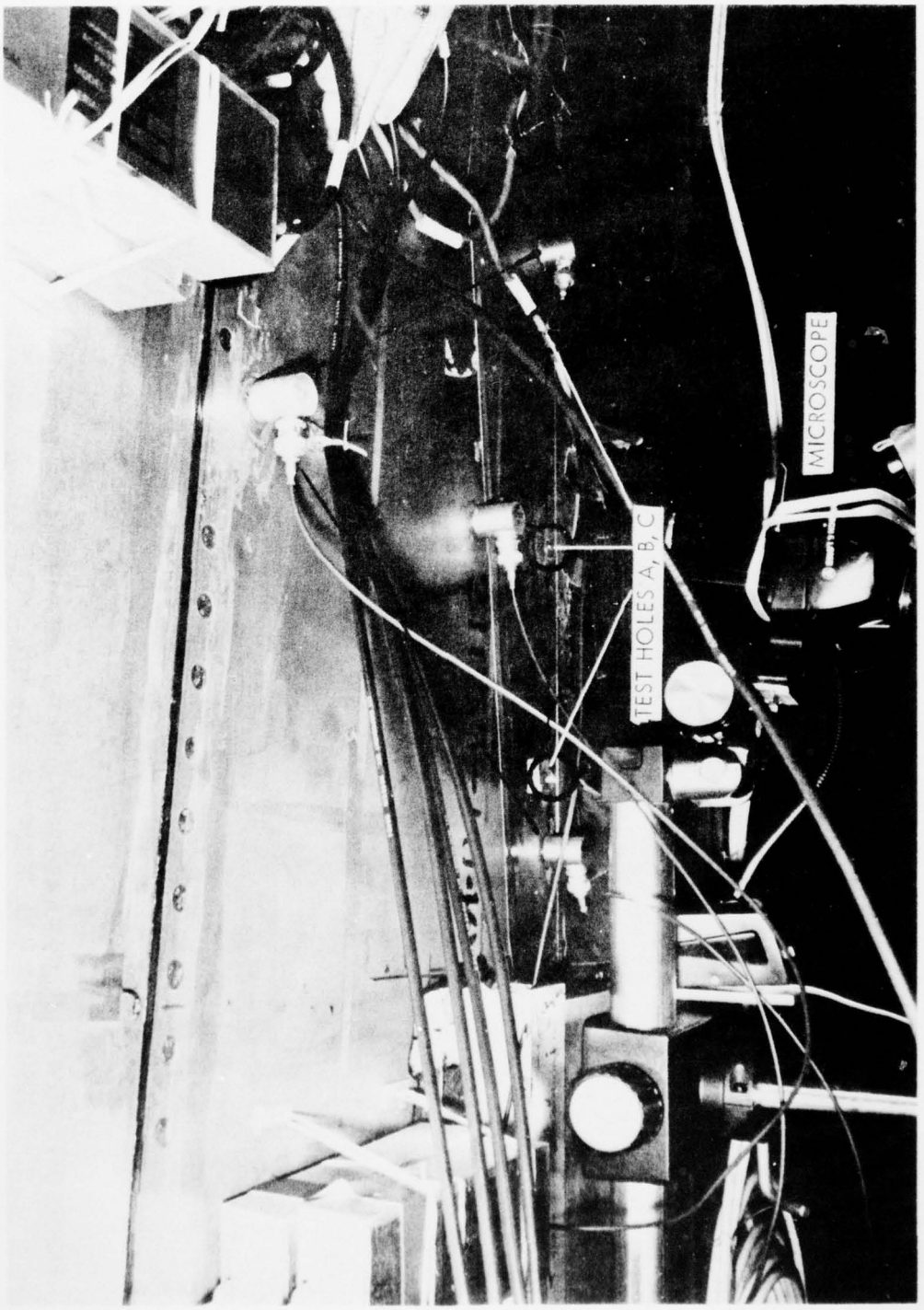

FIGURE D10. VIEW OF TRIANGULAR ARRAY O 'N TEST AREA 1 FOR MONITORING TEST HOLES A, B AND C DURING TEST FLIGHTS 1201 THROUGH 1400

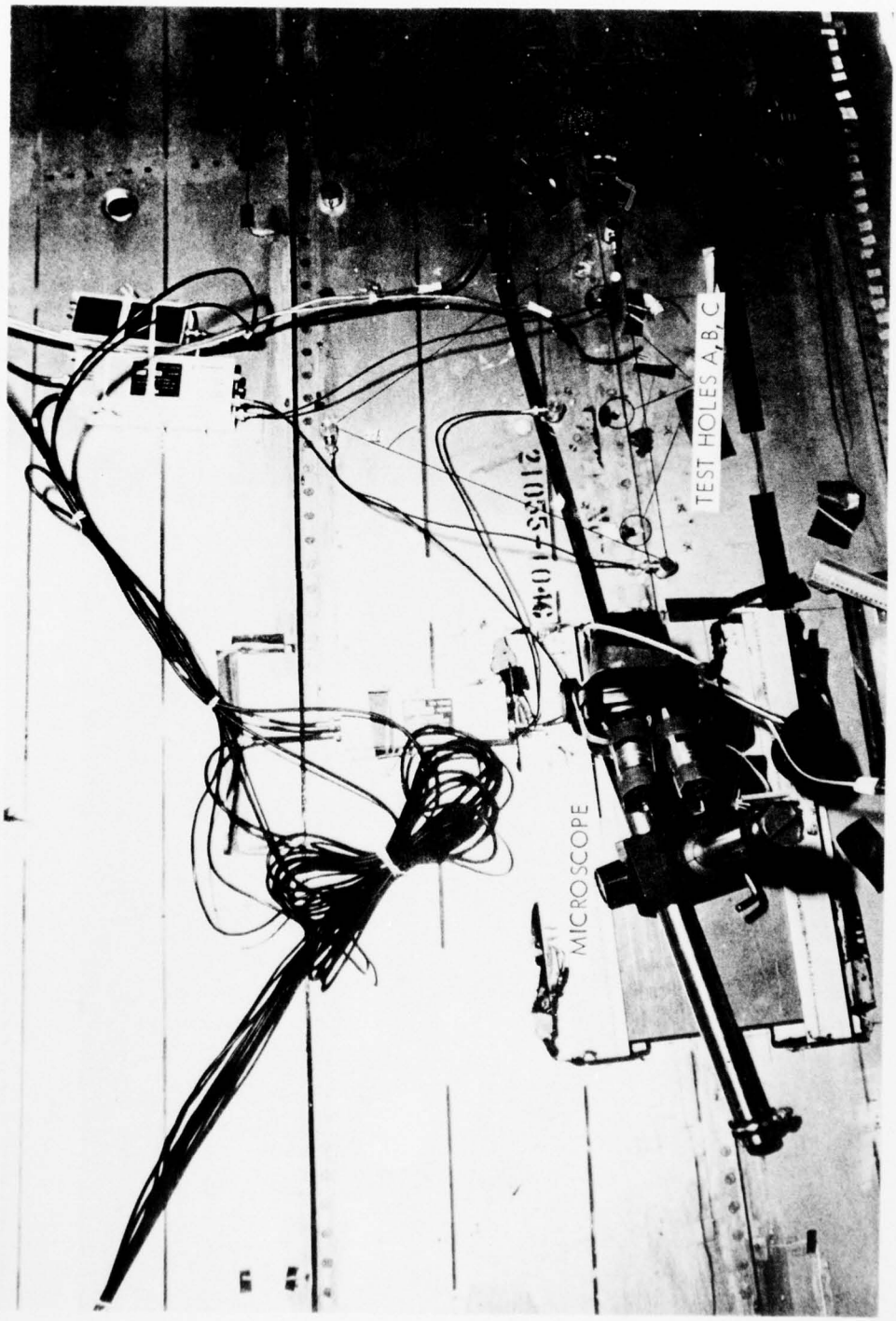

FIGURE D11. VIEW OF TRIANGULAR ARRAY O IN TEST AREA 1 FOR MONITORING TEST HOLES A, B, AND C DURING TEST FLIGHTS 801 THROUGH 1200

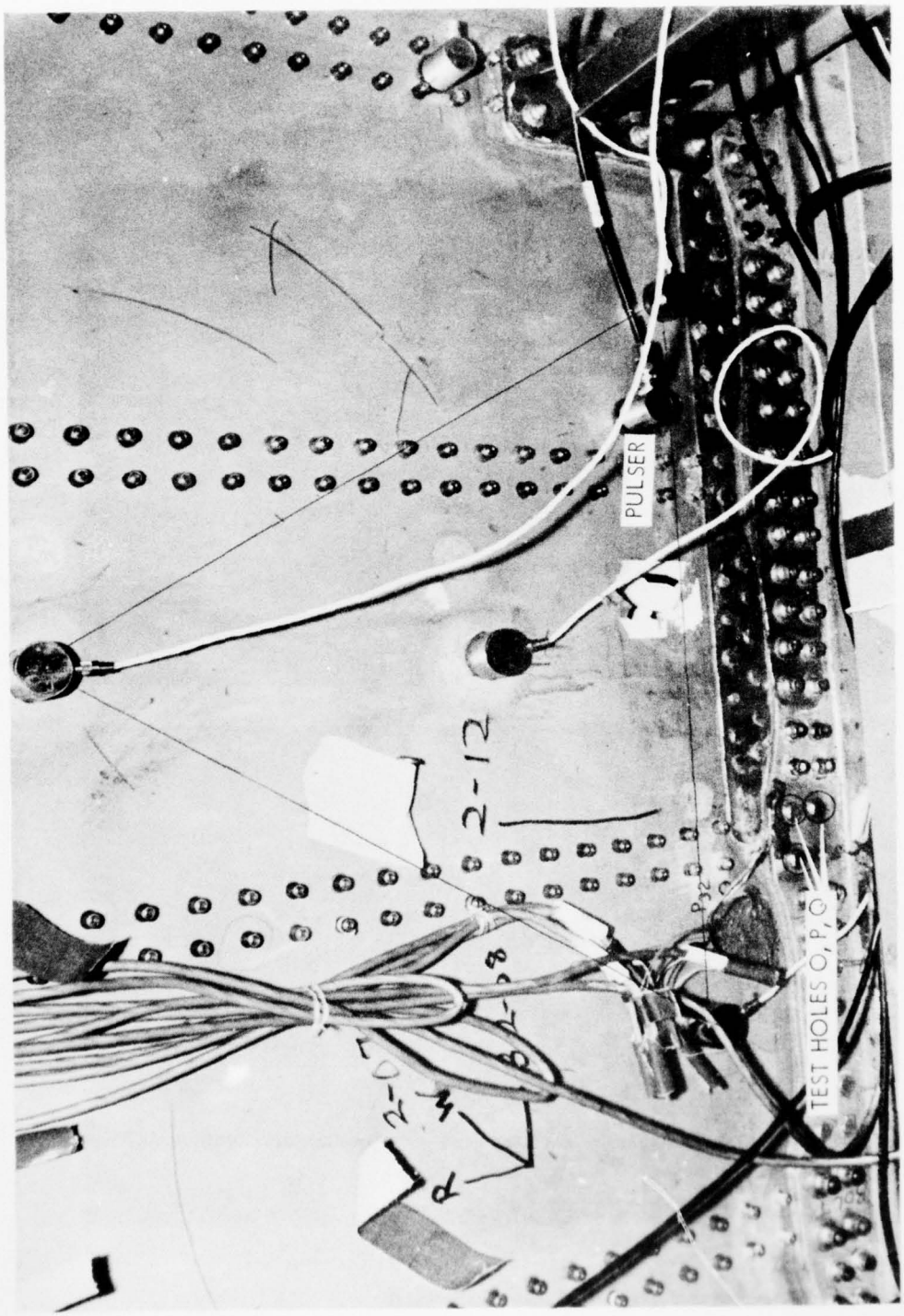

FIGURE D12. VIEW OF TRIANGULAR ARRAY 1 IN TEST AREA 2 FOR MONITORING CRACKS O, P, AND Q DURING TEST FLIGHTS 401 THROUGH 1200

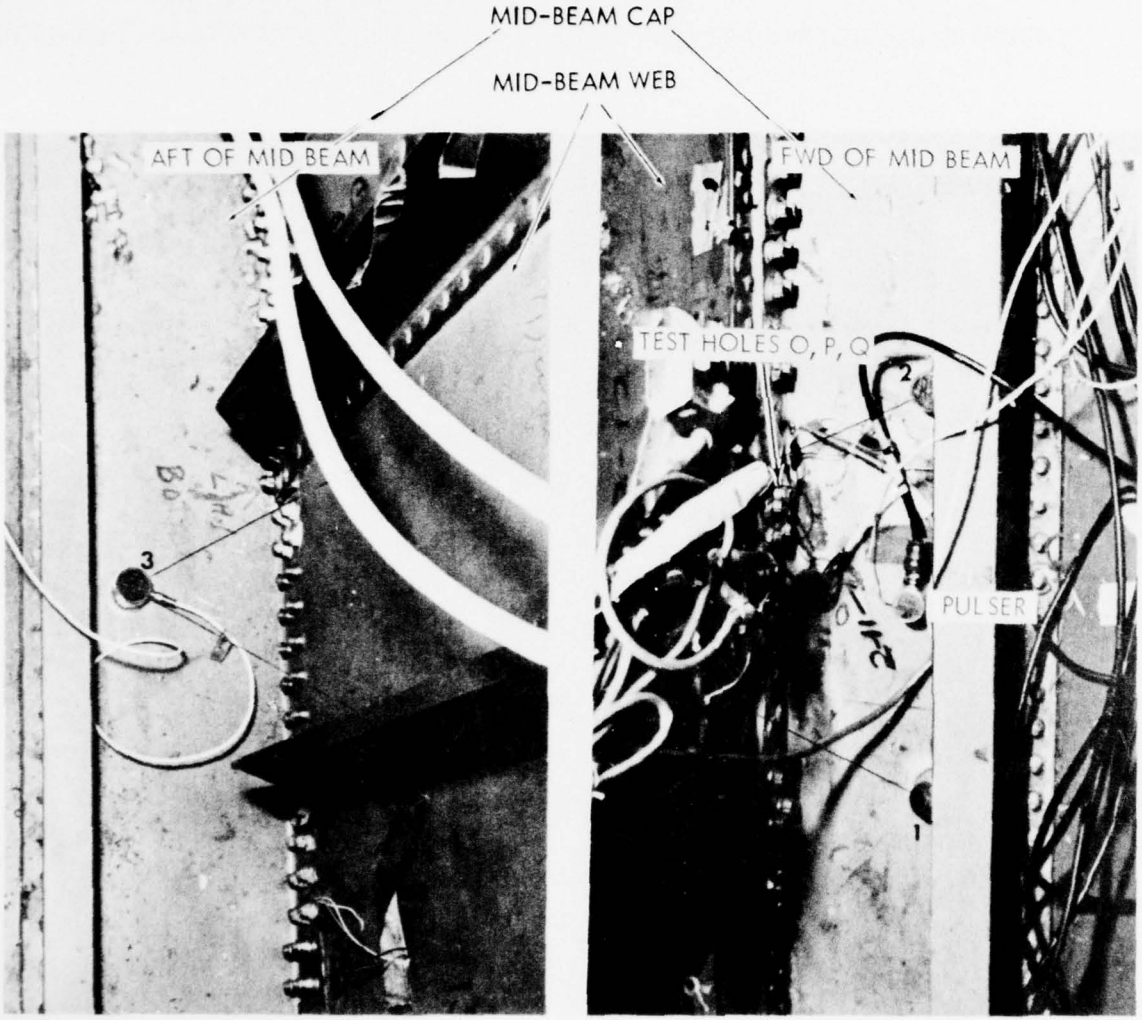

FIGURE D13. SPLIT VIEW OF TRIANGULAR ARRAY 1 IN TEST AREA 2 FOR MONITORING TEST HOLES O, P, AND Q DURING TEST FLIGHTS 1201 THROUGH 1600

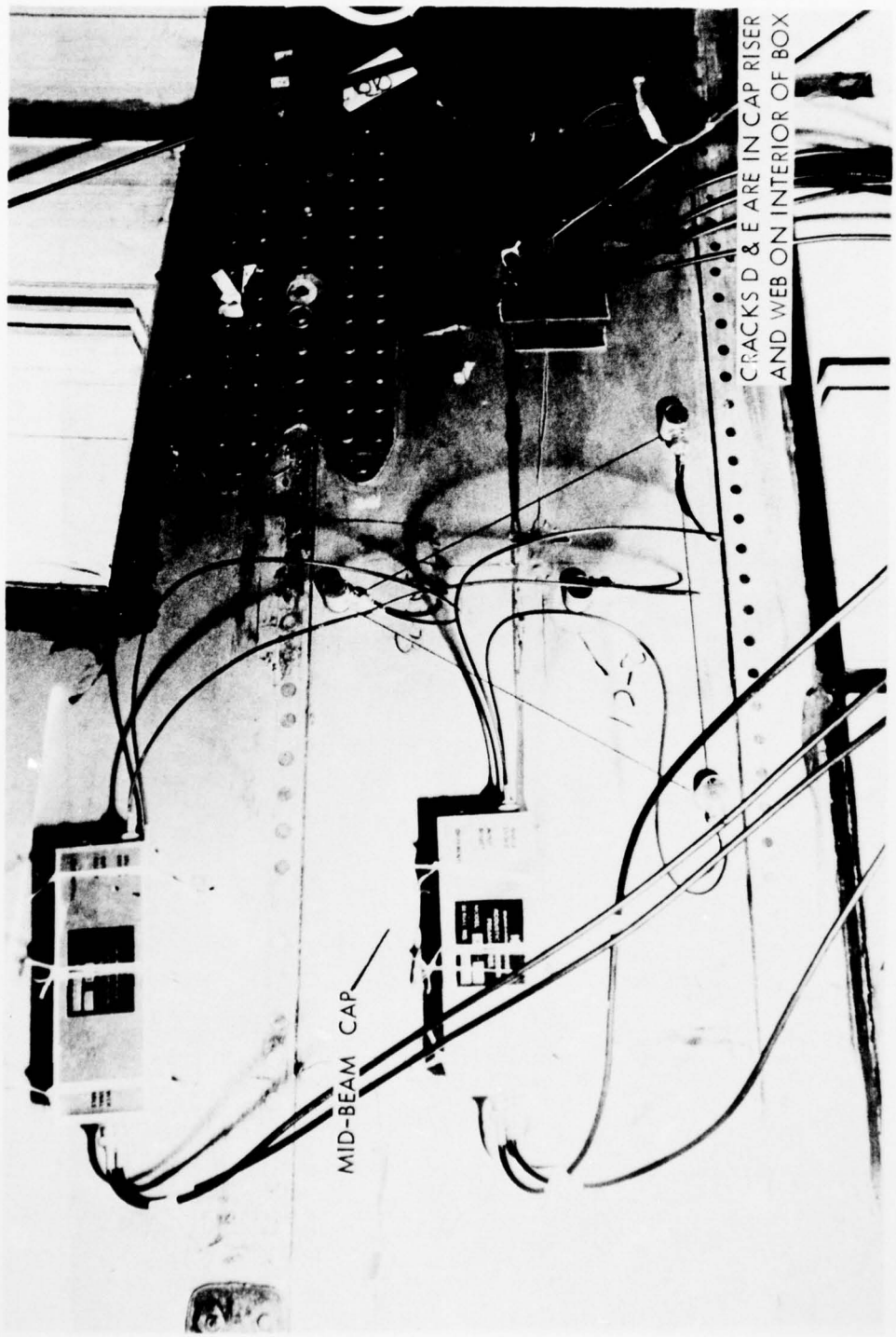

FIGURE D14. VIEW OF TRIANGULAR ARRAY IN TEST AREA 2 FOR MONITORING TEST CRACKS D AND E FOLLOWING FLIGHT 1200

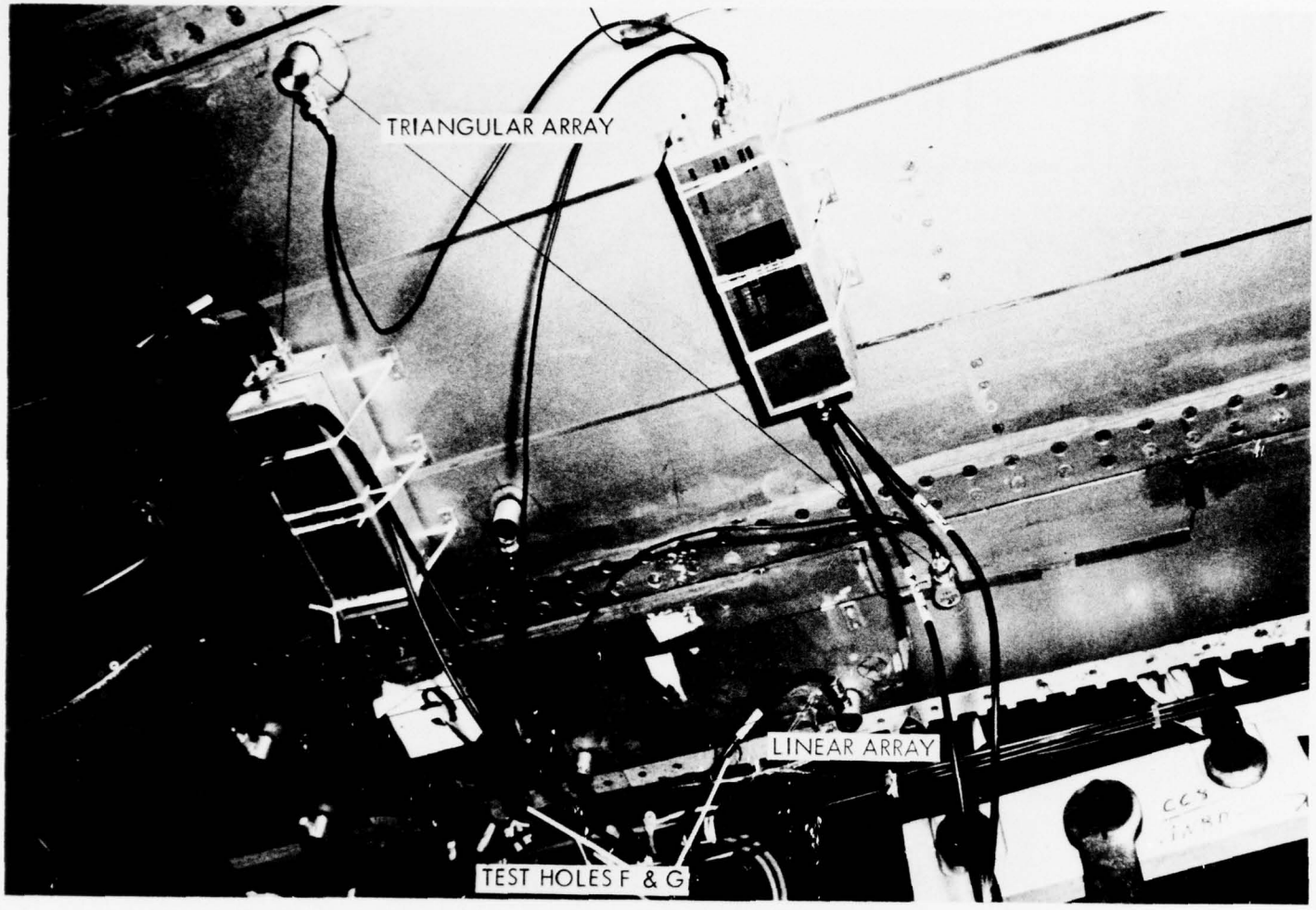

FIGURE D15. VIEW OF TRIANGULAR AND LINEAR ARRAY 2 IN TEST AREA 3 FOR MONITORING TEST HOLES F AND G DURING ALL PRECRACKS AND TEST FLIGHTS

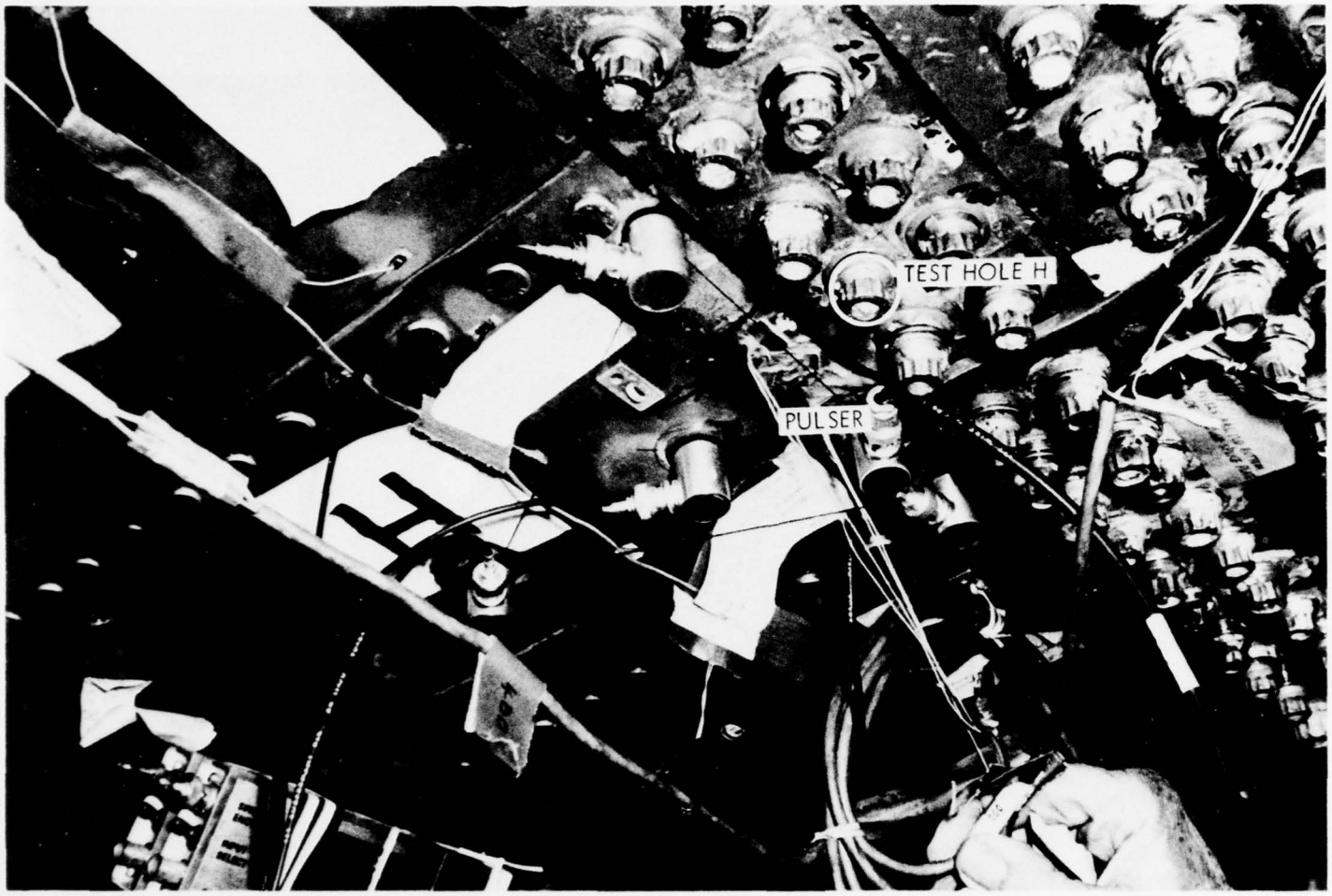

FIGURE D16. VIEW OF TRIANGULAR ARRAY 4 IN TEST AREA 4 FOR MONITORING TEST HOLE H DURING TEST FLIGHTS 141 THROUGH 1200

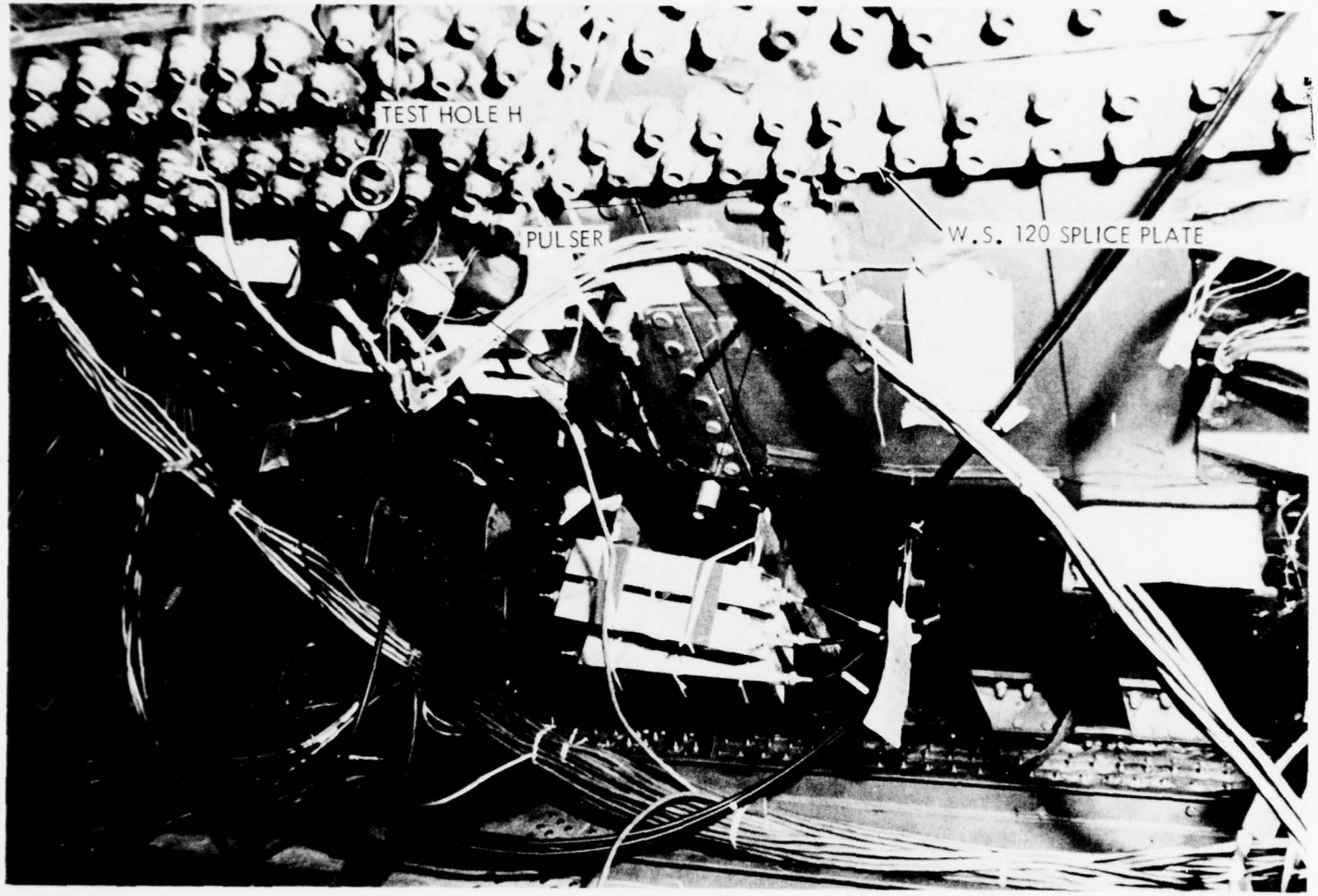

FIGURE D17. VIEW OF TRIANGULAR ARRAY 4 IN TEST AREA 4 FOR MONITORING TEST HOLE H DURING TEST FLIGHTS 1201 THROUGH 1600, INSTALLED ACROSS PLANK JOINT

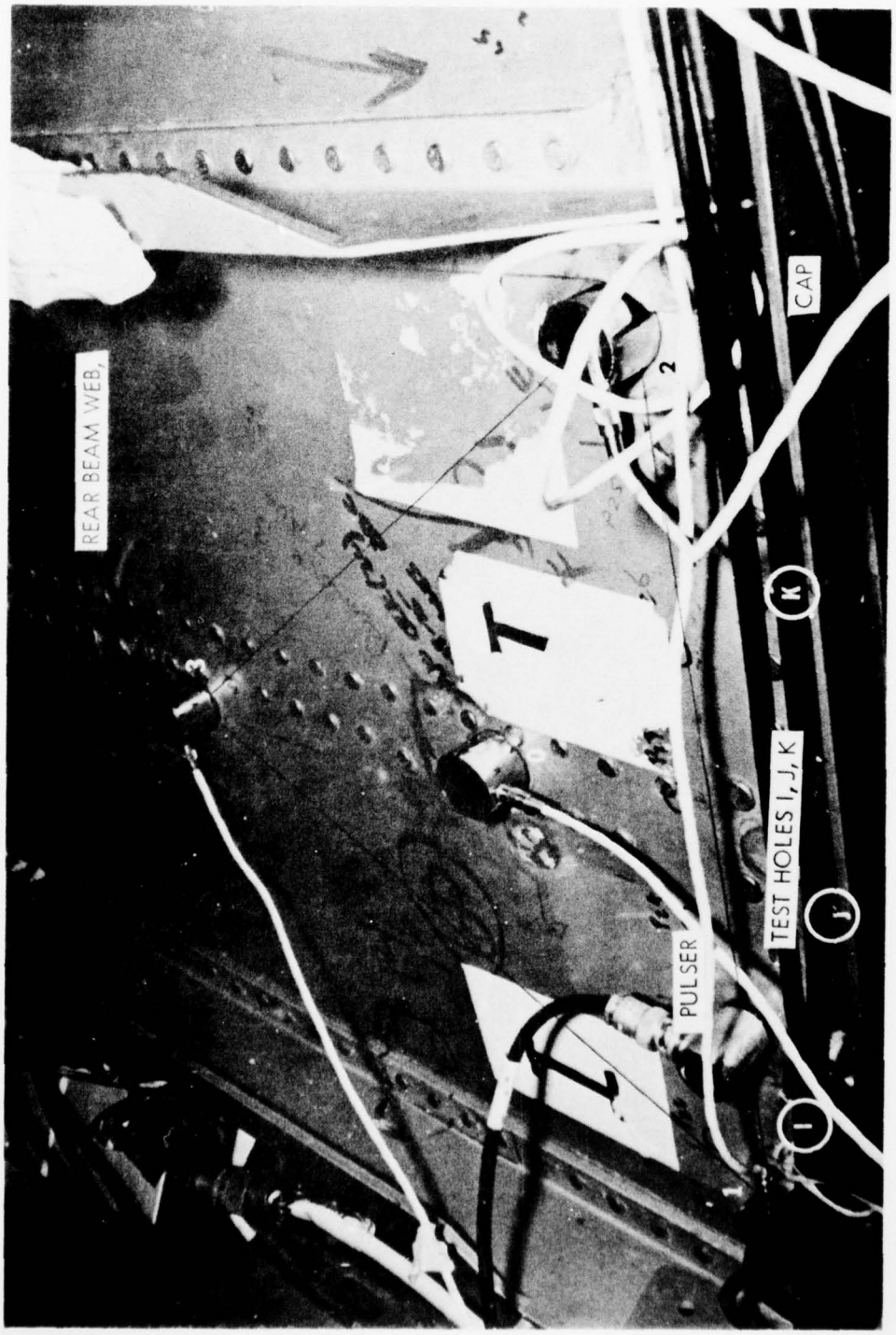

FIGURE D18. VIEW OF TRIANGULAR ARRAY 3 IN TEST AREA 5 FOR MONITORING TEST HOLES I, J, AND K DURING TEST FLIGHTS 401 THROUGH 1200

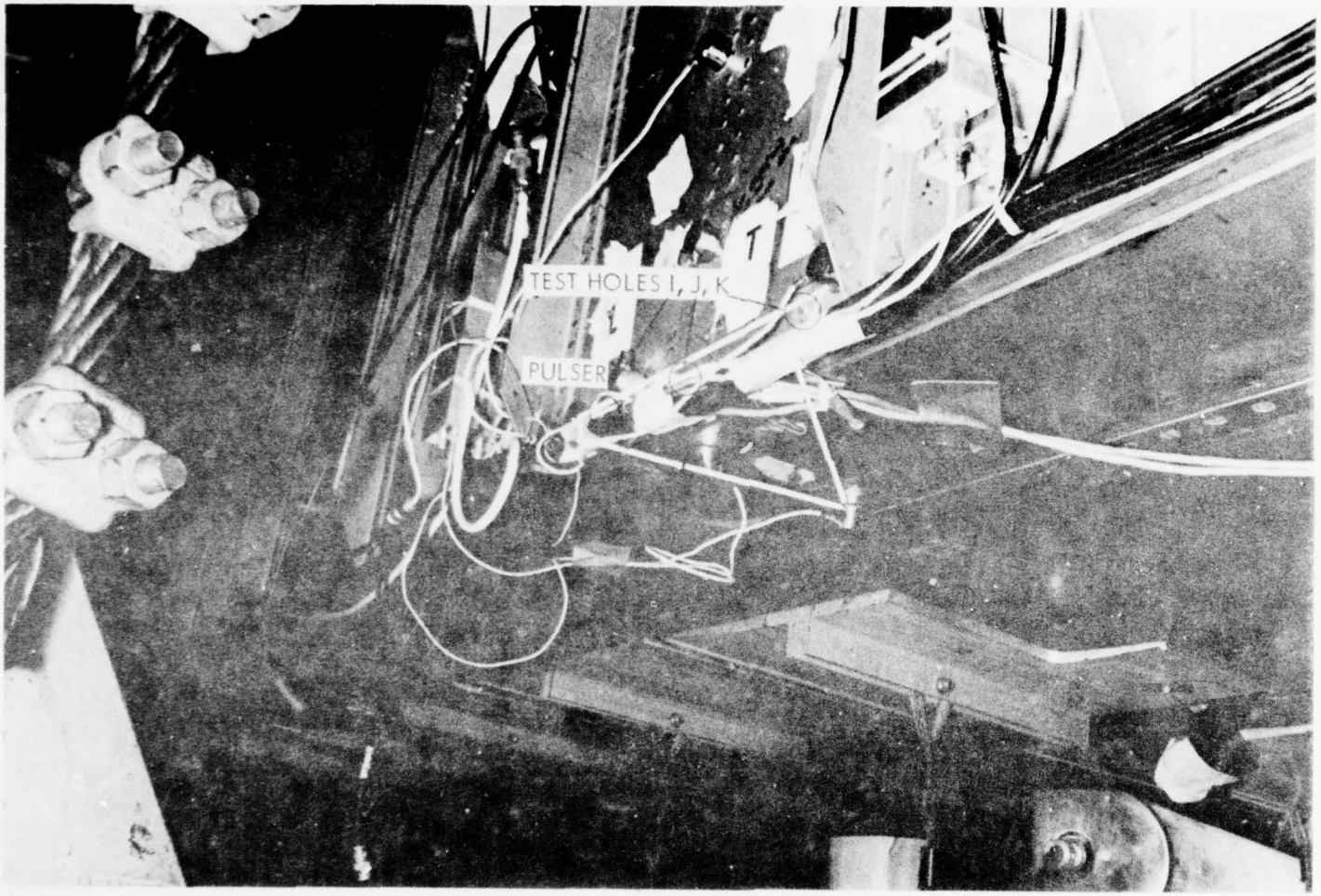

FIGURE D19. VIEW OF TRIANGULAR ARRAY 3 IN TEST AREA 5 FOR MONITORING TEST HOLES I, J AND K DURING TEST FLIGHT 1201 THROUGH 1600. ARRAY IS "FOLDED" ONTO REAR BEAM WEB AND CAP

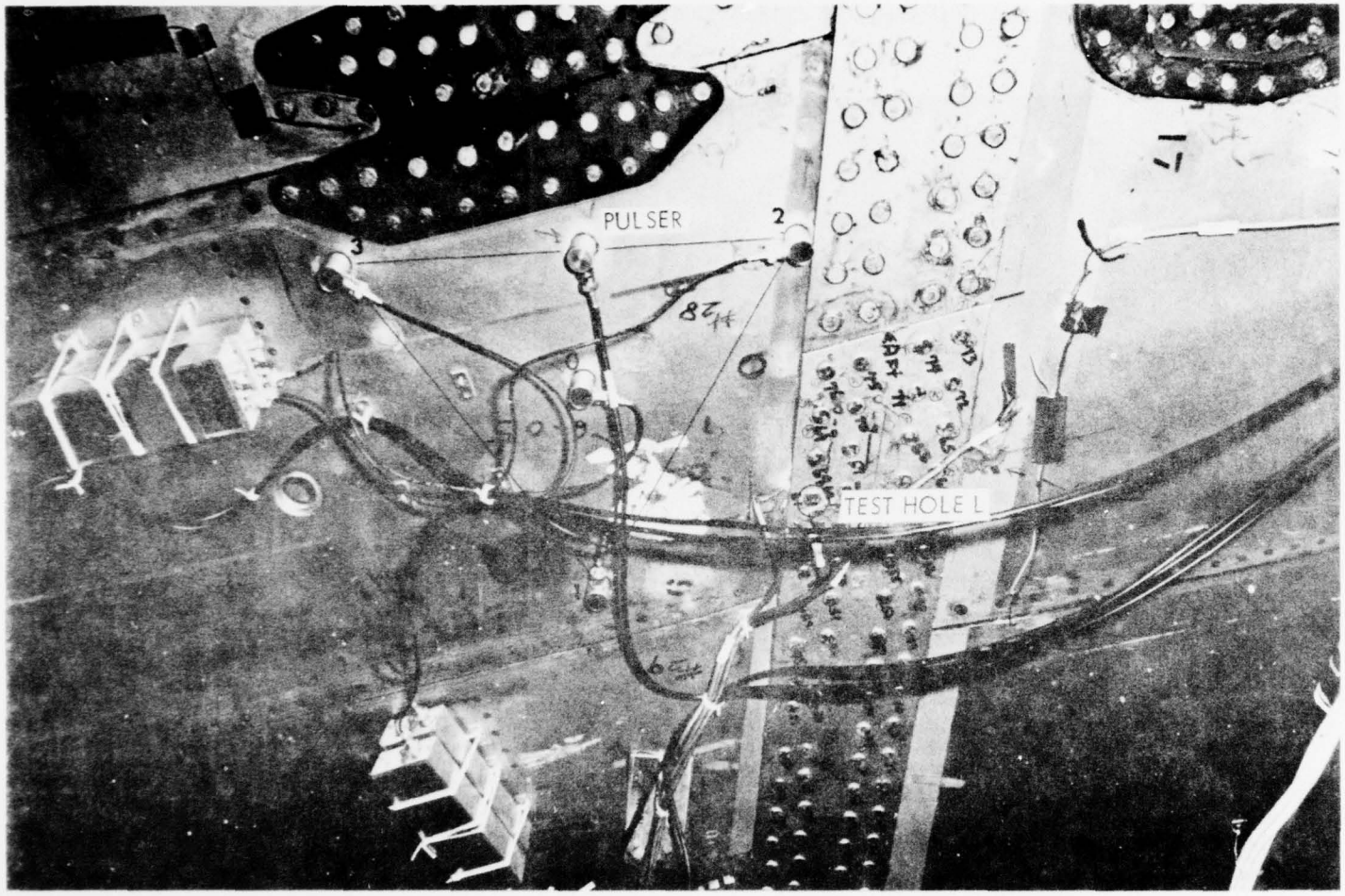

FIGURE D20. VIEW OF TRIANGULAR ARRAY 5 IN TEST AREA 6 FOR MONITORING TEST HOLE L DURING TEST FLIGHTS 437 THROUGH 1600. ARRAY WAS "ROTATED" PRIOR TO FLIGHT 437

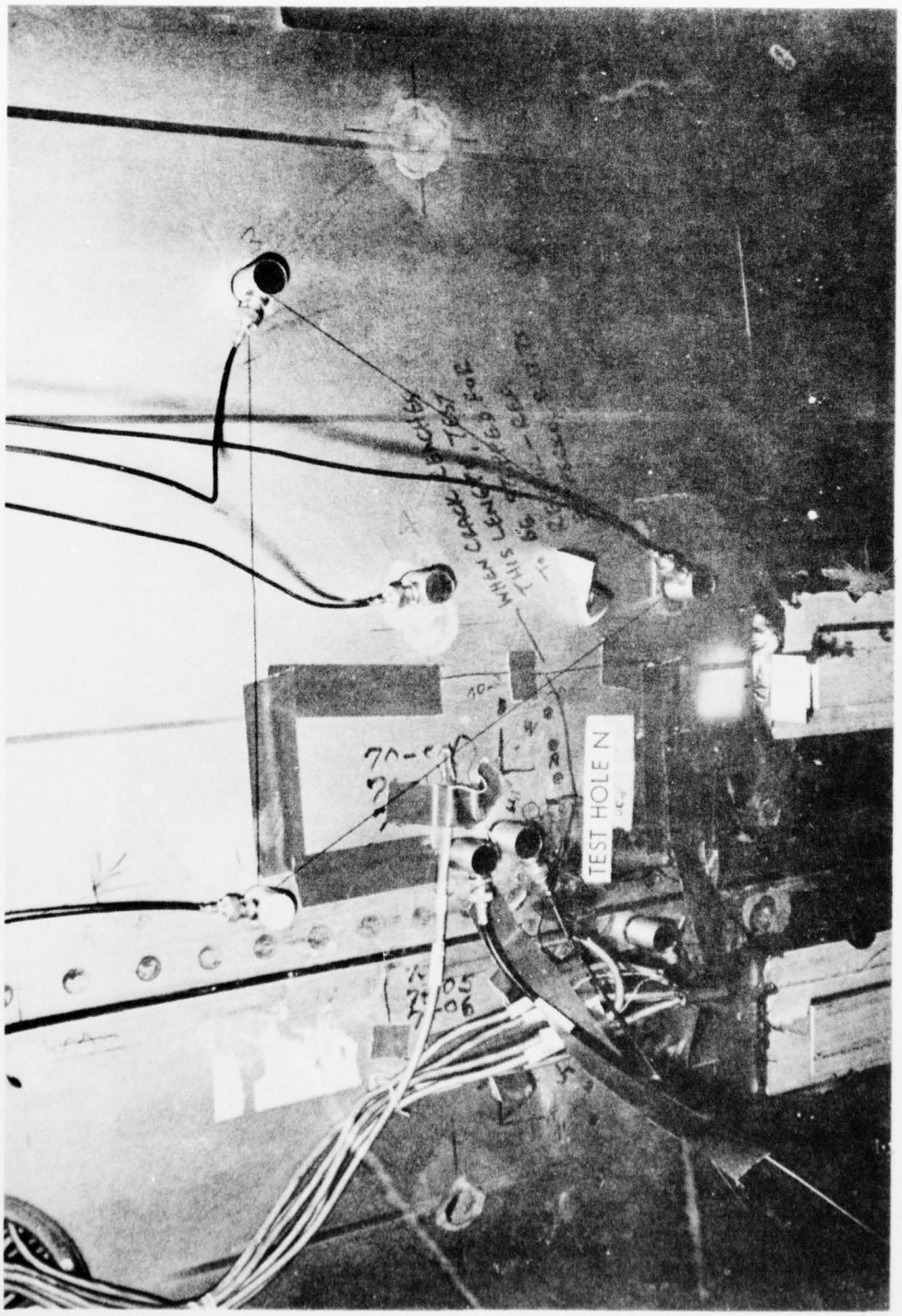

FIGURE D21. VIEW OF TRIANGULAR ARRAY 7 IN TEST AREA 8 FOR MONITORING TEST HOLE N DURING ALL PRECRACK AND TEST FLIGHTS THROUGH 1200. ARRAY WAS "ROTATED" PRIOR TO FLIGHT 438

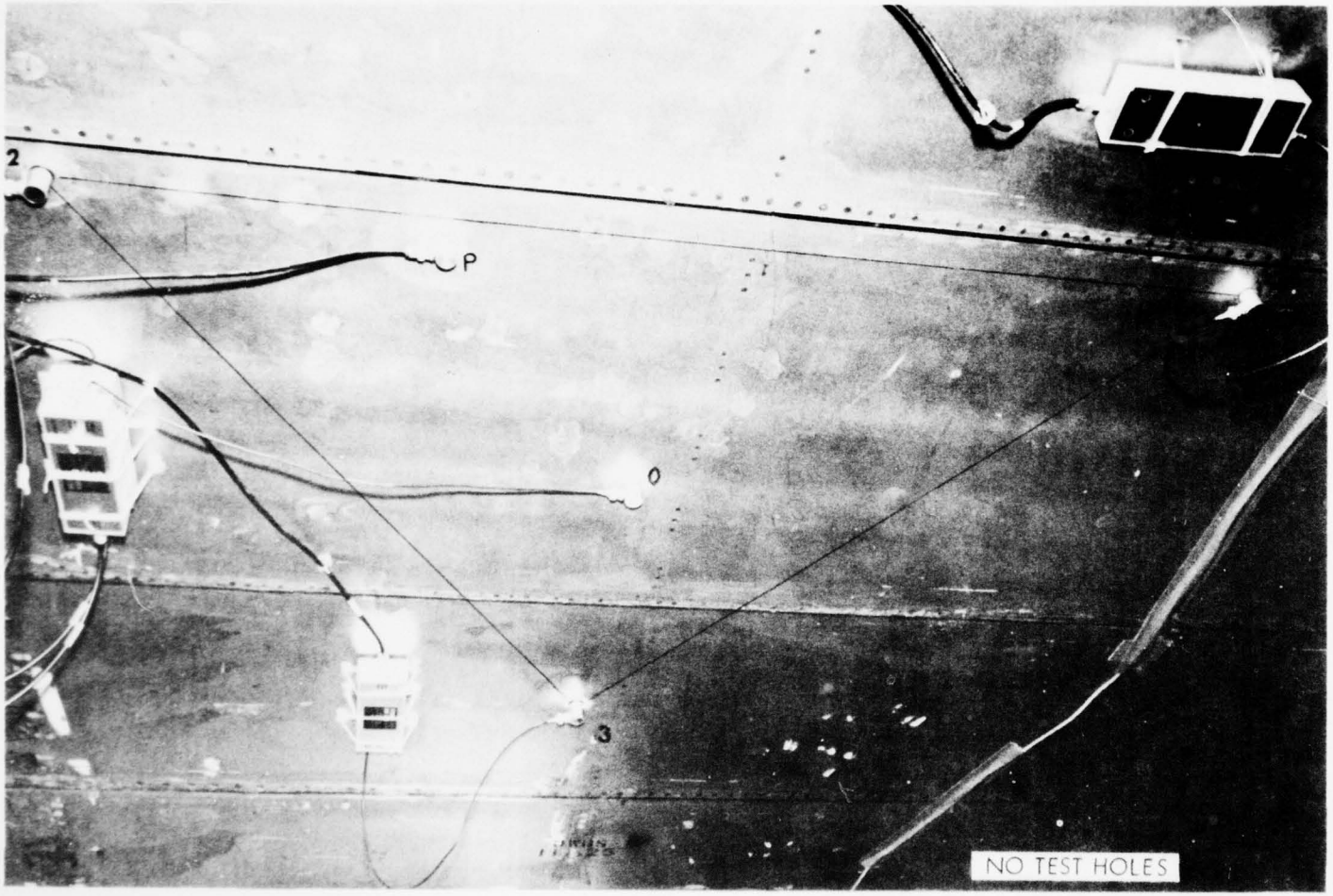

FIGURE D22. VIEW OF TRIANGULAR ARRAY 6 IN AE BASELINE AREA 9 FOR NOISE SURVEY IN A NON-CRACK AREA DURING TEST FLIGHTS 801 THROUGH 1600.

AD-A041 107 LOCKHEED-GEORGIA CO MARIETTA ENGINEERING STRUCTURAL --ETC F/G 11/6
ACOUSTIC EMISSION MONITORING OF CRACK PROPAGATION ON THE EXPEDI--ETC(U)
DEC 76 W M PLESS, C D BAILEY, J M HAMILTON F33615-75-C-5249

UNCLASSIFIED L677ER-0042 AFML-TR-76-214 NL

2 OF 2
AD
A041107

END

DATE
FILMED
7-77

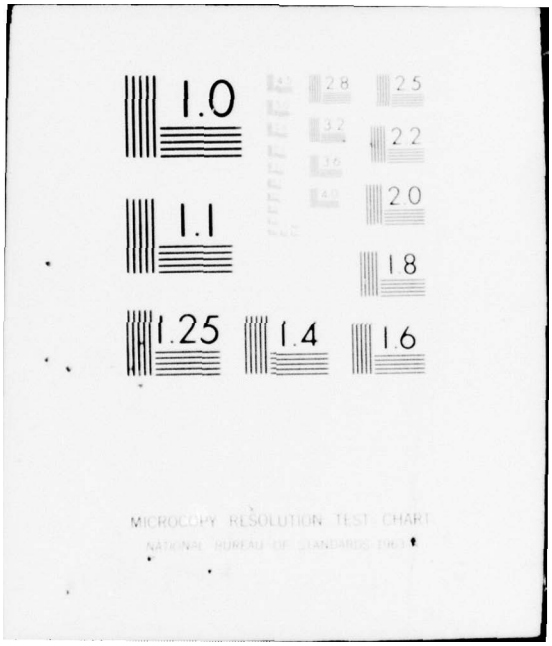
1.0
1.1
1.25
1.4
1.6
2.8
2.5
3.2
2.2
3.6
2.0
4.0
1.8
MICROCOPY RESOLUTION TEST CHART
NATIONAL BUREAU OF STANDARDS 1963-A

APPENDIX E

DATA TAPE CHARACTERIZATION PROCEDURE

APPENDIX E

DATA TAPE CHARACTERIZATION PROCEDURE

1. Select the tape(s) containing the flights to be analyzed (this information is hand-recorded on the cassette ID sticker).

2. Examine the Tape(s) to:

   - o Determine the start and tinish times of each flight by playing the tape and printing content increments on the paper chart.
   - o Group the flights into time segments. A time segment is that period of computer time from the start of the computer time at zero time until the timer is reset to zero. A time segment may contain one or more flights.
   - o Record a marker (Control E) on the data tape to automatically stop the tape transport at the end of each time segment.
   - o Chart record the flight numbers and total number of flights associated with each time segment.
   - o Chart the time segments associated with each side of the data tape.
   - o Determine the flights during which no data were recorded.

The last step enables the analyst to recognize "missing" data during the analysis or to bypass portions of the tape which contains nonrelevant data.

APPENDIX F

CRACK GROWTH HISTORY AND CRACK SURFACE PHOTOGRAPHS

APPENDIX F

CRACK GROWTH HISTORY AND CRACK SURFACE PHOTOGRAPHS

Test Area 1, Test Holes A, B and C. Crack growth occurred in holes A and B, but not in C. In hole A, growth initiated at the sawcuts on the forward side of the hole and grew forward in both members of the lap joint. By flight 800, the crack had growtn almost to the forward edge of wing panel No. 4 and terminated in the formation of a shear lip. The interfacing beam cap experienced parallel crack growth forward of the hole, terminating in the vicinity of a thickness step. A diagram of panel joint, sawcuts, and final cracks is given in Figure F1. Little or no growth occurred after flight 800.

In Hole B, crack growth initiated at the sawcuts on forward and aft sides of the hole in both members of the lap joint. By flight 650, the crack had reached the forward edge of wing panel No. 4 forming a shear lip and had extended to the thickness step in the interfacing beam cap. The crack continued to grow aft of the hole until it reached the edge of the beam cap at flight 1375 and extended 0.90 inches into the wing panel No. 4.

Test Area 2, Test Holes D, E, O, P and Q. Crack growth was experienced in all five holes during the program. A diagram of Test Area 2, the sawcuts, and final cracks is given in Figure F2. Crack D extended from a sawcut in the mid-beam web and grew for 0.087 inches toward the lower edge of the web. No further analysis was made of this crack to correlate growth with test flights. Crack E extended from an existing crack in a lower fastener hole in the mid-beam cap riser. The final crack size was 0.228 inches as measured along the surface. No further analysis was done to segregate the increments of growth occurring during the test flights from the pre-existing size.

Cracks O, P and Q were all in the mid-beam cap riser and extended from pre-existing fatigue cracks. Only crack 'O' was analyzed to segregate the various increments of growth. Crack 'O' length along the surface was 0.202 inches. The pre-existing length was 0.069 inches, and the increment added during the post-test residual strength tests was 0.020 inches - thus, the 2100 flight test program added an increment of 0.113 inches to the growth of crack 'O'. Cracks P and Q were not analyzed for segregation of growth increments. All three cracks apparently grew steadily throughout the 2100 flight test and the post-test residual strength programs.

Test Area 3, Test Holes F and G. Both cracks F and G grew from corner sawcuts during the program test flights. A diagram of Test Area 3, the sawcuts and final cracks is given in Figure F3. Crack F extended 0.035 inches along the 45° bisector toward the aft edge of the rear beam cap hinge lip. Crack G extended 0.035 inches aft and 0.055 inches forward (along 45° bisectors) from the hole. Neither crack received further analysis for correlation to test flights or growth increment segregation.

Test Area 4, Test Hole H. Figure F4 is a diagram of Test Area 4, including the sawcut and final crack. Crack H extended 0.175 inches along the 45° bisector from a corner sawcut in the test hole. This crack was analyzed for growth correlation to test flight and for segregation of growth due to the residual strength test loads. An increment of 0.140 inches of the above growth occurred during the flight-by-flight tests. Growth occurred steadily throughout the latter program.

Test Area 5, Test Hole I, J and K. Crack growth occurred in all three test holes. A diagram of Test Area 5, the sawcuts and final cracks is shown in Figure F5. Crack I grew from a through-sawcut on the upper side of a fastener hole in the web. Growth was 0.050 inches as measured along the surface of the web. Crack J extended 0.247 inches from a through-sawcut on the lower side of a fastener hole to the lower edge of the web. This crack reached the edge of the web just prior to test flight 1200 and no further growth occurred at this hole. Crack K grew 0.033 inches on the upper side of a fastener hole in the web and 0.050 inches on the lower side of the hole - each extending from a through-sawcut in the web. Only Crack J was analyzed for growth correlation to test flights.

Test Area 6, Test Hole L. A diagram of Test Area 6, the sawcut and final crack is given in Figure F6. A crack 0.020 inches as measured along the 45° bisector extended from a corner sawcut in Test Hole L. This crack was not analyzed further.

Test Area 8, Test Hole N. Crack growth occurred at both fore and aft sides of this hole. A diagram of Test Area 8 is given in Figure F7. Growth extended from fatigue cracks existing, prior to the flight-by-flight program and was confined to the wing panel 3 portion of the panel 3/panel 2 lap joint. Initial crack length including the fastener hole diameter was 0.93 inches. The final crack length was 1.56 inches. Since the material containing test hole N was removed from the structure following test flight 1200, the total growth increment of 0.63 inches was due entirely to the flight-by-flight program.

Crack growth histories of analyzed cracks 1A, 1B, 2 '0', 4H and 5J are depicted by data plots shown in Figure F8 (Figures F8A, F8B, F8C, F8D, and F8E, respectively). Photographs of the fracture faces of these cracks are shown in Appendix F which exhibits photos of all the test cracks. In these plots, crack length and average growth per flight are plotted as a function of test flight. The left end of the crack length curves are shown emanating from the boundary dimension of the initial sawcut or intial fatigue crack. The x-axis (flight axis) includes the first 100 "precrack" flights that were applied before the 2000 test flights. Crack growth was experienced at all test holes, except hole 1C, during the 2100 crack initiation and propagation flights. Test cracks not analyzed for growth versus flight history are 2E, 2P, 2Q, 3F, 3G, 5I, 5K and 6L.

APPENDIX F

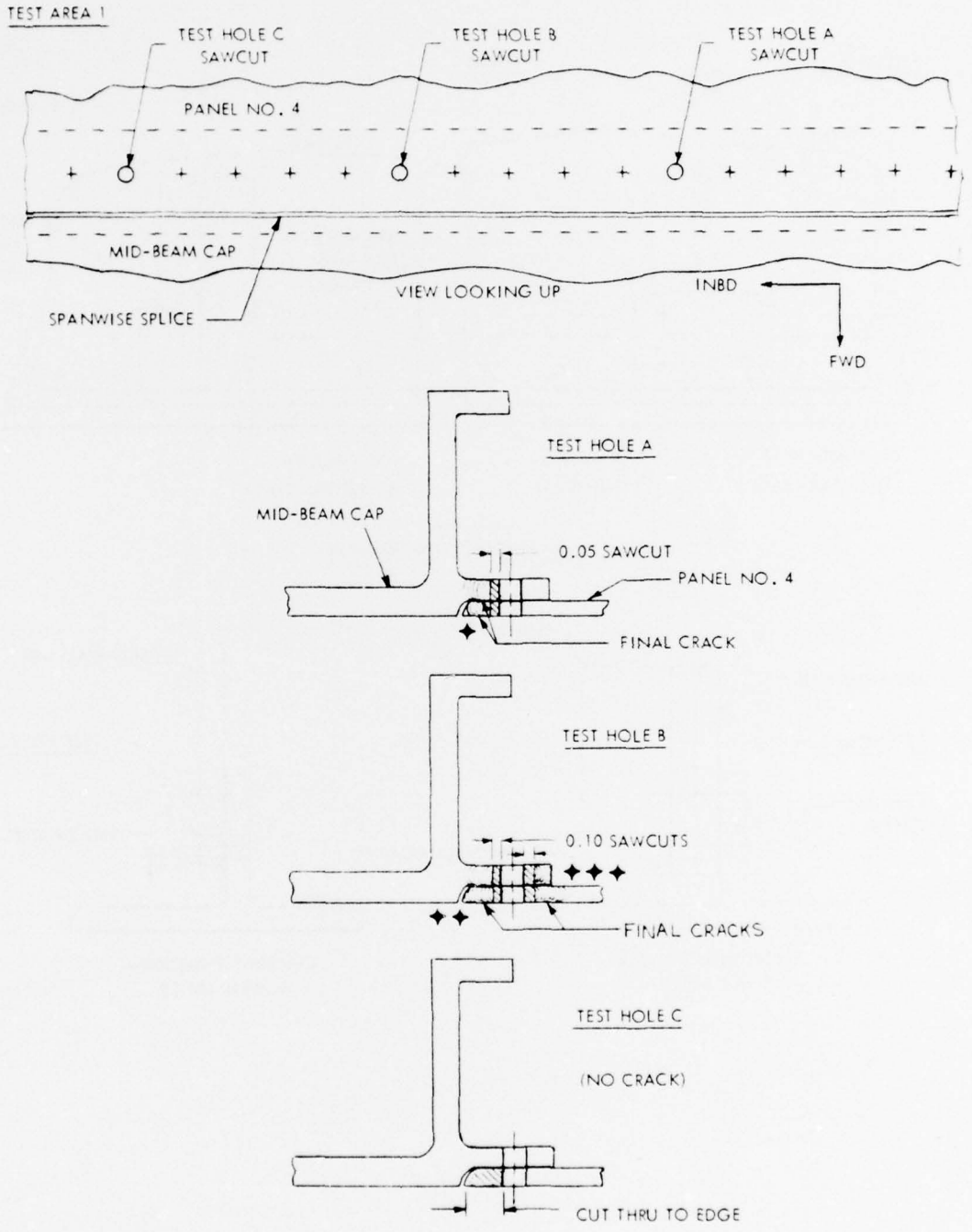

FIGURE F1. CONDITIONS AT TEST HOLES A, B, AND C IN TEST AREA 1

APPENDIX F

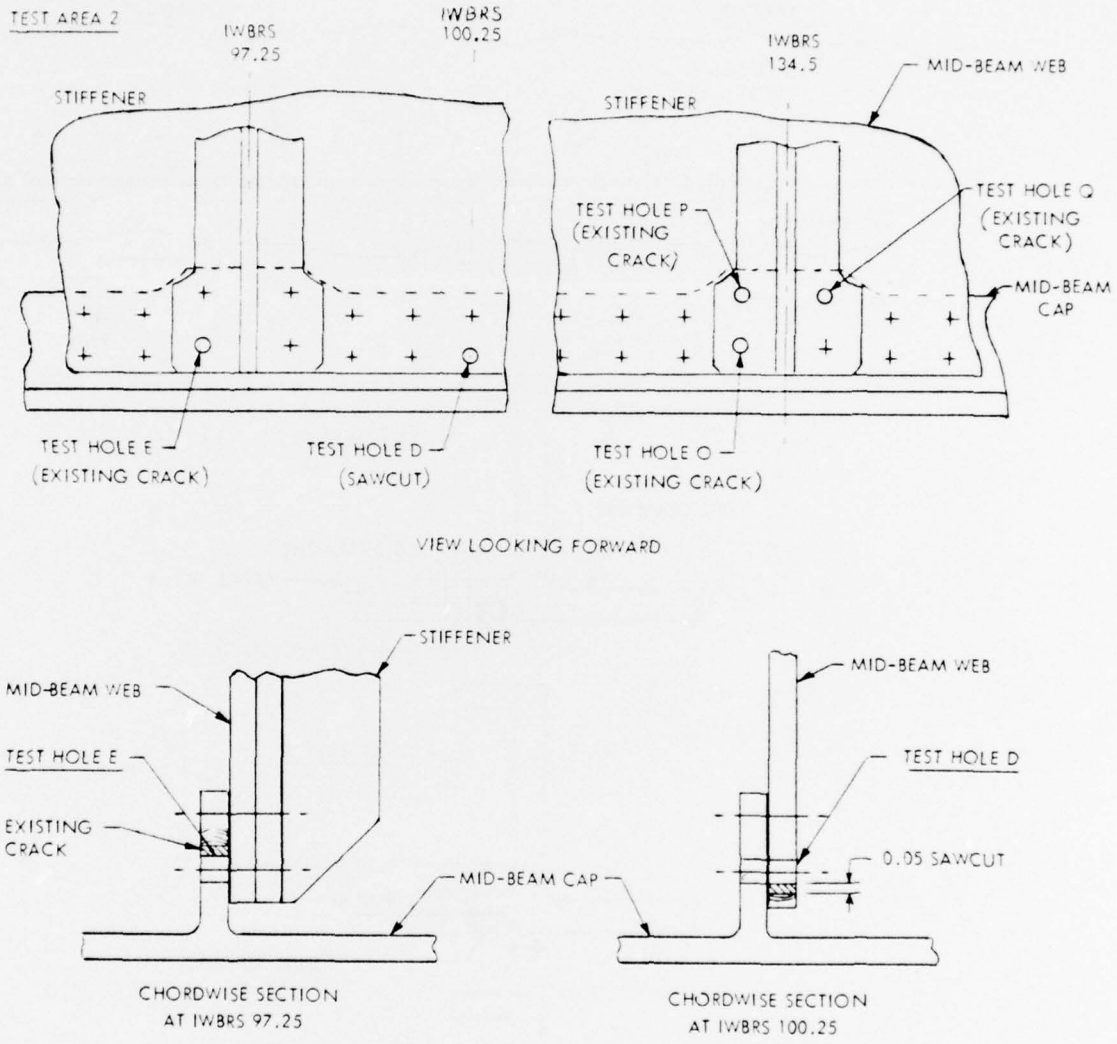

FIGURE F2. CONDITIONS AT TEST HOLES D AND E AND O, P, AND Q IN TEST AREA 2

APPENDIX F

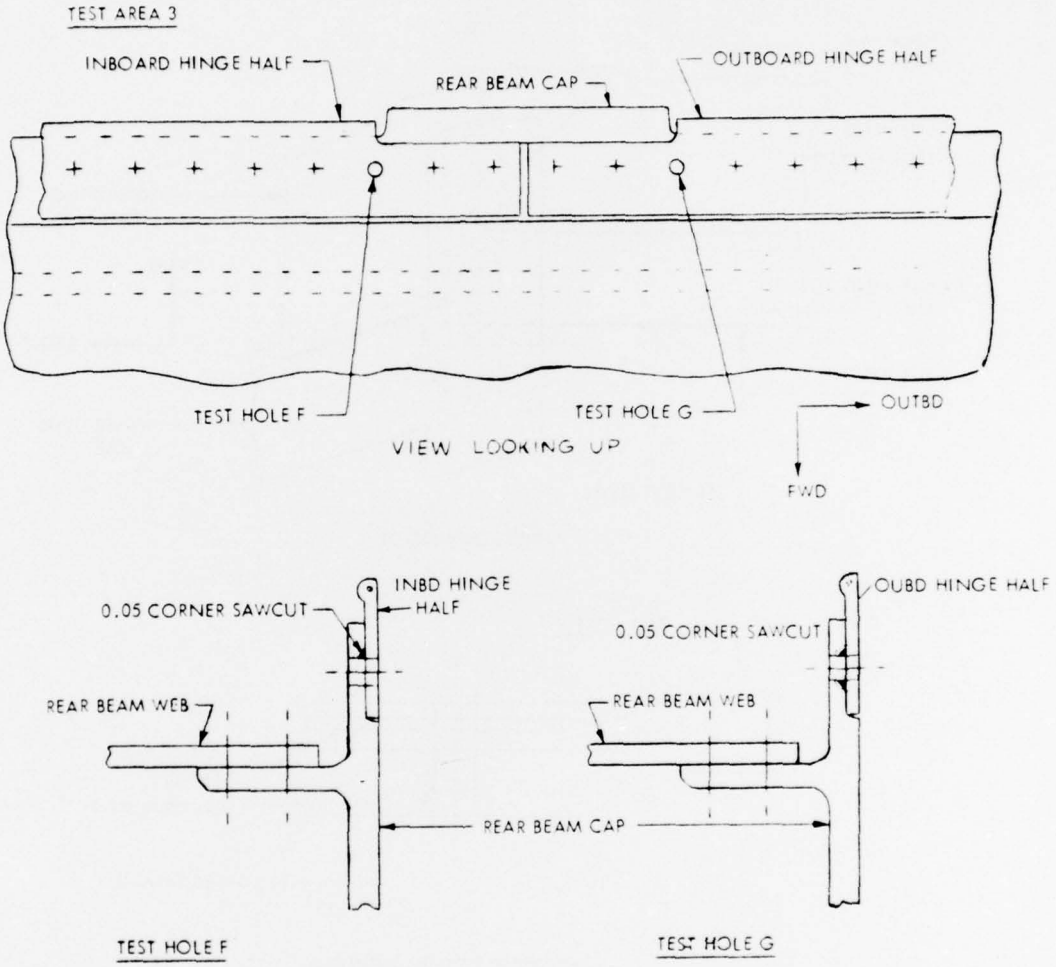

FIGURE F3. CONDITIONS AT TEST HOLE F AND G IN TEST AREA 3

APPENDIX F

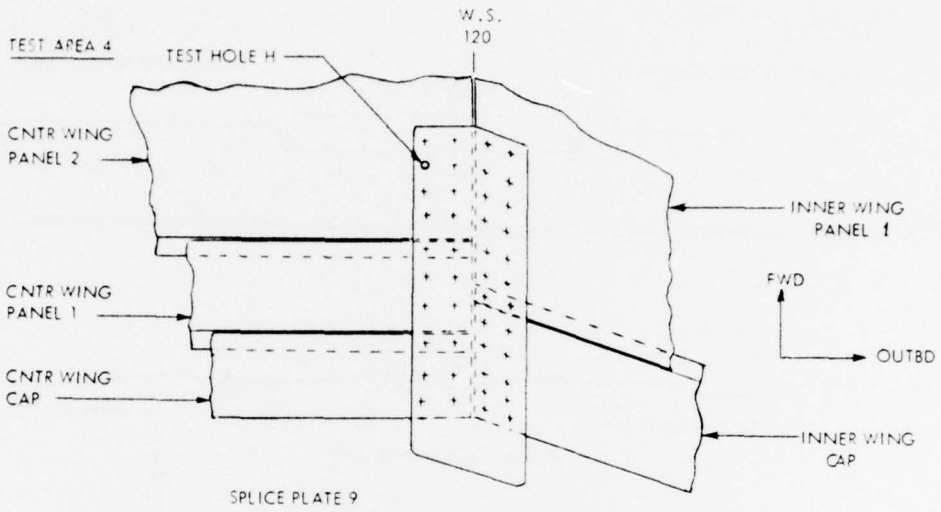

VIEW LOOKING UP

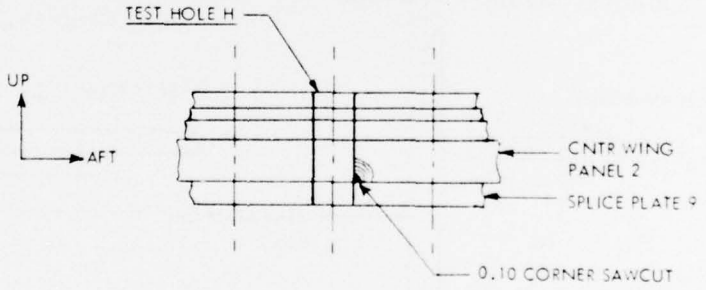

CHORDWISE SECTION THROUGH
TEST HOLE H

FIGURE F4. CONDITIONS AT TEST HOLE H IN TEST AREA 4.

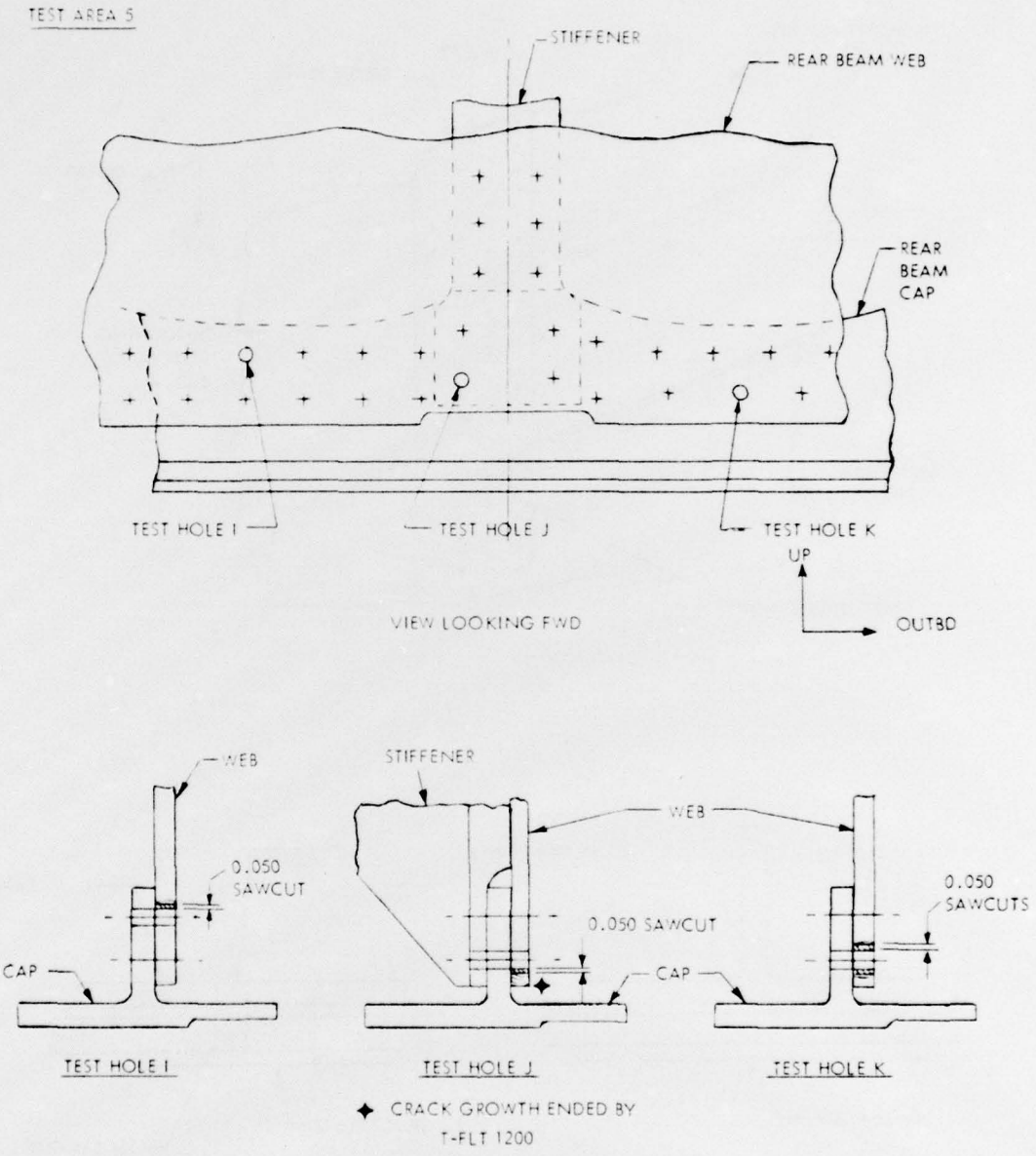

FIGURE F5. CONDITIONS AT TEST HOLE I, J, AND K IN TEST AREA 5

APPENDIX F

TEST AREA 6

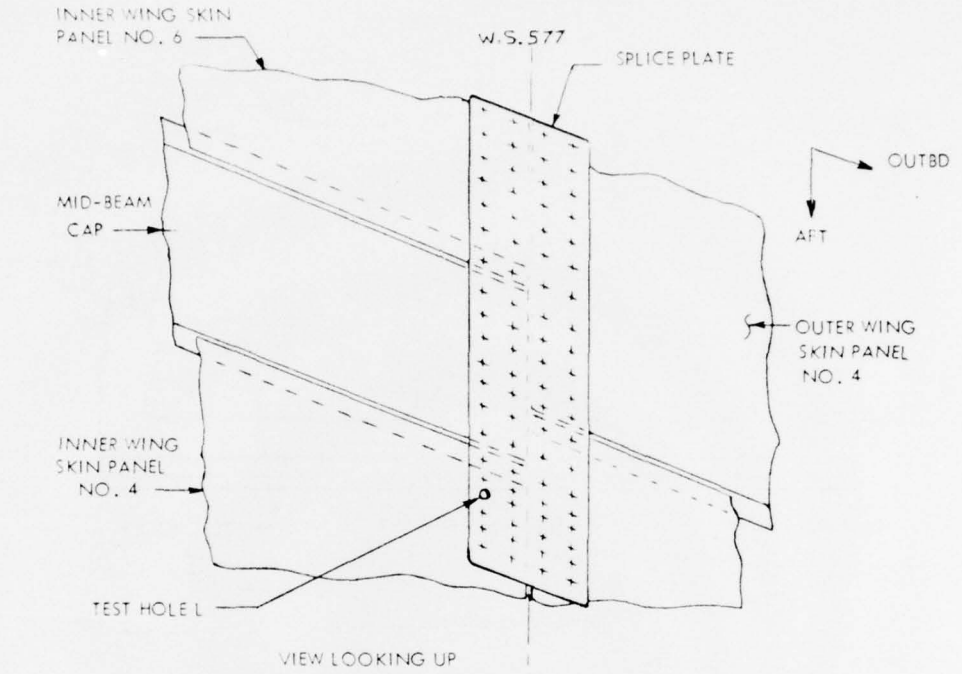

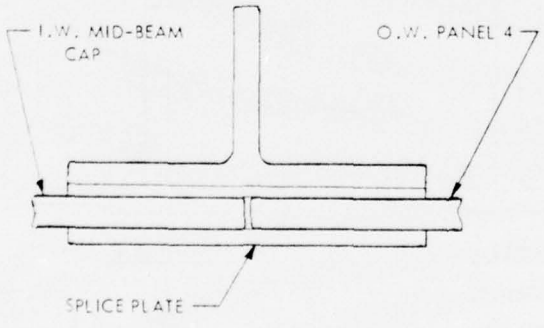

SPANWISE SECTION AT W.S. 577

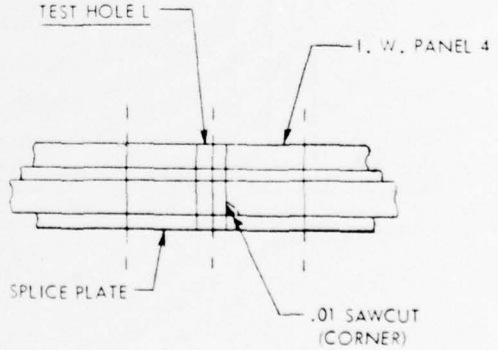

CHORDWISE SECTION THROUGH TEST HOLE L

FIGURE F6. CONDITIONS AT TEST HOLE L IN TEST AREA 6

APPENDIX F

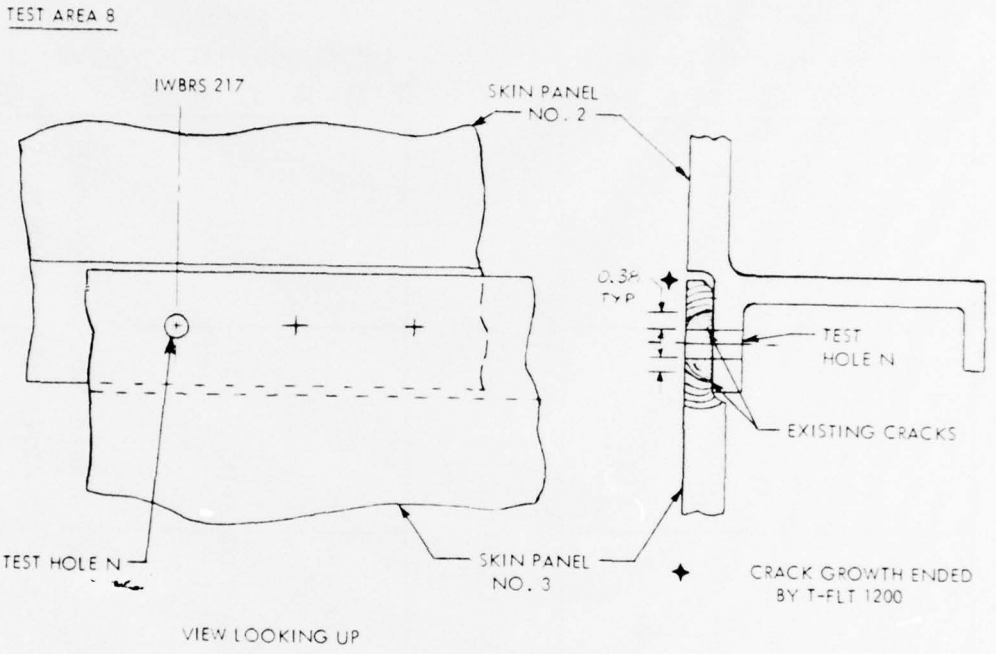

FIGURE F7. CONDITIONS AT TEST HOLE N IN TEST AREA 8

FIGURE F8. CRACK GROWTH VERSUS CUMULATIVE TEST FLIGHTS (1 OF 3)

FIG F8C

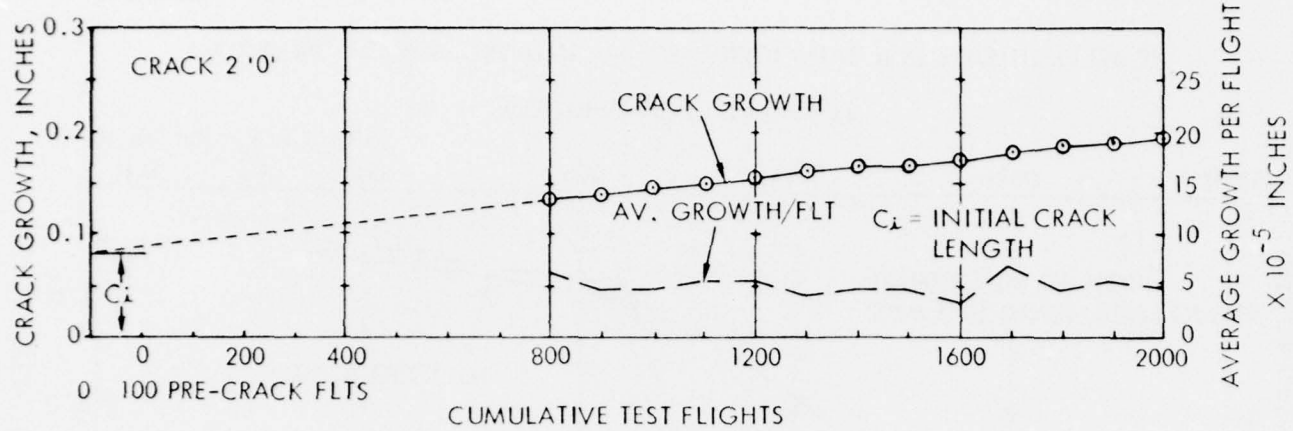

FIG F8D

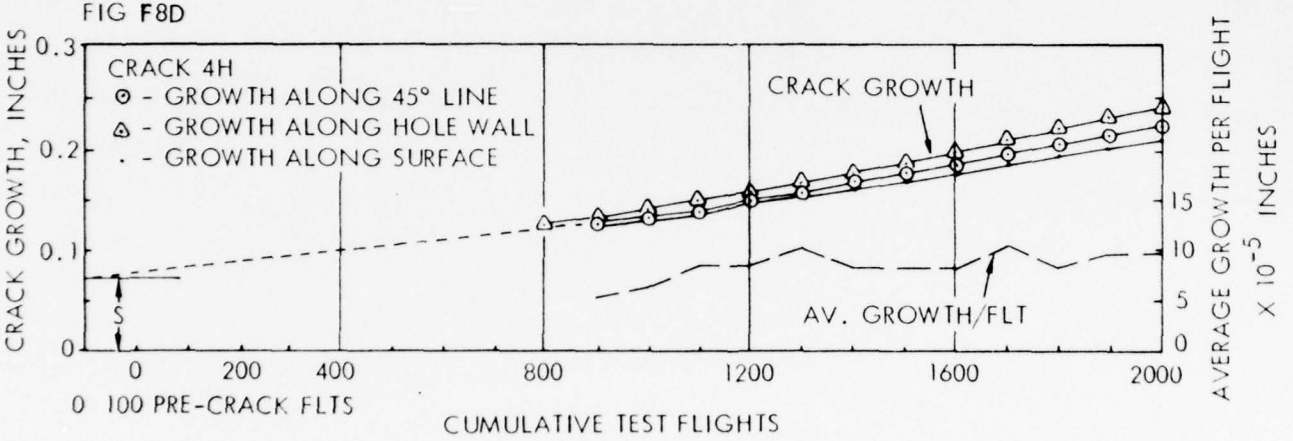

FIGURE F8. CRACK GROWTH VERSUS CUMULATIVE TEST FLIGHTS (2 OF 3)

FIG F8E

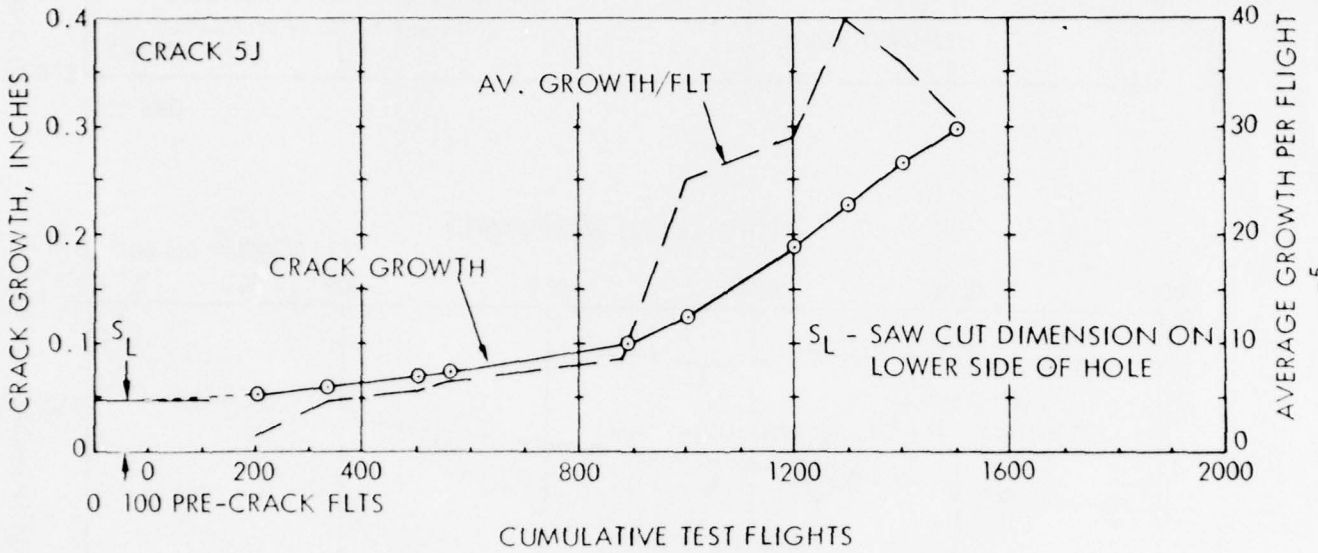

FIGURE F8. CRACK GROWTH VERSUS CUMULATIVE TEST FLIGHTS (3 OF 3)

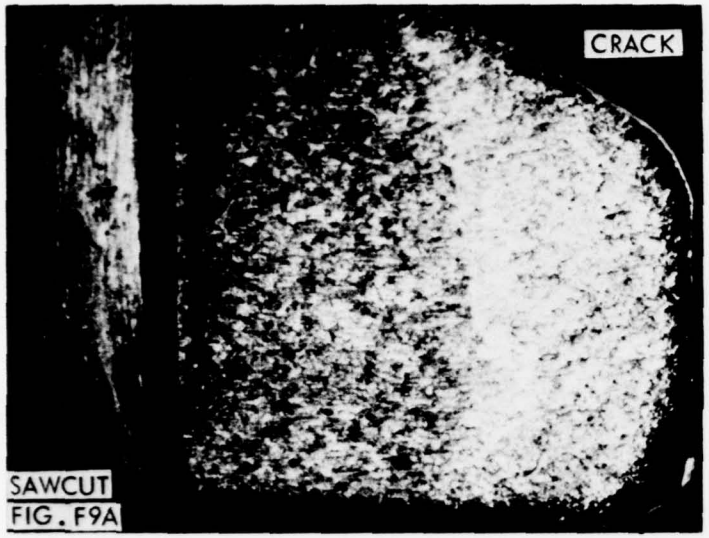

CRACK 1A

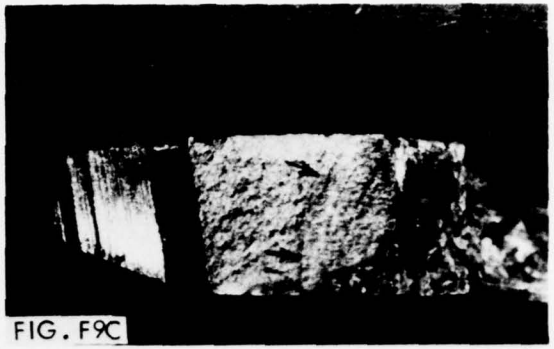

CRACK 2D

TEST HOLE 1C DID NOT HAVE CRACK GROWTH

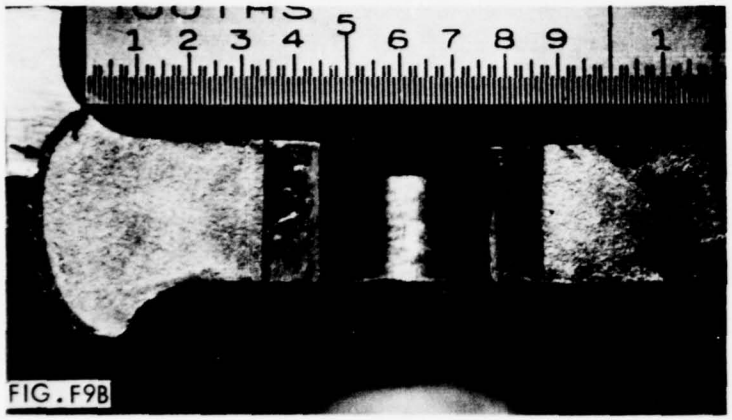

CRACK 1B

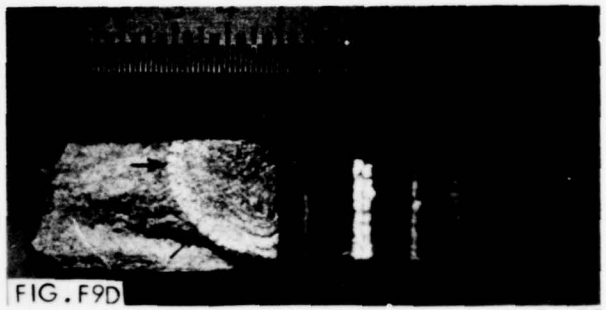

CRACK 2E

FIGURE F9. PHOTOMACROGRAPHS OF TEST CRACK SURFACES (1 OF 3)

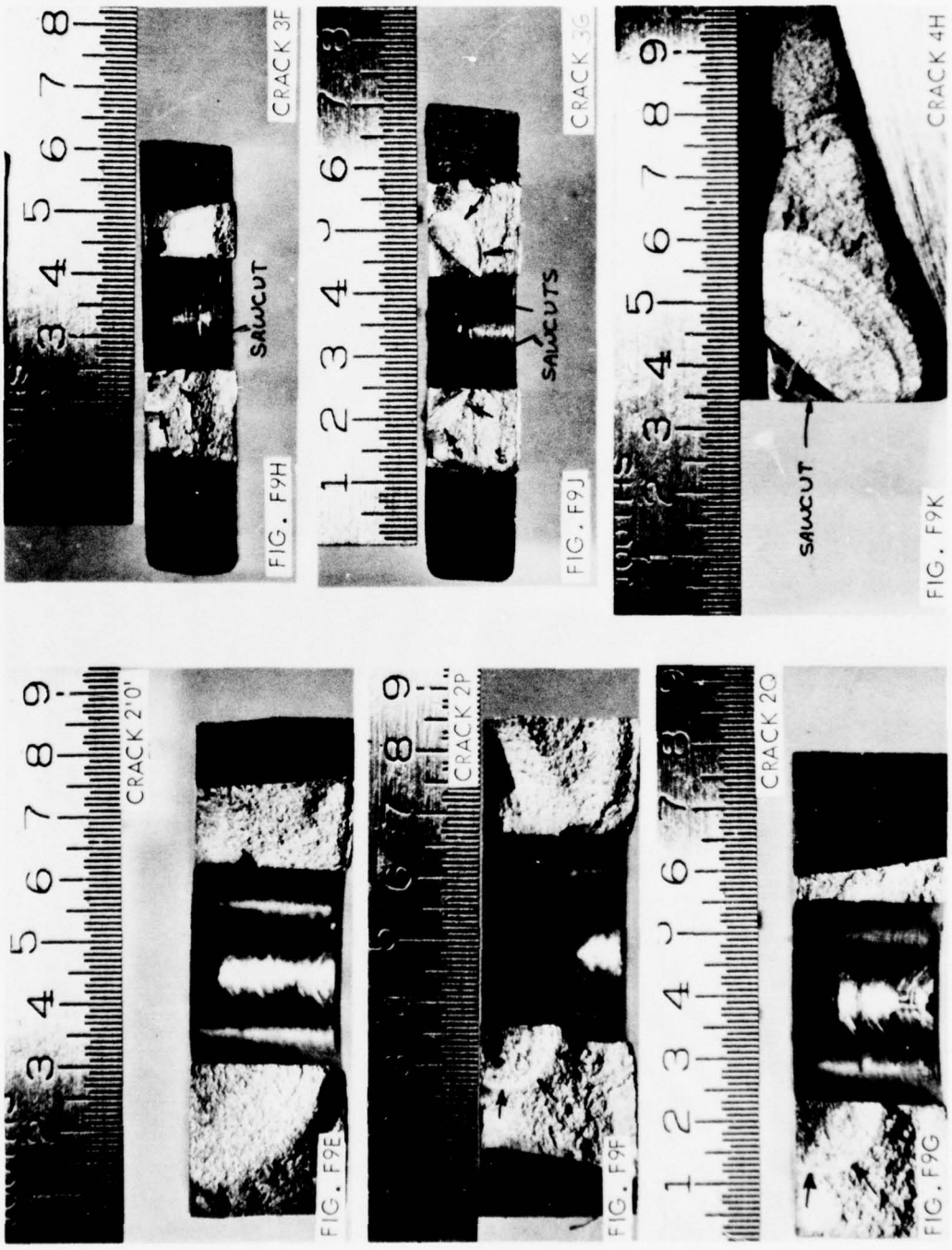

FIGURE F9. PHOTOMACROGRAPHS OF TEST CRACK SURFACES (2 of 3)

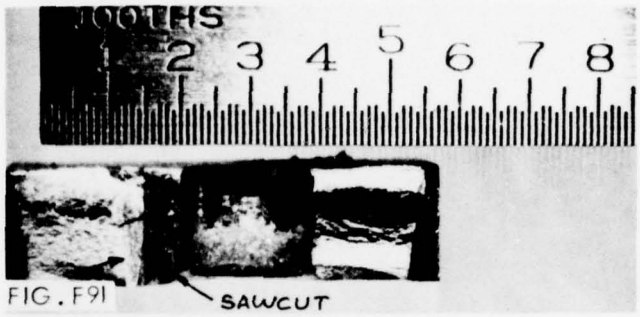

CRACK 5I

PHOTO OF CRACK 5J NOT AVAILABLE

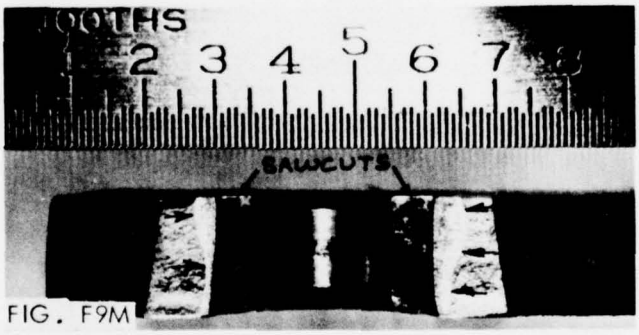

CRACK 5K

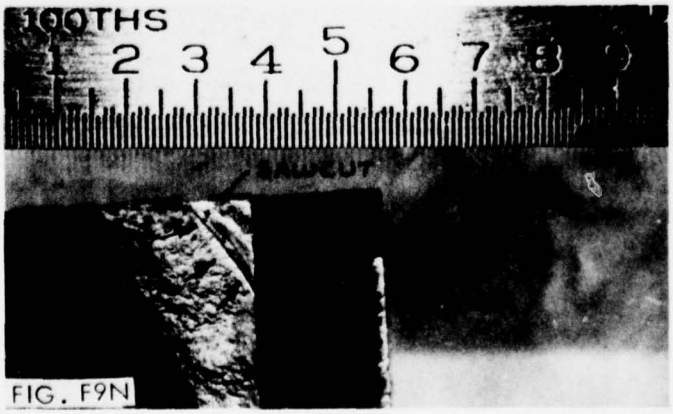

CRACK 6L

FIGURE F9 PHOTOMACROGRAPHS OF TEST CRACK SURFACES (3 OF 3)

APPENDIX G

IN-TEST CRACK LENGTH MEASUREMENTS

APPENDIX G

IN-TEST CRACK LENGTH MEASUREMENTS

In-Test Crack Measurements. Prior to start of the test program, before any flight loads were applied, the visual crack tip location of all existing cracks at test holes were determined using a triangulation measurement technique. The position of the end points of all sawcuts were likewise determined. The triangulation technique involved measurements made from a reference triangle in which two prick marks near each test hole defined the triangle base and the test hole center formed the triangle apex. The prick marks were nominally 2.0 inches apart and the perpendicular distance trom the base to the test hole center was nominally 2.0 inches. Subsequent measurements of crack growth were made from the two prick marks to the crack tip and were expressed as x-y displacements.

A second set of baseline crack tip location measurements was developed following the 100 "precrack" flights which were applied to initiate crack growth at the sawcuts. Thereafter, measurements were made at each accessible test hole after every 25 to 75 test flights, generally, with some variation. Holes containing corner cracks or corner cuts were inspected with ultrasonic and/or eddy current automatic bolt-hole techniques to determine extent of crack growth along the hole wall. TableG1is a compilation of the final in-test crack growth as determined visually or with the NDI methods. Comparison of these determinations can be made with the measurements made with fractographic techniques presented in Table 3.

APPENDIX G

TABLE G-1. VISUAL CRACK MEASUREMENTS

TEST CRACK	FINAL VISUAL GROWTH INCREMENT, IN.	VISUAL MEASUREMENT LOCATION	
1A	0.23	Fwd, Exterior Panel Surface	(1)
1B	0.64	Fwd, Exterior Panel Surface	(1)
	0.20	Aft, Exterior Panel Surface	(1)
1C	0	Aft, Exterior Panel Surface	(1)
2D	0.28	Web Surface, Lwr Edge	
2E	0	Beam Riser Fwd Surface	
2'0'	0	Beam Riser Fwd Surface	
2P	0	Beam Riser Fwd Surface	
2Q	0	Beam Riser Fwd Surface	
3F	0	Fwd, Exterior Cap Surface	
3G	0	Fwd and Aft, Ext. Cap Surfaces	
4H	0.13	Hole Wall	
5I	0	Exterior Web Surface	
5J	0.25	Hole Wall (Intermittent)	(2)
5K	0	Exterior Web Surface	
6L	-		
7M	0.24	Fwd, Interior Panel Surface	
8N	0.36	Fwd, Exterior Panel Surface	
	0.30	Aft, Exterior Panel Surface	
9R	0.12	Fwd, Exterior Panel Surface	(3)

(1) Section Removed from Structure After Flt 1400

(2) Section Removed from Structure After Flt 1650

(3) Discovered at 1406 Flts. Growth Increment Occurred from Flt 1406-1600

APPENDIX H

1032 SYSTEM REAL TIME DATA DISPLAYS

APPENDIX H

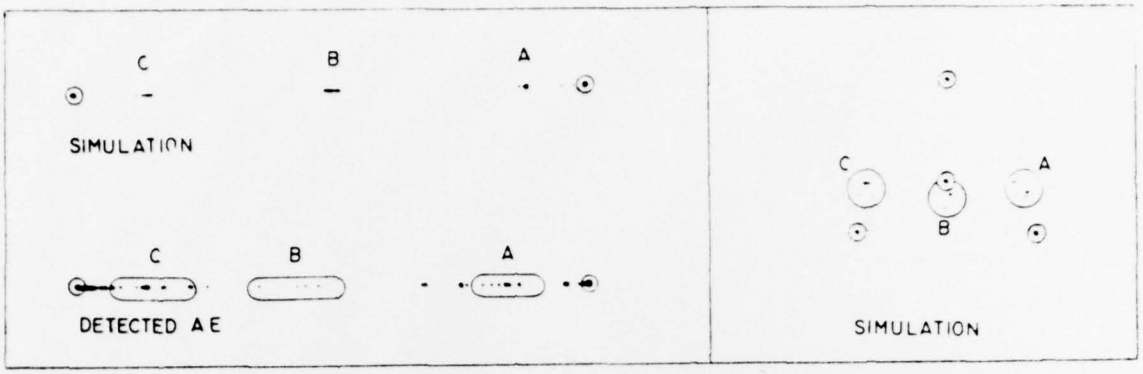

FIGURE H1. AE REPRESENTATIONS FROM TEST AREA 1

The array in Test Area 1 was linear array through Flt 800. The presentations on the left of the block for linear array 0/1 contain a display (top) of simulated signals injected at test holes A, B, and C, and a display of AE signals plus noise detected during Flt 530. The display on the right is a triangular representation of simulated signals injected at the test holes. Since cracks at A and B had little or no growth after this array was deployed, a suitable triangular display of detected AE was not available.

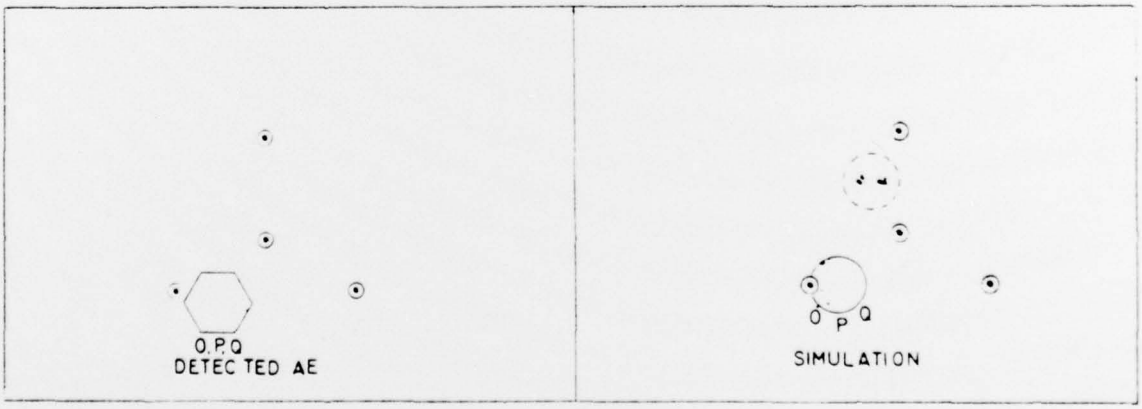

FIGURE H2. AE REPRESENTATIONS FROM TEST AREA 2

The triangular array presentation shows real AE crack growth from test area 2 on the diagram at the left and simulations in the diagram on the right. Other indications on left diagram are primarily nonrepeating random noise signals. The simulation on the right shows a displacement for indications made at the test hole on an adjacent faying member.

APPENDIX H

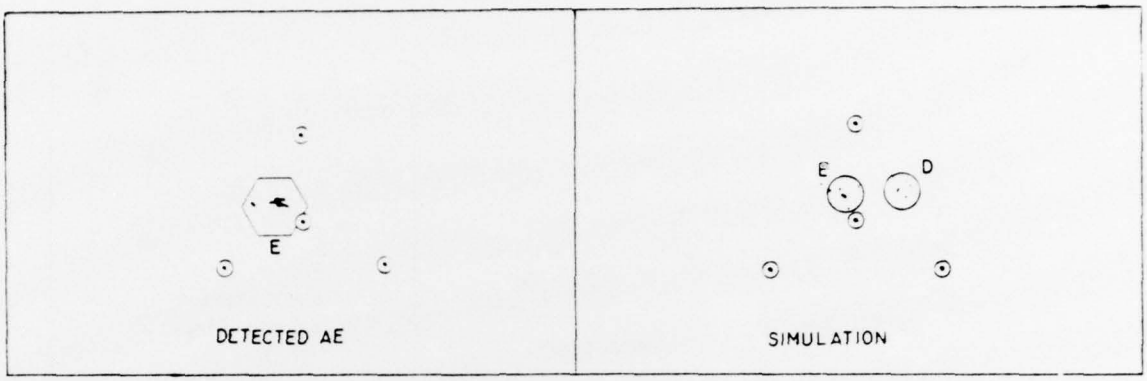

FIGURE H3. AE REPRESENTATIONS FROM TEST AREA 2

Triangular presentation on left is AE detected during flight 1625 from test hole E in test area 2. Right presentation shows simulations made on the mid beam cap riser at test holes E and D.

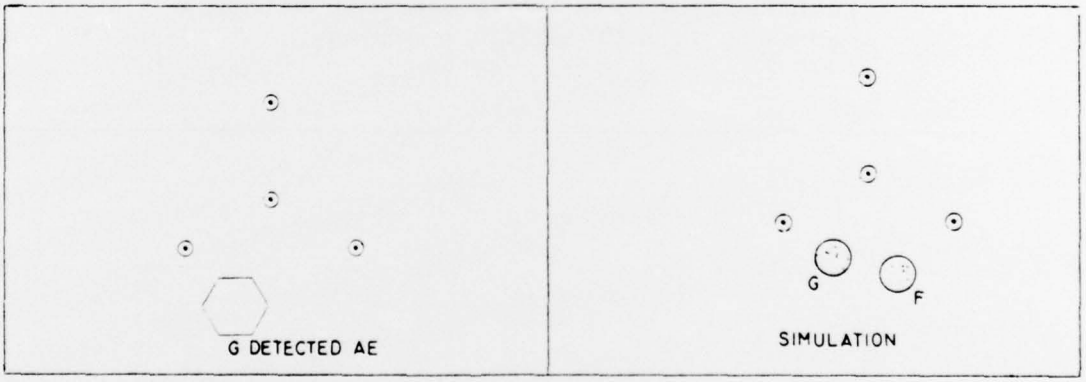

FIGURE H4. AE REPRESENTATIONS FROM TEST AREA 3

Triangular presentations on left are detected AE from test hole G in test area 3. Presentation on right are simulations made of test holes F and G.

APPENDIX H

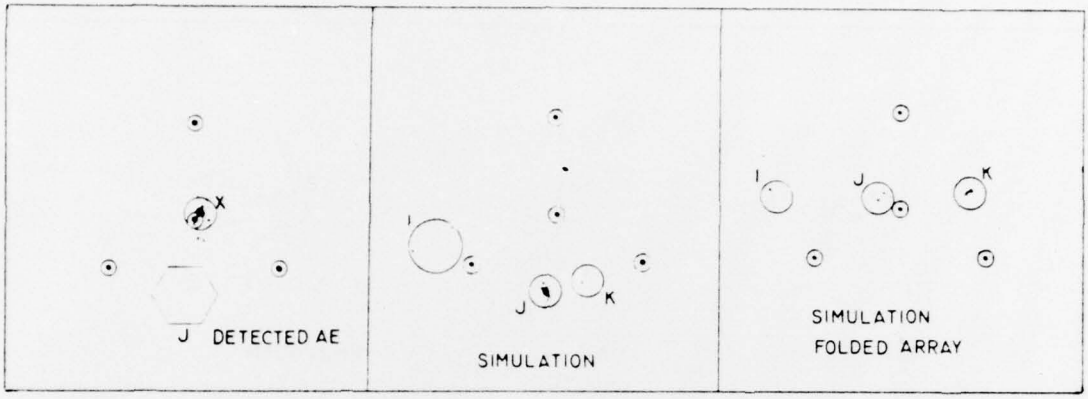

FIGURE H5. AE REPRESENTATIONS FROM TEST ARE 5

Triangular presentation on left includes AE from test hole J in test area 5, repetitious AE from unknown source at X and nonrepeating random noise. Two presentations on right show simulations made at test holes I, J and K for the arrays installed after flights 400 and 1200, respectively.

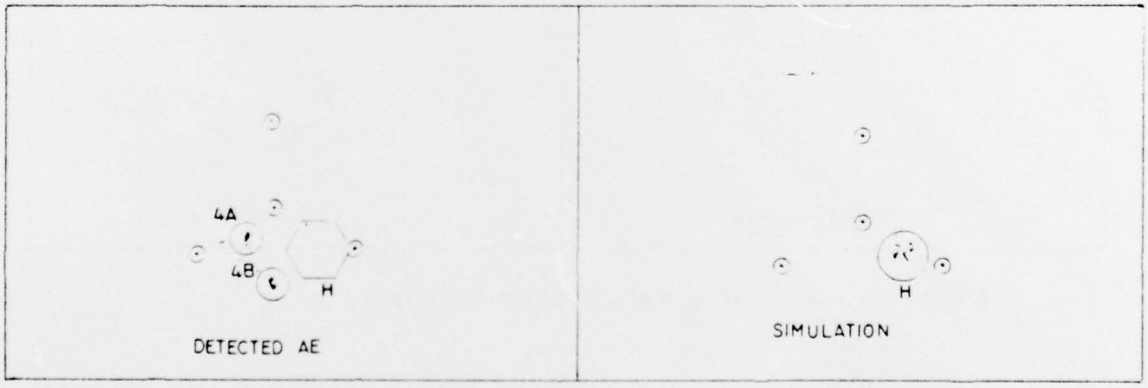

FIGURE H6. AE REPRESENTATIONS FROM TEST AREA 4

Triangular presentation on left shows repetitive AE detected during flights from test hole H and suspect areas 4A and 4B, all in test area 4. The presentation on right shows simulations made at test hole H, with bolt removed.

APPENDIX H

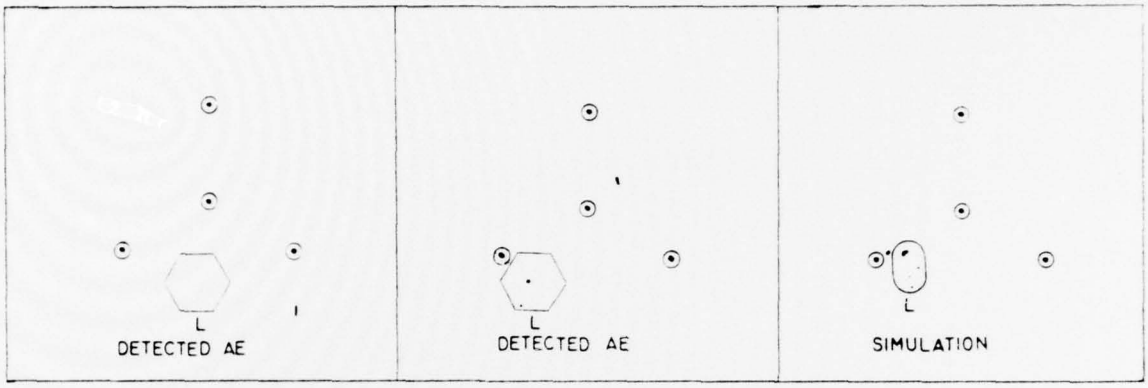

FIGURE H7. AE REPRESENTATIONS FROM TEST AREA 6

Triangular presentation on left shows AE detected during flight loading from test hole L using the "rotated" array. Center presentation is AE from test hole L before the array was rotated (after flight 436). Right presentation are simulations made of test hole L with bolt removed before the array was rotated.

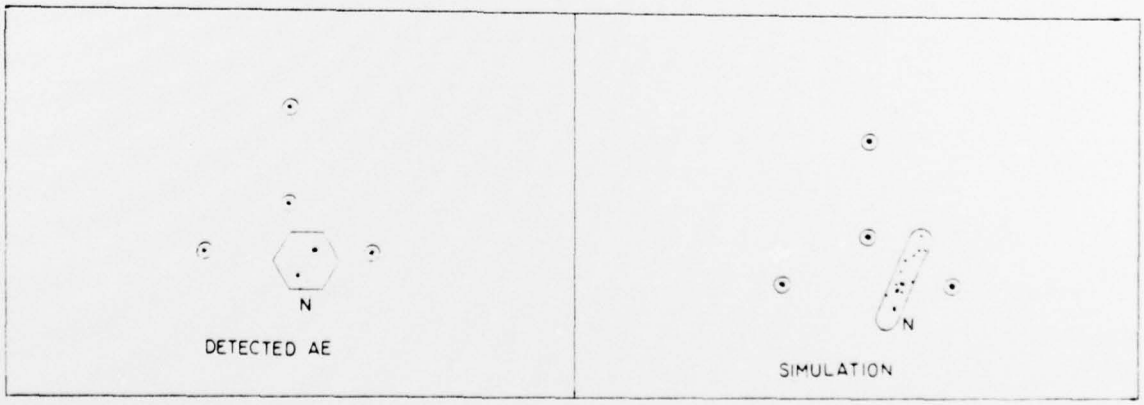

FIGURE H8. AE REPRESENTATIONS FROM TEST AREA 8

Triangular presentation on left is AE detected during flights 790 to 796 at test hole N. Right presentation shows simulations made at test hole N.

APPENDIX I

AE EVENT RESULTS FOR THE TEST AREAS

APPENDIX I

AE RESULTS FROM EACH TEST AREA

Test Area 1, Test Holes A & B. Area 1 was monitored with a linear array through flight 800, which was then replaced with a triangular array. The triangular array was modified again after flight 1200 in an attempt to improve the AE detectability. The latter modification, described in Section 3.1.4C, included a wing joint within the array. Since crack growth had virtually ceased in hole A before flight 800 and growth was continuing aft from hole B only, the triangular arrays did not witness much AE activity. The AE from hole B were intermingled with a relatively high noise incidence and were also being indicated in a virtual location varying from the true position because of structural effects. The previous linear array appeared to indicate AE from holes A and B, but it was not possible to verify them as true crack growth AE in the presence of the high noise. The triangular arrays had the potential of resolving the AE identity difficulties if significant crack growth had continued.

Test Area 2, Test Holes D and E. Early attempts to monitor growth at these test holes were not successful using a linear array. After a triangular array was mounted on the beam cap following flight 1200, this array consistently picked up AE from hole E through flight 2000. These are plotted in Figure 11 and tabulated in Table I. The occasional emissions from hole D lost intensity in propagating from the web to the array and were, therefore, less reliably indicated.

Test Area 2, Test Holes O, P and Q. Early cap-mounted linear and web-mounted triangular arrays could not successfully indicate AE from these holes because of a very high noise incidence in the area. The final triangular array showed an improvement in noise rejection but was not entirely successful in showing separation in noise and AE sources.

Test Area 3, Test Holes F and G. The linear array used to monitor the area during the first 300 flights appeared to indicate AE from both test holes F and G. These were used to compare the results obtained with the AML system whose transducers were mounted in Area 3 parallel to the D/E 1032 transducers. Several noise sources were present which made detection unreliable for the one-dimensional linear array. The triangular array which was installed in the area across the cap-to-panel 1 splice following flight 400, displayed AE from F and G. However, crack growth was slow and the emissions were sparse and scattered. Several noise sources were more active than the cracks, but could be separated on the array's two-dimensional plan view display.

Test Area 4, Test Hole H. This was another noisy area and the early linear array could not reliably show crack growth AE. The 8-inch triangular array installed next allowed scattering of the indications from noise and AE sources, hindering reliable assessment. A larger triangular array was installed and it included the center wing

panel 2-to-panel 3 splice. It successfully displayed AE from test hole H and two other emitters designated 4A and 4B. A plot of AE from test hole H is shown in Figure 11 and the data are tabulated in Table I. A distinct decrease in the AE rate was experienced after modifying the array, but this was eventually corrected by optimizing the channel gains. (Data from 4A and 4B are also tabulated in Appendix E.)

Test Area 5, Test Holes I, J and K. AE from hole J was received by the initial triangular array until the crack reached the lower edge of the web just prior to flight 1600. The crack was removed at the end of 1650 flights for fractographic examination. A plot of the AE from J is shown in Figure 11 and the data are tabulated in Table I. The emission rate was very sporadic throughout the flights. AE from holes I and K were not identifiable as coming from a distinct source. This was attributed to the complex stiffener and cap splice joints and to the positioning of the array so that I and K were in the vicinity of the apex transducers 1 and 2, respectively (see Section 3.1.4B). The final experimental array installed following Flight 1600 did not reliably indicate emissions from holes I and K. Several early extraneous emitters were located at fastener holes in a nearby stiffener attachment area and were found to be related to loose fasteners.

Test Area 6, Test Hole L. The triangular array installed in this area following the 100 precrack flights was improved by "rotating" the array after 435 flights. AE from the small amount of crack growth experienced in hole L was persistent, but not constant. The AE is plotted in Figure 11 and the data are tabulated in Table I. Another unidentified emitter or noise source existed within the chordwise splice in this area.

Test Area 7, Test Hole M. This area was not monitored for AE during the program.

Test Area 8, Test Hole N. AE indications were received from Test Hole N throughout the first 1200 flights, after which the material containing the crack was removed for fractographic examinations. An improvement in detection was obtained when the array was "rotated" prior to flight 438.

Test Area 9, Test Hole R. This area was not monitored for AE.

AE Baseline Area 9. This area, established as an AE noise baseline area, developed a persistent AE emitter following flight 801. The data for the emitter for flights 1201 to 2000 is tabulated in Table I. An old crack, stop-drilled to stop growth, existed in a clip attachment on a panel riser in the vicinity of the emitter. No growth occurred in the crack during the test flights. This crack was not known to exist when the area was selected.

APPENDIX I

TABLE I. CUMULATIVE AE EVENTS FOR X993 TEST CRACKS AND AE SOURCES

	TEST CRACKS & IDENTIFIED EMITTERS						
TEST FLIGHTS	4H*	5J*	2E**	6L	4A	4B	9A
801	(0)	(0)					
838	14	6					
858	16	6					
882	19	7					
900	25	9					
924	39	12					
950	56	15					
987	82	19					
1000	107	21					
1037	240	26					
1107	676	51					
1135	947	66					
1152	1104	72					
1185	1447	91					
1200	1524	98					
1256	1538	116	69	29	94	135	26
1275	1544	116	87	35	134	178	37
1299	1574	117	143	74	248	320	86
1345	1584	123	178	173	304	371	120
1373	1627	129	244	226	423	492	144
1400	1659	142	263	270	496	559	170
1418	1701	182	353	349	587	651	218
1450	1730	210	413	382	660	720	249
1475	1793	241	518	468	798	864	336
1500	1878	262	610	589	936	987	417
1549	1953	272	625	727	1181	1160	520
1600	1989	276	637	828	1360	1332	570
1650	1998		1317	1014			
1700	2017		1751	1198			
1750	2044		2333	1394			
1800	2104		2719	1592			
1850	2253		2925	1791			
1900	2539		3379	2056			
1950	2765		3699	2229			
2000	3035		4019	2462			

*These arrays were modified prior to Flight 1201.

**This array was installed prior to Flight 1201.

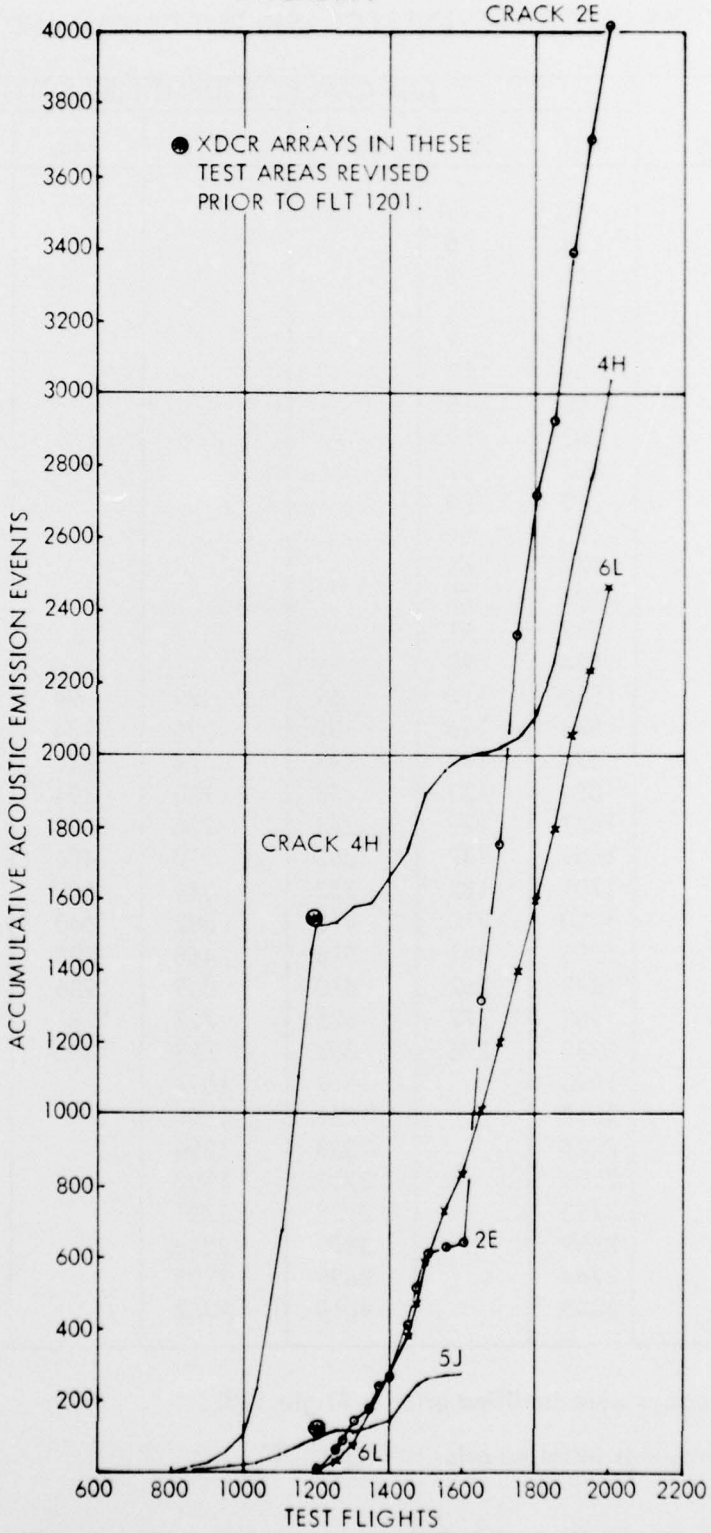

FIGURE 11. ACCUMULATIVE AE EVENTS VERSUS TEST FLIGHTS FOR FOUR TEST CRACKS

REFERENCES

1. C. D. Bailey and W. M. Pless, "Acoustic Emission Used to Nondestructively Determine Crack Locations in Aircraft Structural Fatigue Specimen", IDEP No. 556.45-FH-01. Also, Proceedings of 9th Symposium on Nondestructive Evaluation, April 1973, p. 224f.

2. C. D. Bailey and W. M. Pless, "Acoustic Emission Structure-Borne Noise Measurements on Aircraft During Flight", October 1974, Materials Evaluation, Sept. 1976, p. 189f.

3. Lockheed-Georgia Company, "C-5A Category I Test Results - Expedited Wing Box Fatigue Test (Project Speed), Part II: Second Lifetime," LG1UT73-1-12.

4. R. L. Bell, "Acoustic Emission Transducer Calibration - Transient Pulse Method," Feb. 1973, Technical Report DE-73-3, Dunegan/Endevco, San Juan, Capistrano, Calif.

5. D. M. Anderson and W. M. McGee, "Development and Application of Marker Loads for a Fatigue Crack Growth Study on a Full-Scale Test Article," paper delivered AIAA/ASME/SAE 17th Structures, Structural Dynamics, and Materials Conference, King of Prussia, Pa., May 1976.

6. C. D. Bailey, J. M. Hamilton, and W. M. Pless, "AE Monitoring of Rapid Crack Growth in a Production-Size Wing Fatigue Test Article", NDT International, Dec. 1976, p. 298f.

☆ U. S. GOVERNMENT PRINTING OFFICE: 1977 — 757-001/430